DESIGN OF A DUAL-EXPANDER AEROSPIKE NOZZLE ROCKET ENGINE

by

ERIC STEPHEN MCVAY

RICHARD D. BRANAM, COMMITTEE CHAIR
JOHN BAKER
PATRICK R. LECLAIR

A THESIS

Submitted in partial fulfillment of the requirements for the degree of Master of Science in the Department of Aerospace Engineering and Mechanics in the Graduate School of The University of Alabama

TUSCALOOSA, ALABAMA

2016

ABSTRACT

The University of Alabama's Aerospace Engineering and Mechanics Department is developing a computational dual-expander aerospike nozzle (DEAN) upper stage rocket engine to demonstrate the engine's performance capabilities and to establish a model by which the DEAN can be built. This research expands the base model developed by the Air Force Institute of Technology to more accurately represent the physics involved in both the fluid flow and geometrical properties of the engine. The DEAN engine was modeled using NASA's Numerical Propulsion System Simulation (NPSS) and Chemical Equilibrium with Applications (CEA) software. The methodology implemented in this research was validated by modeling the RL-10A-3-3A upper stage engine in NPSS and comparing resulting outputs with NASA's ROCket Engine Transient Simulator (ROCETS) analysis.

The DEAN uses liquid oxygen and liquid hydrogen as its propellant and is being designed to produce a thrust of 30,000 [lbf] and a specific impulse of at least 465.5 [s], at an oxidizer-to-fuel ratio of 5.88, while also remaining within the size envelope of the RL-10B-2 upper stage engine. The performance and size objectives were established to meet the National Aeronautics and Space Administration's (NASA) Advanced Upper Stage Engine Program (AUSEP) need for an upper stage rocket engine to replace the aging RL-10 series engines that have been in production since the 1960s. Results indicate that optimal performance for the feasible solution space examined in this research occurs at an expansion ratio of 30, a throat area of 23 [in^2], and a characteristic length, L*, of 90 [in]. The optimal DEAN design point was

shown to achieve a thrust of more than 5,000 [lbf] greater than the RL-10B-2, a I_{sp} of 1.8 [s] greater, and a significantly reduced size envelope.

LIST OF ABBREVIATIONS AND SYMBOLS

a	=	cooling channel half-spacing
a_{H_2}	=	speed of sound of H_2
a_{O_2}	=	speed of sound of O_2
A	=	cross-sectional area
A_c	=	chamber area
$\frac{A_c}{A_t}$	=	chamber contraction ratio
A_e	=	nozzle exit area
A_{phys}	=	annular flow area
A_t	=	throat area
AR	=	cooling channel aspect ratio
b	=	width of cross-sectional area
c	=	effective exhaust velocity
c^*	=	characteristic velocity
c_{CR}	=	chamber ratio coefficient
c_n	=	nozzle truncation factor
c_p	=	heat capacity of the fluid
C_d	=	discharge coefficient
C_F	=	thrust coefficient
CEA	=	Chemical Equilibrium with Applications

CET93	=	Chemical Equilibrium with Transport Properties
CV	=	cooling volume
d	=	depth of cross-sectional area
d_{hyd}	=	hydraulic diameter
D	=	diameter
D_c	=	chamber diameter
DEAN	=	dual-expander aerospike nozzle
f	=	Darcy friction factor
FPT	=	fluid property table
g_0	=	gravity constant
Δh	=	change in enthalpy
h	=	enthalpy
h	=	cooling channel height
h_{gr}	=	hot gas heat transfer coefficient, Bartz equation
h_l	=	liquid heat transfer coefficient, Colburn equation
H_p	=	pump head pressure rise
I_{sp}	=	specific impulse
k	=	thermal conductivity
K	=	loss-factor
L	=	length
L^*	=	characteristic length
L_c	=	chamber length
L_e	=	engine length

L_n = nozzle length

LOX = liquid oxygen

LH_2 = liquid hydrogen

LCH_4 = liquid methane

$LRPS$ = liquid rocket propulsion system

m = mass

m_f = final mass

m_o = initial mass

$\dot{m}$ = mass flow rate

$\overline{M}$ = molar mass

M = Mach number

M_e = exit Mach number

n = number of channels

$NASA$ = National Aeronautics and Space Administration

$NIST$ = National Institute of Standards and Technology

$NPSS$ = Numerical Propulsion System Simulation

O/F = oxidizer-to-fuel ratio

ΔP = pressure drop

P_a = ambient pressure

P_c = chamber pressure

P_e = exit pressure

P_e/P_c = pressure ratio

P_{Ti} = turbine inlet pressure

P_{Td} = turbine discharge pressure

$p_{T,pr}$ = turbine pressure ratio

$\dot{Q}$ = heat flow rate

$\bar{R}$ = gas constant

Re = Reynolds number

ROCCID = ROCket Combustor Interactive Design

ROCETS = ROCket Engine Transient Simulator

RTE = Rocket Thermal Evaluation

r_c = chamber radius

r_t = throat radius

SA = surface area

SRPS = solid rocket propulsion system

t = cooling channel-combustion chamber wall thickness

T = temperature

TDK = Two-Dimensional Kinetics

T_0 = total temperature

T_c = combustion temperature

T/W = thrust-to-weight ratio

ΔV = change in velocity

v = velocity

V_e = exhaust velocity

V_c = chamber volume

w = cooling channel half-width

x	=	axial position
y	=	surface contour equation
α	=	nozzle half-angle
ε	=	expansion ratio
γ_c	=	ratio of specific heats of combustion in chamber
η_P	=	pump efficiency factor
η_T	=	turbine efficiency factor
λ	=	nozzle efficiency factor
μ	=	absolute viscosity
ϕ_B	=	Bartz equation correction factor
ϕ_{curv}	=	Colburn equation correction factor for tube radius of curvature
ρ	=	density

ACKNOWLEDGMENTS

I would first like to express my sincere appreciation to Dr. Richard Branam, my research advisor and committee chair, for his guidance, encouragement, and support throughout this research. I would like to thank Dr. John Baker for sitting on my research committee and, more importantly, for reestablishing the astronautics coursework and research foundations within the Aerospace Engineering and Mechanics department. Thank you to Dr. Patrick LeClair for sitting on my research committee and for being patient with my constant questions regarding relativity, physics, and metaphysics.

Thanks to Dylan Stapp, my research colleague and lab mate, for the wise words and support throughout this endeavor – "coffee is my working fluid." I would like to thank The University of Alabama Graduate School for providing me the Graduate Council Fellowship, which allowed me to pursue my master's degree and complete this research. Finally, a special thank you to my beautiful wife Allyssa – your love, support, and sacrifice has been the glue for our family over these past five years; I cannot wait to continue our journey together.

CONTENTS

LIST OF TABLES

LIST OF FIGURES

I. INTRODUCTION

The dual-expander aerospike nozzle (DEAN) upper stage rocket engine design methodology is aimed at improving engine performance by increasing specific impulse (I_{sp}) and thrust-to-weight ratio (T/W) while maintaining similar or better thrust levels than other engine concepts. The DEAN operates using a LOX/LH_2 dual-expander cycle – the fuel and oxidizer each run through separate expansion cycles before entering the combustion chamber. The aerospike plug nozzle is used to improve efficiency over the entire flight envelope and reduce the overall engine mass.

While solid rocket propulsion systems (SRPS) do exist for upper stages, the majority of current upper stage rocket engines are fueled from liquid rocket propulsion systems (LRPS). LRPS have significantly higher I_{sp} than SRPS and LRPS also provide throttle control. SRPS only offer a one-time burn.

The four main LRPS thermodynamic cycles include staged-combustion, pressure-fed, gas-generator, and expansion. The staged-combustion, gas-generator, and expansion cycles utilize hot or warm gases to drive the turbine, which then drives the fuel and oxidizer pumps. The staged-combustion cycle introduces a small amount of oxidizer to the fuel flow and pre-burns the flow. The warm gases drive the turbine and are fed into the combustion chamber with the oxidizer. The pressure-fed cycle operates by utilizing a separate gas supply to pressurize the fuel and oxidizer tanks, thus reducing the system complexity and eliminating the need for turbopumps – this is the simplest engine cycle[1].

The gas-generator cycle operates by feeding 2-5% of the total flow (fuel and oxidizer) into a separate combustor; the hot gas then drives the turbine and is exhausted overboard. The major losses for this cycle occur because the entire flow is not converted to thrust, though this cycle has significant simplifications over the staged-combustion cycle – namely that the pressure drop across the exhaust injector is independent of the combustion chamber pressure. The expander cycle operates by feeding high-pressure propellant through cooling jacket channels (heat exchangers) to simultaneously cool the nozzle and vaporize the propellant. The warm gas then drives the turbine and is fed into the combustion chamber[1].

The DEAN implements a dual-expander cycle in which both the oxidizer and fuel function in two separate expansion cycles. The use of two expander cycles increases the engine complexity significantly because of the two required power balances (one for each cycle) and the requirement of the propellant to meet at the thrust chamber at the same pressure. This research demonstrates whether or not the engine performance will outweigh the added complexity drawbacks. The DEAN expansion cycle is shown in Fig. (1).

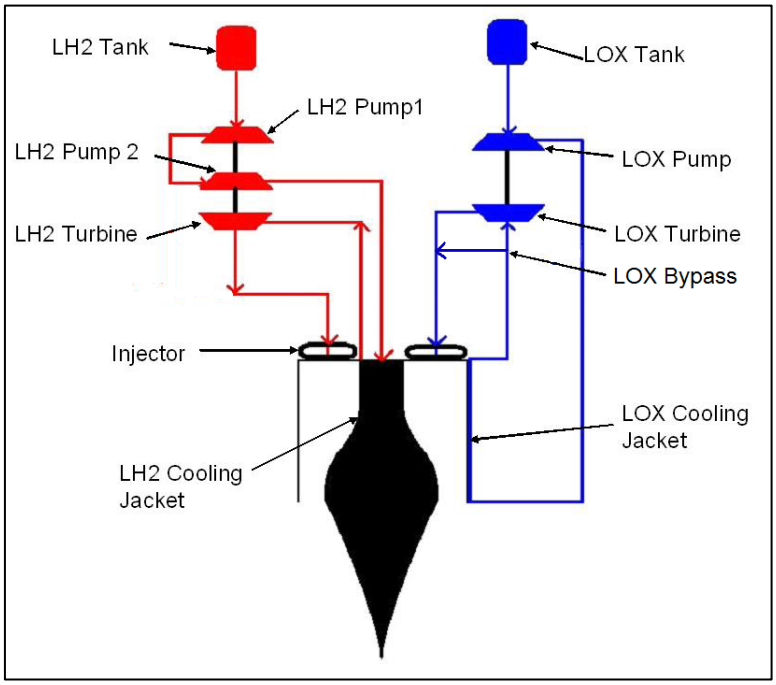

Fig. 1 DEAN Expansion Cycle[2]

The oxidizer (liquid oxygen) path is colored blue and the fuel (liquid hydrogen) path is colored red (government work with permission).

I.1 Motivation

Greason has shown that a 3% increase in I_{sp} will result in a 10% increase in delivered payload to orbit[3]. With costs for current launch systems at greater than $8,000/lb to deliver to low-earth orbit and more than $11,000/lb to deliver to geosynchronous orbit, launch services are always looking for ways to increase their payload to orbit[3]. Increasing the specific impulse directly increases payload and therefore revenue. Additionally, NASA is currently constrained by payload mass to the surface of Mars. Increasing the performance of the rocket engines enables NASA to further increase their payload as well, providing a pathway for a manned mission to Mars, or other celestial body.

The advantages of the DEAN architecture are significant in terms of performance yield. The aerospike geometry allows the DEAN to be altitude compensating; the flow expands ideally

with changes in altitude (changes in pressure). Because the DEAN is altitude compensating, it produces a higher total impulse than the standard bell nozzle engines for the same mission profile. The bell nozzle only exhibits fully expanded flow at the design altitude (pressure). Below the design altitude, the bell nozzle has problems with overexpansion of the flow[4] – when the ambient pressure is greater than the nozzle exit pressure – thus reducing the thrust and I_{sp} achieved. Above design altitude, the bell nozzle has problems with underexpansion of the flow[4] – when the exit pressure is greater than the ambient pressure. In both the underexpanded and overexpanded cases, the engine performance and efficiency decrease and can create mechanical failures. The DEAN's major advantage over the bell nozzle, however, lies in its weight – the DEAN weighs less than similarly performing bell nozzle engines (e.g. RL-10B-2)[5]. Even so, the aerospike may even be truncated to reduce the weight even further. Initial research suggests that the aerospike may be truncated to as much as 50% with minimal performance losses[5].

Another major advantage is the improved operability and reliability of the dual-expander cycle. The fuel and oxidizer streams are entirely independent of each other until being injected into the combustion chamber, as seen in Fig. (1). For this reason, an inter-propellant seal is not necessary, therefore reducing the cycle's critical failure mode (i.e. propellant mixing and combustion before reaching the combustion chamber) when compared to gas-generator or staged-combustion cycles, for example.

The DEAN architecture is throttle-able in two ways: the oxidizer-to-fuel-ratio is actively adjusted in each of the two individual expansion cycles, thereby adjusting the performance properties; the second being that the aerospike nozzle itself is a plug nozzle that can be moved axially to control the throat area, thus throttling the flow and modifying the performance of the engine.

The DEAN engine, though currently being designed as an upper stage engine, has potential application for Mars access (i.e. entry, descent, landing, and ascent) vehicles currently being engineered. We consider NASA's Mars Design Reference Architecture[6] as a baseline example. Methane (LCH_4) has been selected as the ideal fuel for the Mars architecture because it is easily space-storable for long duration missions, whereas liquid hydrogen requires substantial amounts of energy to maintain for long duration missions in deep space with significant losses from boil-off. Liquid hydrogen (LH_2) requires lower temperature requirements, which directly increases total power (cryocooler power consumption) and mass requirements (namely from increased insulation and larger storage tanks). Future work will be completed to model the DEAN as a Mars access engine and to demonstrate the feasibility, sustainability, and efficiency of its implementation into NASA's Mars mission architectures. This future research will include a propellant trade study to determine the effectiveness of methane as a fuel for the DEAN architecture. Major payoffs could be realized if the DEAN were to maintain better performance metrics at lower weight, as has been projected by previous studies. The Mars vehicle design will need propulsion for entry, descent, landing, and ascent. The DEAN's advantageous performance at lower altitudes and throughout the entire flight envelope would be an ideal choice.

I.2 Research Objectives

The objectives for this research are threefold: 1) simulate the performance of a LOX/LH_2 dual-expander cycle, 2) validate results using the RL-10A-3-3A, and 3) determine the optimal design parameters within the scope of this analysis and the limitations of the dual-expander model in order to provide a next generation upper stage engine. Table 1 outlines the design points for the DEAN engine and provides a comparison with RL-10B-2 performance values.

Table 1 DEAN & RL-10B-2 Performance Comparison

Parameter	[Unit]	DEAN	RL-10B-2[7,8]
Thrust	[lbf]	30,000	24,750
Specific Impulse	[s]	465.5	465.5
Diameter	[in]	<60	43.8*
Length	[in]	<90	86.5*

*Dimensions Do Not Include Nozzle Extension

The performance and size goals are based on NASA's Advanced Upper Stage Engine Program need for an upper stage rocket with thrust levels between 25-35,000 [lbf][9] to replace the RL-10 series engines that have been in production since the 1960s. The performance goal is for the DEAN to operate at a higher thrust while maintaining the same specific impulse. Additionally, the RL-10B-2 performance values are for a fully extended nozzle, but the size values are for an unexpanded nozzle; the DEAN objectives are to achieve better performance within this unexpanded size envelope. Previous studies indicate that this performance gap is likely even greater than our goals suggest, with a potential I_{sp} of over 490 [s][2].

Researchers at the Air Force Institute of Technology initially developed the DEAN as an upper stage engine in support of the Department of Defense Integrated High Payoff Rocket Propulsion Technology program. Martin, Hall, and Simmons have provided a framework for the current LOX/LH_2 DEAN research[2,5,10]. Martin's work demonstrated that the architecture had the potential to produce the desired outputs, but further work was needed to increase the resolution and fidelity of the model[10]. Hall and Simmons continued this research by simplifying Martin's model and adding parametric variables to be used in optimization and trade studies using Phoenix Integration's ModelCenter[2,5]. This research takes the simulation to a new level of development for the LOX/LH_2 DEAN architecture. The current simulation includes embedded thermodynamics (equation of state and compressible flow). The embedded thermodynamics package has reduced the number of independent inputs by tying parameters together through

geometrical and physical principles. The reduced parameter set allows more engine configurations to be considered in much less time and improves the overall utility of the simulation. The simulation architecture has incorporated the flexibility needed to further consider the use of methane in support of the NASA Mars mission architecture.

II. BACKGROUND

Chapter II presents the theory and background behind rocket engine and nozzle design, the dual expander aerospike nozzle, and past research on the DEAN engine.

II.1 Current Upper Stage Rocket Engines

Rocket engines provide several essential operations: specifically, launch from Earth, orbit transfers, thrust maneuvering required for orbit maintenance, docking with other spacecraft, and attitude control[7]. The propulsion systems completing these maneuvers are grouped into three categories: launch vehicles, upper stage engines, and reaction control system thrusters. Our focus in this research is the upper stage rocket engine. As these stages are inherently "payloads" on the launch vehicles, it is necessary to minimize their weight and maximize their performance (specific impulse). For in-space vehicles, the primary performance concern is the specific impulse, whereas the thrust is the primary performance concern for launch vehicles. In the near future, the task of re-entry (via retropropulsion) and ascent from planetary or orbiting bodies will be added to these performance demands of upper stage rocket engines.

In order to determine the competitiveness of the DEAN as an upper stage engine, it is necessary to review other LOX/LH_2 upper stage engines that are either currently in operation or are in development for use in the near future. Table 2 presents three of these engines in tabular format.

Table 2 Performance Comparison of LOX/LH_2 Upper Stage Engines[7,11]

Engine	Thrust, Vacuum [lbf]	I_{sp} [s]	Weight [lbf]	T/W [ ]
RL-10B-2	24,750	465.5	664	37:1
J-2X	294,000	448	5,450	54:1
RL-60*	60,000	460	700	86:1

*In development

The RL-10B-2 and RL-60 engines both implement a single expander cycle with a regeneratively cooled nozzle[12]. The J-2X operates using a gas generator cycle and a regeneratively cooled nozzle[11]. Each of the engines shown in Table 2 share common cycle and cooling methods with the DEAN. Sections II.2 and II.4.E discuss rocket engine cycles and cooling methods for rocket engines, respectively.

II.2 Rocket Engine Thermodynamic Cycles

The staged combustion cycle – shown in Fig. (2) – mixes some oxidizer into the fuel flow in the pre-burner (government work with no copyright). The exhaust gases and the unburned fuel flow are used to drive the turbomachinery and are then injected into the thrust chamber, where the remaining combustion occurs. Staged combustion cycles are advantageous because all the mass flows through the throat area (produces thrust) and because they provide high chamber pressures. High chamber pressures result in smaller thrust chambers and larger expansion ratios – meaning the nozzles are more efficient at lower altitudes. The main disadvantage of this cycle is the complexity of the engine creating difficult operating conditions, specifically for the turbomachinery. The added complexity also adds mass to the engine, reducing the overall thrust to weight[13].

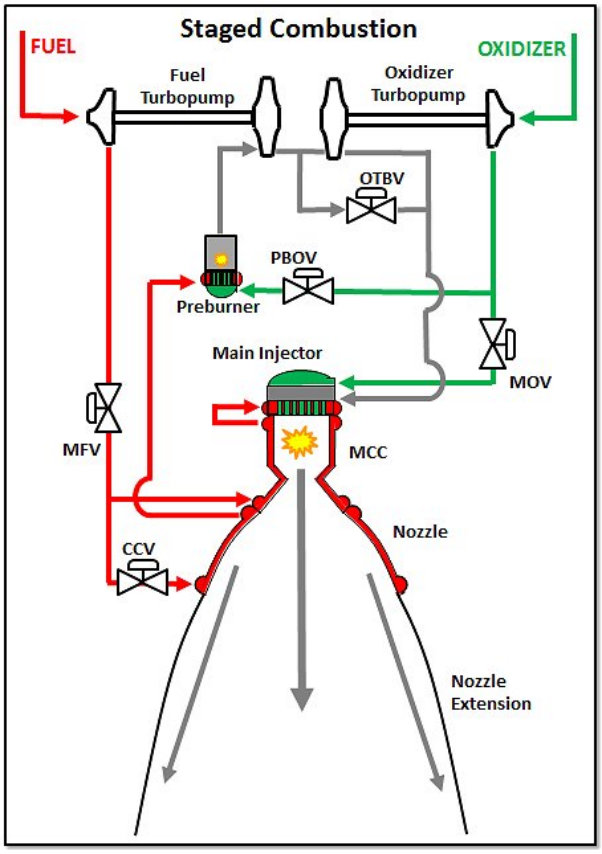

Fig. 2 Staged Combustion Cycle[14]

The second engine cycle is the pressure-fed cycle. The pressure-fed cycle uses a separate gas supply to pressurize the propellant tanks – the supplied pressure must be greater than the chamber pressure in order to maintain flow and prevent backflow. This is the simplest of the engine cycles and sustains highly reliable performance, particularly for on-orbit maneuvers and attitude and control. Pressure-fed systems are limited by tank pressure that they can provide, which limits thrust chamber pressure. If the pressures in the tanks are too high, the tank thickness and the supporting structure become too heavy, reducing performance[15].

The gas generator cycle – shown in Fig. (3) – feeds small amounts of propellant to a separate combustion chamber (government work with no copyright). The products of that combustion are used to drive the turbomachinery to pump the propellants to the thrust chamber. Once the combustion products provide power to the turbines, the gases are exhausted

downstream of the throat. Performance is lost because these exhaust products are not expanded through the main nozzle. While the gas generator cycle is not necessarily the most efficient, the main advantage is the simplicity of the thermodynamic cycle and the higher turbine pressure ratios available[16].

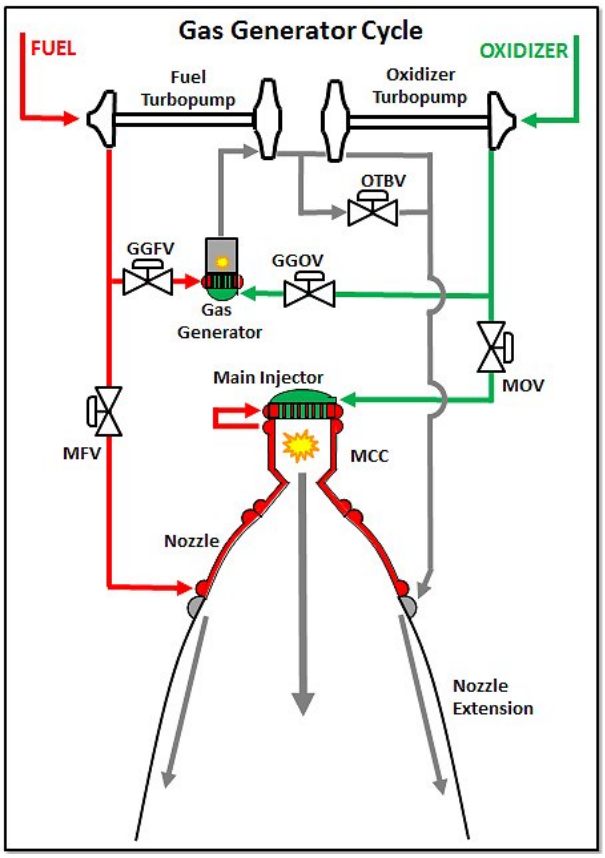

Fig. 3 Gas Generator Cycle[14]

The closed expander cycle in Fig. (4) pumps the propellant through cooling channels along the nozzle and thrust chamber (government work with no copyright). These cooling channels operate as heat exchangers, transferring energy to the working fluid (propellant). The warm, high-pressure fluid is typically supercritical. The propellant is then expanded across the turbine, transferring the energy necessary to run the cycle, before being injected into the thrust chamber. The expander cycle is considered "closed" because all the propellant goes through the thrust chamber, thus allowing for maximum thrust for the operating condition (increases engine

efficiency)[16]. The DEAN rocket uses a variation of this cycle, the dual-expansion cycle, where both the fuel (liquid hydrogen) and oxidizer (liquid oxygen) operate in separate expansion cycles.

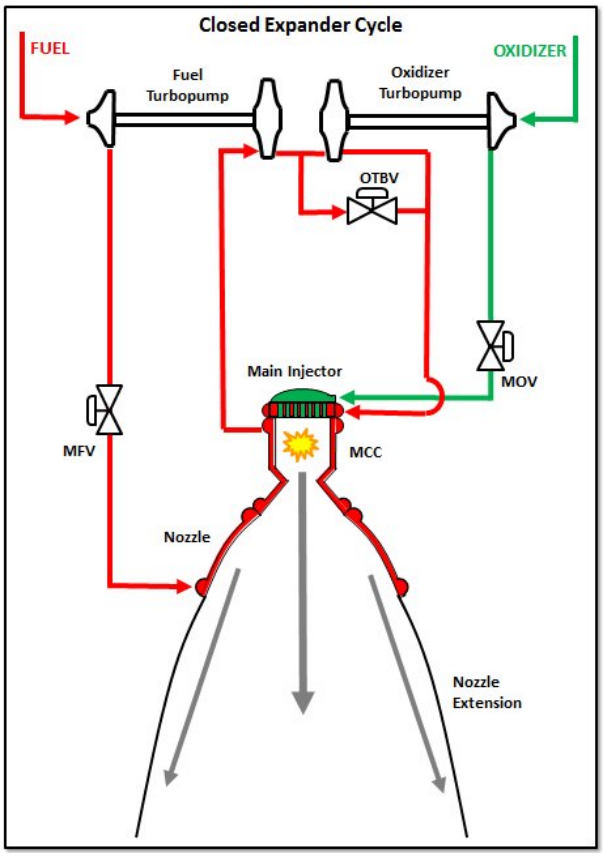

Fig. 4 Expander Cycle[14]

The square-cube law limits expander cycles. The expander cycle functions by the amount of heat transferred through the surface area of the nozzle and chamber. The cooling volume of the propellant in the heat exchanger increases faster than the surface area. Increasing surface area increases the amount of energy available to the turbine to pump the propellant. The increased volume increases the pressure loss, and therefore the amount of horsepower required by the pump. The energy balance creates a maximum size condition for which any growth will negatively affect the performance of the engine or even make the engine cycle entirely inoperable.

The implementation of the dual-expansion cycle introduces significant complexity to the engine. The separate DEAN expansion cycles for a LOX/LH_2 engine are shown in detail in Fig. (5)[2], with the primary plumbing and flow directions listed (government work with permission).

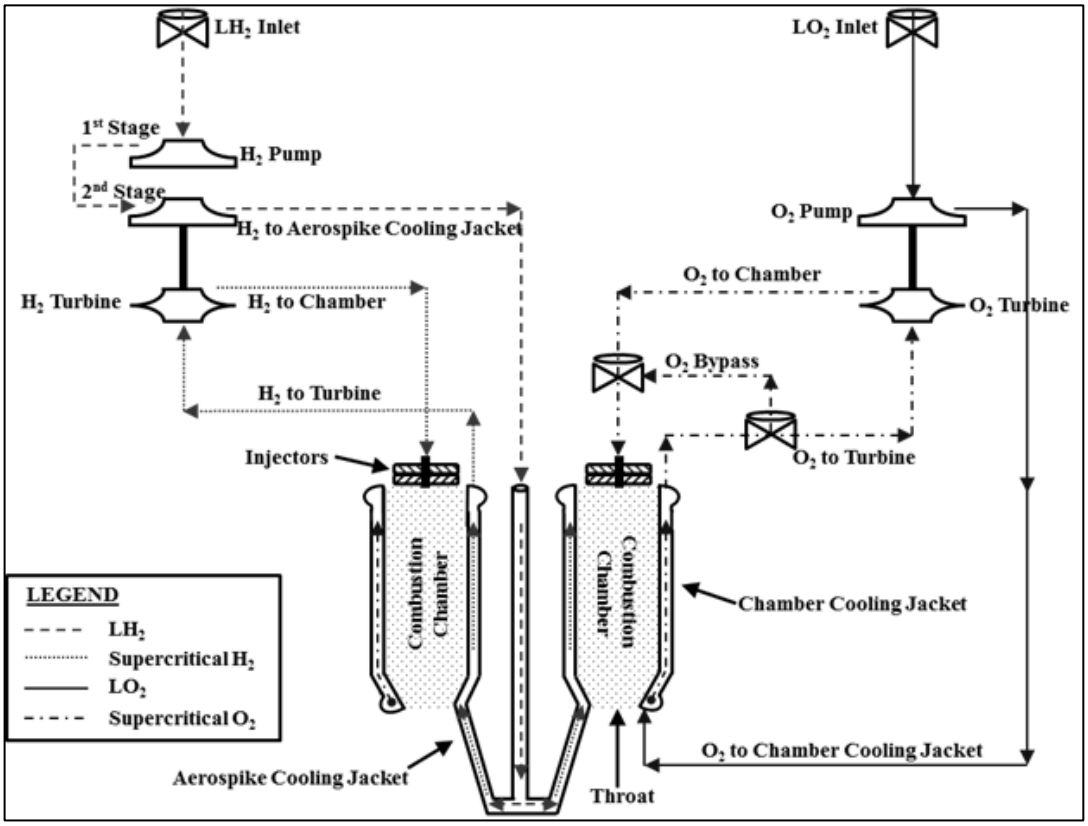

Fig. 5 DEAN Expansion Cycle[2]

As shown, the LOX flows through the combustion chamber cooling jacket and the LH_2 flows through the aerospike cooling jacket, with both cooling jackets operating as heat exchangers. Similar development engines (Upper Stage Demo, Air Force Research Lab) have used separate pumps for the propellants, but turned both turbines with the fuel. The separate cycle scheme eliminates an inter-propellant seal, which mitigates the critical failure mode associated with propellant mixing and combustion prior to the combustion chamber.

II.3 Rocket Engine and Nozzle Performance

Implementation of multi-stage rockets is primarily to drop the inert mass after each stage is complete, but also provides the ability to design each stage based on its specific operating altitude. Altitude performance generally applies to three flight path phases – liftoff, flight, and in-space – with nozzles and engines being optimized for each particular segment. At lower altitudes, where the gravity well dominates, thrust is the major performance parameter of interest. As the spacecraft achieves higher altitude, the thrust and I_{sp} will both increase, and the performance interest shifts to I_{sp}. Additional mass savings are realized in the design and manufacturing of staged rockets because each engine is designed to the specific operating conditions. For stages whose operating conditions are near-vacuum, such as an upper stage, I_{sp} is the driving performance parameter.

Specific impulse is a measure of an engine's efficiency – the ratio of engine thrust to propellant burned. Higher specific impulse correlates to longer burn durations (all else constant), which is synonymous with a car's efficiency correlating to miles per gallon. Specific impulse (Eq. (1)) is determined directly from thrust and mass flow or as a relationship of combustion characteristics (specifically temperature, propellant molecular weight, and ratio of specific heats)[1].

$$I_{sp} = \frac{Thrust}{\dot{m} g_0} = \frac{1}{g_0}\left[\sqrt{2\frac{\gamma \mathcal{R}}{(\gamma-1)}\frac{T_c}{\mathcal{M}}\left[1-\left(\frac{P_e}{P_c}\right)^{\frac{(\gamma-1)}{\gamma}}\right]} + A_e\left(\frac{P_e - P_a}{\dot{m}}\right)\right] = \frac{V_e}{g_0} \quad (1)$$

The calculation is simplified for the design condition, $P_e = P_a$ (or "fully expanded flow"). The characteristic velocity (c*) is also used as a method for measuring the engine efficiency and is directly proportional to I_{sp}. The effective exhaust velocity, c, is then related to c* by multiplying c* by the thrust coefficient, C_F, given by

$$C_F = \frac{Thrust}{A_t * P_c} \tag{2}$$

In reality, the effective exhaust velocities calculated by Eq. (1) are higher than the actual measured exhaust velocity because of combustion inefficiency[17].

The engine performance is related to the rocket performance by the overall change in velocity, or ΔV. The impulse required to complete a given orbital maneuver defines the required change in velocity needed for a rocket system[1]. The total ΔV provided by a spacecraft is directly proportional to the specific impulse.

$$\Delta V = I_{sp} * g_0 * \ln\left(\frac{m_o}{m_f}\right) \tag{3}$$

This relationship (Eq. (3)) shows how higher engine specific impulse will reduce the demand for propellant mass, reducing the overall mass of the space vehicle. This research does not focus on ΔV as a design variable, so we instead manipulate this equation to solve for the product of I_{sp} and g_0, which is equivalent to exhaust velocity, V_e. The effective exhaust velocity, c, can be determined by the following relationship:

$$c = V_e + \frac{(P_e - P_a) * A_e}{\dot{m}} \tag{4}$$

The specific impulse relationship in Eq. (1) also suggests a reliance on higher chamber pressure (P_c). Achieving higher chamber pressure has a much more pronounced impact on thrust chamber size than it does on specific impulse[1]. For a given thrust level, increasing chamber pressure requires that the throat area of the chamber must decrease (Eq. (5)). As the throat area decreases, the nozzle exit diameter and the chamber diameter can be reduced, reducing the engine mass.

$$\dot{m} = \frac{A_t P_c}{\sqrt{T_c}} \sqrt{\frac{\gamma \mathcal{M}}{\mathcal{R}}} \left(\frac{\gamma+1}{2}\right)^{-\frac{\gamma+1}{2(\gamma-1)}} \tag{5}$$

The pressure ratio, or ratio of exit pressure to chamber pressure, is given by Eq. (6):

$$\frac{P_e}{P_c} = (1 + \frac{\gamma_c - 1}{2} * {M_e}^2)^{\frac{\gamma_c}{1-\gamma_c}} \quad (6)$$

For fixed chamber pressures, we can determine the exit pressure along the flight path. The expansion ratio (Eq. (7)) describes the relationship between the throat area and the nozzle exit area. Engines are currently designed with a fixed expansion ratio for a given design altitude (pressure). The engine's design altitude, when nozzle exit pressure is equal to the atmospheric pressure, is characterized by ideally, or fully, expanded exhaust flow.

$$\varepsilon = \frac{A_e}{A_t} = \frac{1}{M_e}\left[\left(\frac{2}{\gamma_c + 1}\right)\left(1 + \frac{\gamma_c - 1}{2} {M_e}^2\right)\right]^{\frac{\gamma_c + 1}{2(\gamma_c - 1)}} \quad (7)$$

In order to achieve the high specific impulses of the RL-10B-2, designers needed to use an expansion ratio of 285:1 (achieved using an extendable nozzle)[8]. The DEAN obtains the same performance (specific impulse) with a significantly lower expansion ratio (in the range of 25-30:1), resulting in a significantly lighter engine.

II.4 Rocket Engine Components

Rocket engines are extremely advanced, complex systems that require meticulous detail in their design, manufacturing, testing, and evaluation. As Dr. Dave Akin once said, "Space is a completely unforgiving environment. If you screw up the engineering, somebody dies (and there's no partial credit because *most* of the analysis was right...)"[18]. This section discusses some of the major rocket engine components and the equations used in their design. Most of the techniques and equations listed are first- and second-order approximations and are described in order to allow the reader to understand the complex design challenges involved with rocket design.

A. Propellant Feed System

The propellant feed system involves everything between the propellant tanks and the combustion chamber, which, among other components, includes the turbomachinery (turbines and pumps), cooling jacket, and injector. The goal of the propellant feed system is to minimize the line losses (pressure drop) while delivering the needed mass flow to achieve the desired thrust. The following pressure analysis is described through application of general fluid mechanics theory[1].

Assuming incompressible flow, Bernoulli's equation – shown by Eq. (8) – gives us a way in which to determine the pressure drop (ΔP) resulting from the dynamic pressure of the moving fluid.

$$\Delta P_{dynamic} = \frac{1}{2}\rho v^2 \tag{8}$$

From Bernoulli's equation, we see that increasing kinetic energy (velocity) leads to increased pressure drop (decreased pressure). This pressure mechanism, in combination with the Venturi effect, requires that the velocity must increase for a decreased area, thus also increasing the total pressure drop. The size (area) of the propellant tubing can be determined by applying the mass flow equation (Eq. (9)) and by ensuring that the conservation of mass law is not being violated.

$$\dot{m} = \rho v A \tag{9}$$

These physical relationships show how decreasing the pressure losses can be achieved by increasing the cross-sectional area of our feed lines. Increasing the cross-sectional area requires heavier plumbing, which is in direct contrast to our primary objective of minimizing the engine's weight. The challenge, then, is to determine the balance between pressure loss and engine mass. An additional consideration in our engine cycle is the heat transfer in the cooling volumes.

Increasing propellant velocity enhances the heat exchange through the cooling jacket and provides more energy to operate the turbomachinery.

The feed line loss is the pressure drop due to friction as a fluid flows through a length of tubing. The Darcy-Weisbach equation gives us a means to accurately estimate the pressure drop:

$$\Delta P_{feed} = f\left(\frac{L}{D}\right)\frac{\rho v^2}{2} \tag{10}$$

Here, f is the Darcy friction factor and is determined by the characteristics of the pipe and fluid, as well as the fluid velocity. The Darcy friction factor is also implemented under the assumption that the fluid is incompressible. The flow conditions for both propellants are nearly incompressible. For the supercritical hydrogen, the compressibility factor only ranges between 1.0 and 1.1 over the entire range of operation ($28 < P < 2500$ [psia]; $72 < T < 990$ [°R])[19].

The pressure profile analysis generally begins with the thrust chamber because the chamber pressure is such a significant variable in the performance of the rocket engine. Knowing the desired chamber pressure (set by choosing thrust and throat area) and approximate geometry of the propellant feed system, the pressure profile for the entire engine may be determined section-by-section. Without considering the addition of turbomachinery, the required storage tank pressure is defined as

$$P_{tank,req} = P_c - \Delta P_{dynamic} - \Delta P_{feed} - \Delta P_{cool} - \Delta P_{inj} \tag{11}$$

If Eq. (11) is satisfied for a reasonable propellant storage tank pressure, then the propulsion system may be built without requiring a pump – though more in-depth analysis may prove otherwise. If the equation yields pressures that exceed storage tank capacity, then a pump must be implemented. The latter option usually applies to larger systems, such as the DEAN engine. Figure (6) shows a possible pressure profile for a pump-pressure-fed system.

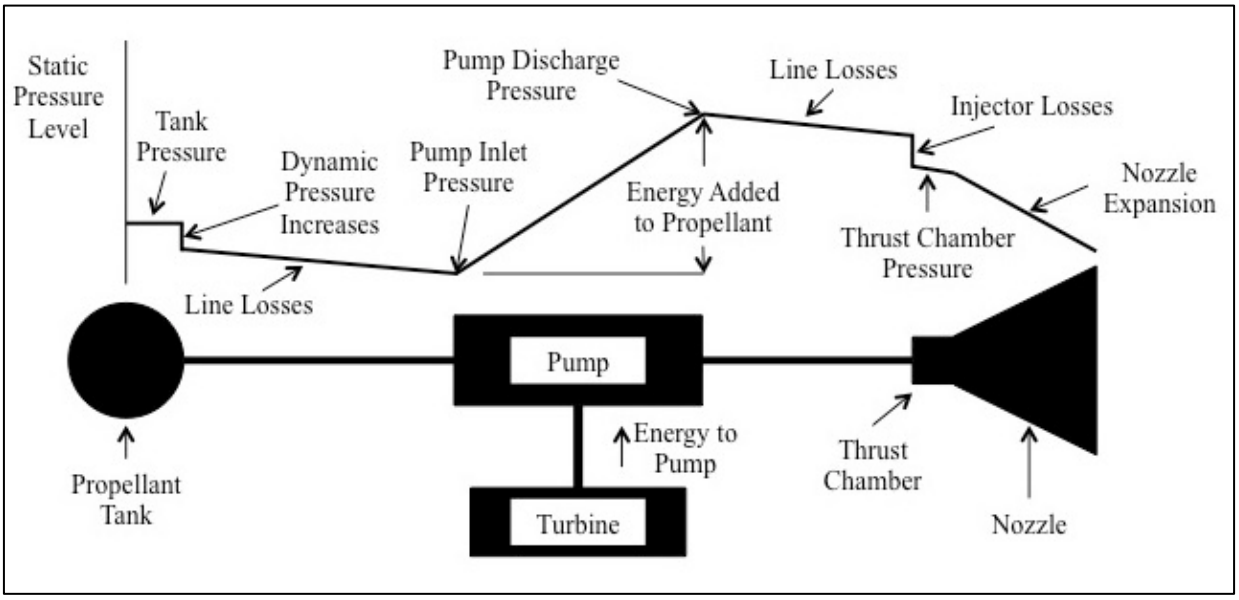

Fig. 6 Pressure Profile (Inspired by Humble, et al.)[1]

The propellant feed system may also include the following components: tank and fill drain valves, on/off valves, control valves, isolation valves, check valves, pressure regulators, filters, transducers, and heaters[1]. Many of these also have pressure drops associated with them – in fact, some function solely to modify the feed pressure. The actual pressure drop for each of these components is determined as the design resolution increases.

B. Turbomachinery

The turbopump is necessary for engines requiring significantly high chamber pressures demanded by thrust needs and significant pressure loss between the propellant tanks and the thrust chamber. Tank pressures for engines with turbopumps are inherently lower, reducing the tank mass and overall system weight[17]. A turbopump, by definition, contains a turbine and a pump. In some cases, the turbopump system may contain more than one pump. The DEAN liquid hydrogen pump requires two stages, mainly because of the low density and the high pressure rise demanded. NASA's monograph *Turbopump Systems for Liquid Rocket Engines* states that the primary design requirement is that the turbopump must "operate within the limits

of the engine system while delivering propellants at the conditions required by the engine thrust chamber"[20]. Turbopumps are extremely complex components both from an engineering perspective and in terms of their functions. An example of the intricacies within the turbopump system is shown in Fig. (7)[20] (government work with no copyright).

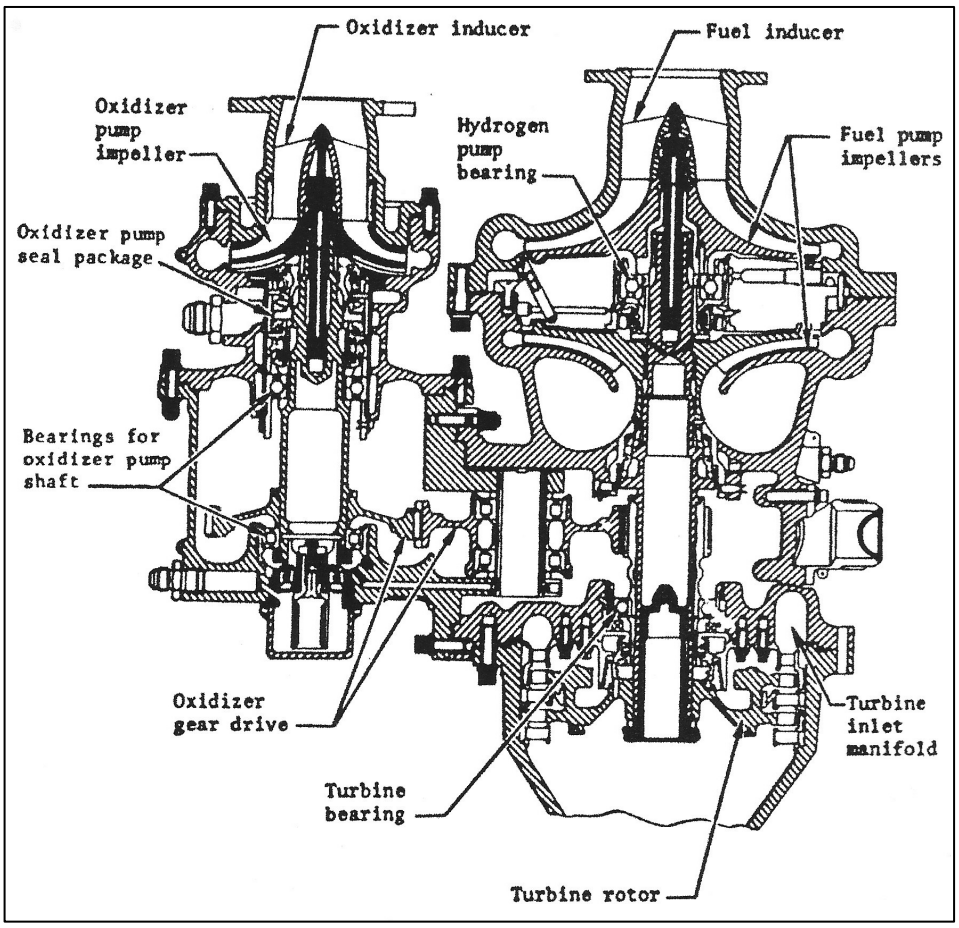

Fig. 7 RL-10A-3-3A Turbopump Assembly[20]

This research incorporated preliminary fuel and oxidizer turbopump designs from Arguello and Strain (both Air Force Institute of Technology). Arguello's research focused on the design of the hydrogen turbopump, which consisted of a turbine and two pump stages – the schematic and solid model of the hydrogen turbopump are shown in Figs. (8) and (9), respectively[21] (government work with permission).

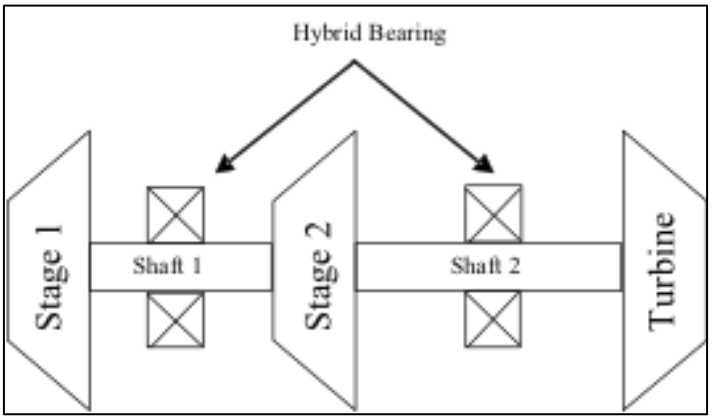

Fig. 8 Hydrogen Turbopump Schematic[21]

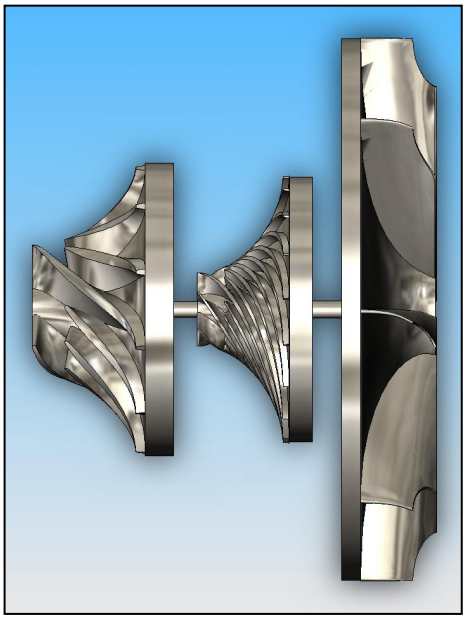

Fig. 9 Hydrogen Turbopump Solid Model[21]

Strain's research focused on the design of the liquid oxygen turbopump, which consisted of a turbine and single stage pump – the schematic and solid model of the oxygen turbopump are shown in Figs. (10) and (11), respectively[22] (government work with permission).

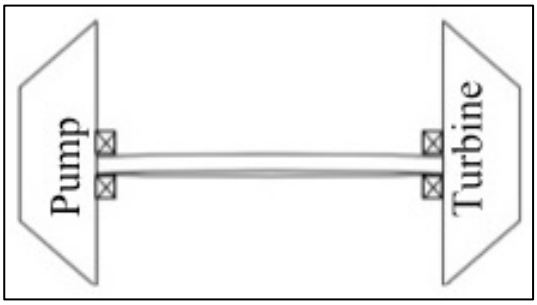

Fig. 10 Oxygen Turbopump Schematic[22]

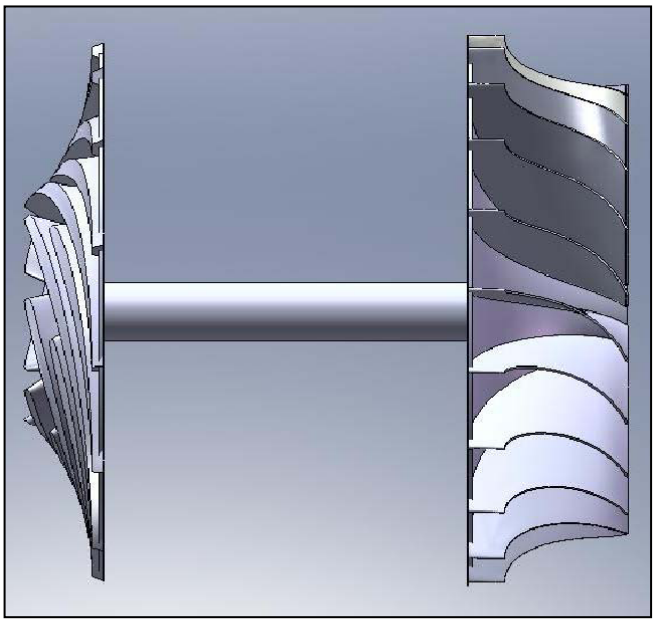

Fig. 11 Oxygen Turbopump Solid Model[22]

These turbopump assemblies are designed with a single shaft connecting the turbine to the pump(s). The other two shaft configurations are geared shaft and dual shaft[20].

The supercritical fluids absorb energy in the cooling jacket and then expand across the turbine providing the needed power for the pump(s). In the case of the DEAN engine, the two separate expansion cycles drive two separate turbines (one for the fuel and one for the oxidizer). At the design point, the power supplied by the turbine matches the power required by the pump.

We can analyze the power balance by equating the relationships defining the pump power required (P_{req}) and the power available from the turbine (right hand side of Eq. (12)).

$$P_{req} = \frac{g_0 \dot{m} H_p}{\eta_p} = \eta_T \dot{m}_T c_p T_i [1 - \left(\frac{1}{p_{T,pr}}\right)^{\frac{\gamma-1}{\gamma}}] \tag{12}$$

Here, $p_{T,pr}$ is the turbine pressure ratio given by Eq. (13).

$$p_{T,pr} = \frac{P_{Ti}}{P_{Td}} \tag{13}$$

Where P_{Ti} is the turbine inlet pressure and P_{Td} is the turbine discharge pressure. The power balance ensures the design process delivers a viable cycle.

Huzel and Huang characterize turbopump system performance by the following three parameters: 1) component weight, 2) required pump-inlet suction pressure head, and 3) turbine gas flow rate[23]. The first parameter is important because, as with all end-state components, the higher the weight for a set performance, the less payload to orbit[23]. The second parameter is necessary to consider because the greater the pump-inlet suction pressure head is, the greater pressure is required by the propellant tank, which then drives up the total weight of the system and drives down the payload weight to orbit[23]. Regarding the third parameter, lower flow rates decrease the engine's overall specific impulse, which then decreases the total payload weight to orbit[23]. This research provides turbopump design results and ensures the systems are within current capabilities for hydrogen and oxygen turbomachinery.

C. Injector

The role of the injector is to insert atomized propellant flow into the combustion chamber, to gauge the mixture of the propellants so the combustion process operates as designed, and to be used as a mechanism for throttling the rocket engine, if needed. This component must remain functioning at the highest level while also operating in the harsh environment of the

thrust chamber. Six major objectives must be completed for any given injector to ensure adequate implementation in the rocket engine: combustion stability, performance, structural integrity, hydraulic qualities, combustion chamber thermal protection, and special requirements[23].

Combustion stability considers how the injector introduces propellant to the thrust chamber, thereby affecting combustion. The injector must ensure smooth combustion while also managing not only how much propellant is in the chamber, but also the timing of injection – adding complexity as rockets may operate at different mixture ratios for different flight phases (i.e. transient start-up, steady-state, throttling, and transient shut-down). Injectors directly influence the combustion stability through the state at which the propellants are introduced (i.e. gaseous, liquid, or both) and the atomization and vaporization processes[23]. Injectors are evaluated on their performance based on how well the injected propellant is distributed, the mixture ratios of that propellant combustion, the rate of heat input, and the chemical reaction rates[23]. In general, better-mixed and evenly distributed propellants will achieve desired performance levels quicker. For liquid rocket propulsion systems, the injector is essentially a combustion chamber wall (usually the top of the chamber), which means that it must be structurally able to withstand the chamber pressures and temperatures throughout the entire engine operating cycle. From a materials perspective, the injector, like the chamber and nozzle walls, must also be cooled in order to prevent structural failure.

Injectors are sized to enable different pressure drops for a range of propellant flow rates, and should be able to atomize the propellants effectively over that range. From a design standpoint, small pressure drops over the injector means reduced turbopump performance requirements. The lower bound, however, is determined based on the engine operating profile

and how much pressure drop is needed for effective propellant atomization[23]. The injector pressure drop (Eq. (14)) is set by the mass flow rate (Eq. (9)) and the design choices for cross sectional area (A), injector type (C_d), and injector configuration.

$$\Delta P_{inj} = \frac{\rho}{2g_0}\left(\frac{V}{C_d}\right)^2 = \frac{1}{2g_0\rho}\left(\frac{\dot{m}}{C_d A}\right)^2 \quad (14)$$

Historical values for ΔP_{inj} are between 15-20% of the chamber-nozzle stagnation pressure[23] for unthrottled injectors, and 30% for throttled injectors[1]. The injector pressure loss for the DEAN is set to a 15% pressure drop, which is similar to other expander cycle upper stages.

Injector designs must take into consideration the location of injection, ensuring that no spots develop on the chamber wall and for maximum mixing. Additional fuel injectors are placed near the walls to reduce the temperature of the gas near the wall. This implementation has a secondary affect in that it also effectively cools the chamber wall, as discussed in the cooing jacket discussion in Section II.4.E. The injector design must operate robustly to off-design conditions such as abnormal propellant mixture ratios and off-design thrust levels[23]. In terms of injector predesign, Huzel & Huang note that, "For a given propellant combination, the chemical reactions and the kinetics of stream breakup, mixing, droplet formation, and heat transfer should be studied and clearly understood, before the approach to the design of an injector is established"[23]. Understanding the physics of combustion and heat transfer will inevitably be more cost- and performance-effective for the engineer.

Injector configurations generally fall into two classes: impinging and non-impinging. The former refers to propellant streams impacting one another at a pre-determined position in the thrust chamber – this method assists in more complete atomization of the propellants. The latter method relies on turbulence and diffusion to achieve mixing, though is not currently in use[17]. Two applications of the impingement techniques are the doublet and triplet. In the doublet

configuration, the oxidizer jet and fuel jet are arranged, and set to impinge, in pairs – this configuration's disadvantage is the formation of an angular momentum angle caused by the unbalanced collision of the streams[23]. The triplet configuration works similarly, but there are three streams where two are symmetrically impinging on the one, removing any angular momentum angle[23].

The pintle injector is an example of an impinging injector and allows for high combustion efficiency, deep throttling, and injector face shutoff[24]. The coaxial injector is another example of an impinging injector where the relatively high-density, low-speed liquid interacts with low-density, high-speed gas and the velocity difference between the two fluids results in a shear action, causing the atomization of the liquid oxygen and then combustion. Figure (12) is an example of a pintle injector and Fig. (13) is an example of a shear coaxial gas/liquid injector, both obtained from Martin[10] (government work with permission).

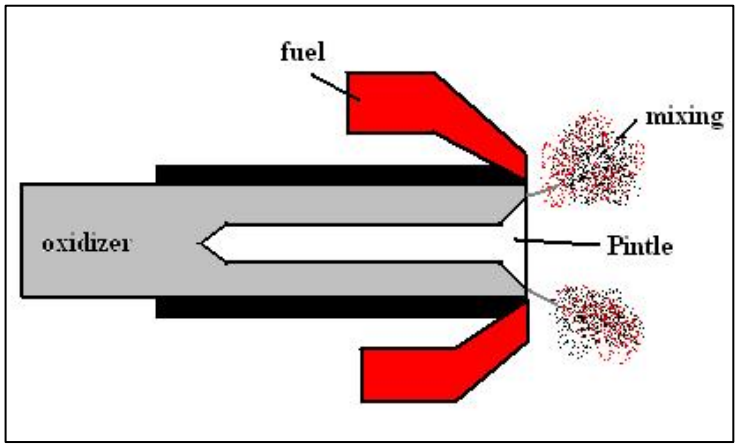

Fig. 12 Pintle Injector Configuration[10]

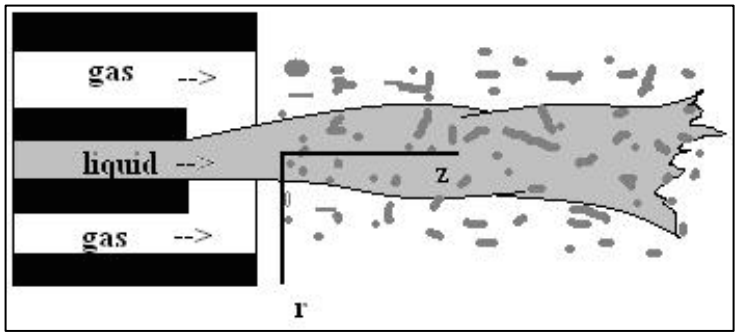

Fig. 13 Shear Coaxial Injector Configuration[10]

The current DEAN configuration is baselined with a pintle injector but could benefit from a coaxial injector as well. The pressure drop across the injector is currently defined for this study. Typical injector assemblies contain dozens to hundreds of injectors[1]. The main advantage of the pintle injectors is its efficiency at delivering propellant quickly to the thrust chamber. Future work will include injector design to increase model fidelity and provide a more accurate representation of the pressure loss in the injector system. Implementation of a gas-gas coaxial injector should also be examined to determine system impact.

D. Combustion Chamber

The most significant performance parameter in the chamber is the mixture ratio. The characteristic velocity characterizes how the mixture ratio is set in the engine through combustion temperature and molecular mass of the products of combustion[25]. In this sense, we can derive characteristic velocity entirely from combustion variables:

$$c^* = \sqrt{\frac{1}{\gamma}\left(\frac{\gamma+1}{2}\right)^{\frac{\gamma+1}{\gamma-1}} \frac{\bar{R}T_0}{\bar{M}}} \tag{15}$$

The typical characteristic length of a combustion chamber is defined to ensure the chamber is long enough to ensure theoretically ideal combustion – the optimal value has a strong relationship with O/F ratios. L^* is defined as a function of specific volume, propellant mass flow rate, and combustion residence time. The relationship may be expressed more simply as

$$L^* = \frac{V_c}{A_t} \tag{16}$$

A larger L^* value implies more complete combustion, but also means that the thrust chamber is longer, which is problematic in regards to minimizing engine weight. A smaller L^* value implies less complete combustion and therefore some of the chemical energy will not be converted to thrust. L^* is also an important value in terms of how much surface area is available for heat exchange. In the case of the DEAN engine, for example, a larger L^* may be required to ensure that enough thermal energy is transferred to the working fluid to run the turbomachinery.

The chamber contraction ratio (also referred to as simply "chamber ratio") is a measure of the volume required for combustion and is a function of the speed and thermochemistry of the reactants. Designing the propellant feed system to deliver the propellants at a low Mach number (0.1-0.6) ensures longer residence time for propellant mixing and combustion to occur. The calculation for chamber ratio is similar to the expansion ratio (Eq. (17)).

$$\frac{A_c}{A_t} = \frac{1}{M}\left[\left(\frac{2}{\gamma+1}\right)\left(1 + \frac{\gamma-1}{2}M^2\right)\right]^{\frac{\gamma+1}{2(\gamma-1)}} \tag{17}$$

Huzel and Huang note that the chamber ratio can be optimized by the following design considerations: 1) combustion performance and the injector design; 2) chamber gas flow pressure drop; 3) chamber wall cooling requirements; 4) combustion stability; 5) weight; 6) space envelope; and 7) ease of manufacturing[23]. This research effort took advantage of available engine information to meet the considerations identified by Huzel and Huang. The chamber ratio has a relationship with existing LOX/LH_2 upper stage engines[23]. This relationship is shown in Eq. (18), below.

$$\frac{A_c}{A_t} = c_{CR}(11.057 - 1.264 * \log(A_t)) \tag{18}$$

The chamber ratio coefficient, c_{CR}, allows for this engine simulation to consider variations of the

engine operation with respect to historical trends. The DEAN surface area is highly sensitive to chamber ratio – this trend will be discussed in-depth in Chapter III.

For most rocket engines, the oxidizer-to-fuel (O/F) ratio is different from the mixture ratio for stoichiometric combustion (the propellant mixture ratio where maximum temperature and heat release occurs)[23]. In general, O/F is selected to maximize specific impulse and minimize total vehicle mass. Rocket propulsion systems burn fuel-rich to minimize component exposure to hot oxidizer (failure mode) and because I_{sp} increases for lower molecular weights. Specific impulse also increases with exhaust temperatures; so maximum I_{sp} is, in many cases, constrained by the thermal properties of the engine and nozzle. Figure 14 presents the theoretical I_{sp} and combustion temperature for a throat area of 25, expansion ratio of 25, and chamber pressure of 1000 [psia].

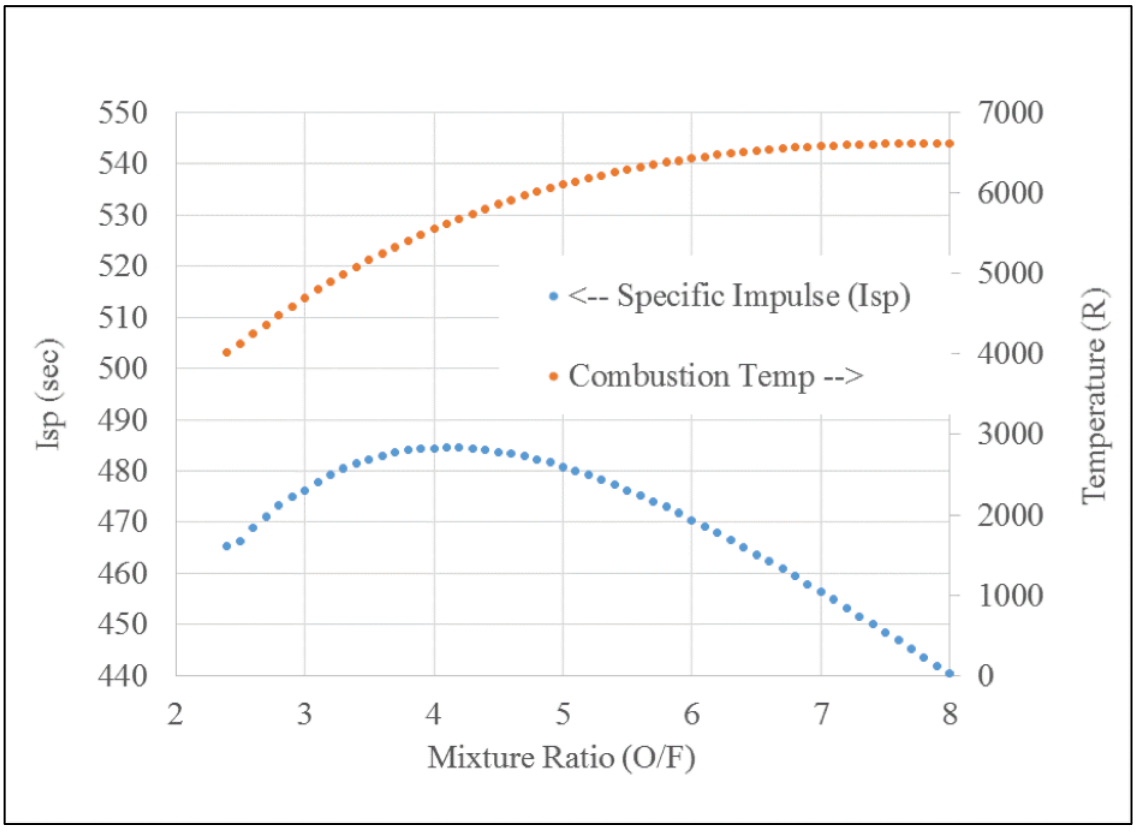

Fig. 14 Theoretical I_{sp} and Combustion Temperature as a Function of Mixture Ratio

The total mass flow rate at the throat area may be determined by manipulating Eq. (1) to give

$$\dot{m} = \frac{Thrust}{I_{sp} * g_0} \tag{19}$$

Given a design O/F, we can then determine the separate oxidizer and fuel mass flow rates, which help to determine the required output from the turbopumps and are also required inputs to manage the engine's power balance. Equations (20) and (21) show the oxidizer and fuel mass flow rates:

$$\dot{m}_{Ox} = \dot{m} * \frac{\frac{O}{F}}{\frac{O}{F}+1} \tag{20}$$

$$\dot{m}_{Fuel} = \frac{\dot{m}}{\frac{O}{F}+1} \tag{21}$$

Liquid oxygen and liquid hydrogen were selected as the oxidizer-fuel mixture for this research. At the point of injection, both propellants are supercritical fluids and behave as a gas-gas injection scheme. The ideal combustion equation for oxygen and hydrogen is shown in Eq. (22):

$$2H_2 + O_2 \rightleftarrows 2H_2O \tag{22}$$

The molecular weights for hydrogen and oxygen are approximately 2 [g/mol] and 32 [g/mol], respectively. From this equation, we see that the oxidizer-fuel mixture ratio for stoichiometric combustion of oxygen and hydrogen is nearly 8:1. While the ideal reaction produces only water, the realized reaction yields up to eight potential products: H, O, OH, H_2, O_2, H_2O, HO_2, and H_2O_2[26]. In the case of liquid oxygen and liquid hydrogen, the optimal O/F is between 3.5 and 4.5 (Fig. 14). The system requirements usually increase the O/F between 5.0 and 6.0 due to low hydrogen density. Operating at lower O/F will increase the size of the hydrogen storage tanks, driving the system mass up and the payload down[1]. Additionally, operating at stoichiometric

conditions would produce the highest temperatures in the combustion chamber and would require more complex materials and cooling schemes to prevent catastrophic failure. Even though the O/F for stoichiometric combustion is about 8.0, operating between 5.0 and 6.0 is still running fuel-rich, though less than the ideal 3.5.

The selection of LOX/LH_2 was made primarily because that mixture provides the highest performance for a chemical rocket system and to serve a means of comparison to past DEAN research and the RL-10 series upper stage engines – which have been highly successful throughout their flight history. There has been some research on a LOX/LCH_4 DEAN engine[27], which will be used for reference in future work when a trade study is completed using different oxidizer-fuel mixture combinations. It is important to note, however, that methane is currently the fuel of choice for NASA's Mars exploration architectures. Table 3 lists the properties of each propellant, including methane, for further discussion.

Table 3 Propellant Properties[23,28]

	Molecular Weight [g/mol]	**Boiling Point [°R]**	**Critical Pressure [psia]**	**Critical Temperature [°R]**	**Density at Boiling Point [lbm/ft^3]**	**Specific Heat [BTU/lbmR]**
Liquid O_2	32.00	162.3	735	277.7	71.23	0.406
Liquid H_2	2.016	36.77	187.8	59.37	4.42	2.336
Liquid CH_4	16.04	200.2	668.6	343.1	26.37	0.831

Liquid hydrogen has a very low density and must be maintained at an extremely low temperature to prevent boil-off. These low operating ranges require higher system mass requirements for propellant tanks, insulation, and cryocooling, as well as increased power draws for those systems. In general, propellants with high specific heat and high boiling and/or decomposition temperatures are ideal for rocket engine cooling. Cryogenic hydrogen works exceptionally well for expansion cycles because of its strong heat absorption capabilities – as can be seen in Table 3 by its relatively high specific heat – as well as the fact that it does not

decompose[17]. Liquid oxygen and liquid methane operate at much more manageable temperature ranges and are significantly denser, which is partly why they were selected for the current Mars architecture – the other part being in-situ propellant production.

E. Cooling Jacket

Propellant combustion and exhaust develops very high temperatures and, therefore, very high heat exchange, to the surrounding walls. Cooling of the thrust chamber and nozzle are necessary in order to control the wall temperatures and ensure that the structure's thermal limits are not exceeded. Common techniques used to cool rocket engines are regenerative cooling, ablative cooling, radiation cooling, and film/boundary layer cooling.

The regenerative cooling technique is implemented by pumping cold propellant (usually fuel) through cooling volumes in the chamber and nozzle walls. The heat from combustion and the exhaust conducts through the walls and is absorbed by the propellant, which then expands across the turbine and transfers its energy to the turbopump system. In this case, the total energy losses are considered negligible because nearly all the thermal energy is used by the working fluid and the subsequent turbine[1,17].

Ablative cooling relies on walls lined with a layer of material (usually silica, quartz, or carbon cloth and resin composites) that vaporizes as the exhaust gases pass over it. The thickness of the ablative material is determined by the burn duration to ensure that enough ablative is available[1].

Radiation cooling relies on the chamber and nozzle walls radiating energy to the surroundings. Radiation cooling requires walls that are designed with high temperature materials and that are thick enough to perform under steady-state chamber pressure without affecting the structural integrity of the liner and wall[1,17].

The final cooling method is film/boundary layer cooling. In this technique, cold liquid propellant (usually fuel) is injected directly onto the chamber walls, creating a film. As the propellant moves down the wall, it cools the wall surface through convection and combusts with the other propellant (usually oxidizer). Once it reaches the throat, the film is nearly completely vaporized[1].

The DEAN engine implements a regenerative cooling method and therefore requires cooling jackets for both the nozzle and the thrust chamber. In this design, the hydrogen cools the nozzle and the oxygen cools the chamber. The implementation of two separate cooling jackets presents two unique design challenges. The first challenge is that the cooling volumes need to be large enough so that the necessary heat exchange can occur, but narrow enough so that the structural integrity of the channel is not compromised and the pressure drop across jacket is not beyond the operational capability of the pump. The hot-side wall (i.e. the wall exposed to the combustion/exhaust) and the cold-side wall (i.e. wall exposed to the working fluid) are both primary structural components that support the inner channel walls against the high chamber pressures. The second design challenge comes with the design of the nozzle. For normal bell-shaped nozzles, the cold-side wall is surrounded by cooler ambient air. The DEAN engine includes an aerospike nozzle, which is completely surrounded by the exhausted combustion products. Figure (15) shows a regenerative cooling diagram for the DEAN thrust chamber[5] (government work with permission).

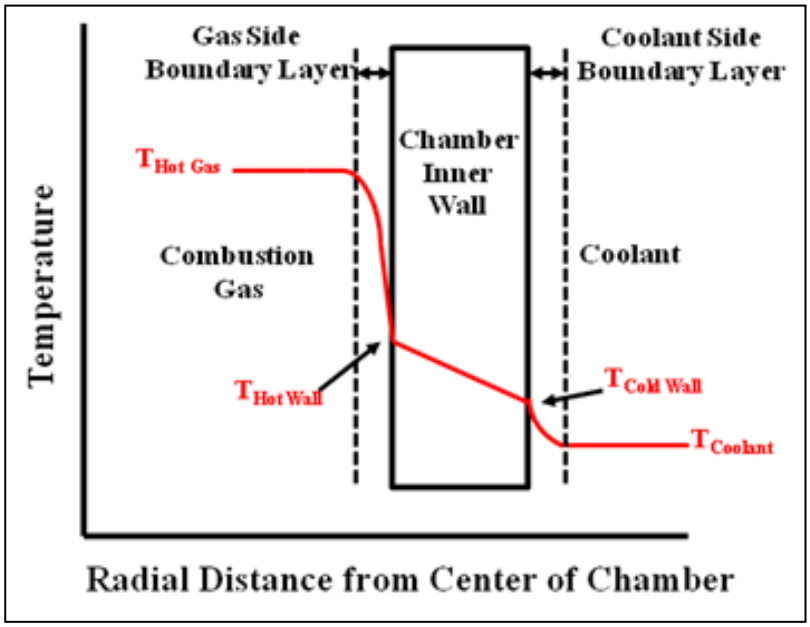

Fig. 15 Thrust Chamber Regenerative Cooling Diagram[5]

The radial temperature distribution shows the hottest temperature at the center of the combustion chamber and the coolest temperature as the coolant temperature in the cooling volumes. For the nozzle side, it is important to note that this trend would be switched (i.e. the temperature would be cooler closest to the center of the nozzle).

There are three types of heat exchange: convection, conduction, and radiation. Convection occurs as fluid passes over a surface and heat is exchanged; there must be a temperature gradient in order for the heat exchange to occur[29]. Inside the thrust chamber, hot gas passes over the chamber wall as it is exhausted through the throat and nozzle. During this process, heat is transferred from the hot gas to the cooler wall. On the fluid side of the chamber wall, the coolant (liquid oxygen in the case of the DEAN) passes over the surface and absorbs the heat from the wall in the same fashion. Conduction occurs as heat is transferred through a medium under the influence of a temperature gradient; this occurs primarily in solids[29]. In the case of the regenerative cooling cycle, heat is conducted through the inner chamber wall, as shown in Fig. (15). Finally, radiation is the emission of thermal energy from the hot gases to the

inner walls and from hot hardware to the surroundings; radiation may contribute between 3 and 40% of the heat transfer to the chamber and nozzle walls[17].

The DEAN's dual expander cycle can be described using three heat transfer sections, in the following order: 1) convection and radiation from the hot gas to the cooler chamber inner wall; 2) conduction within the chamber inner wall; and 3) convection from the hot wall to the cooler liquid oxygen. This same process occurs for the aerospike cooling jacket, except hydrogen is the working fluid. We can complete a first-order heat transfer analysis by applying the first law of thermodynamics (energy conservation equation)[1].

$$\dot{Q}_{in} = \dot{Q}_{out} + \Delta h \tag{23}$$

Here, $\dot{Q}$ is the heat flow in or out of the control volume, and Δh represents any change in enthalpy within the control volume. For our analysis, we model the process as one-dimensional heat exchange, which effectively negates the conduction section and assumes that the temperature on the hot-side is the same as the temperature on the cold-side. For the regenerative cycle, Humble, Henry and Larson show the energy conservation equation becomes[1]

$$(\dot{Q}_{rad} + \dot{Q}_{con})_{in} = (\dot{Q}_{rad})_{out} + \dot{m}_{coolant} c_p (T_{out} - T_{in}) \tag{24}$$

Here, the heat flow subscripts are for heat addition due to radiation and heat addition due to convection, $\dot{m}_{coolant}$ is the mass flow rate of the coolant, c_p is the heat capacity of the fluid, and T is the temperature of the fluid entering or leaving the cooling volume. Both the oxidizer and fuel are in a supercritical state through the regenerative cooling process.

Heat exchange from the chamber/nozzle to the cooling channels serves two purposes: to cool the chamber/nozzle surfaces, and to provide enough heat to the working fluid to run the turbomachinery. This study found a need to increase the heat exchanged over a surface area. The most effective ways are to elongate the thrust chamber, roughen the cold-side walls in the

cooling volumes, or widen the cooling channels. The first option increases the engine mass and the second option has tradeoffs between higher heat transfer rate and higher pressure losses. For these reasons, we will further examine the cooling channel width as a means of providing more surface area for the heat exchange to occur over.

Rectangular cooling channels are geometrically described by their aspect ratio (AR) – the channel's height divided by the channel's width. The AR serves as a method to describe the surface area for heat transfer. Previous research has shown one method to reduce hot-side wall temperature is to implement an increased number of cooling channels with high aspect ratio (greater than 5.0)[30]. Examples of low AR and high AR are depicted in Fig. (16)[5] (government work with permission).

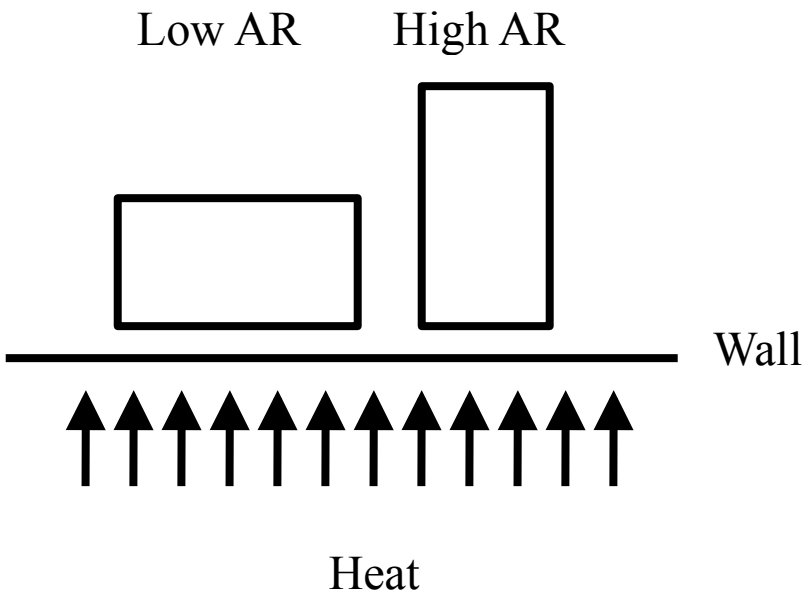

Fig. 16 Channel Aspect Ratio Comparison[5]

The cooling channel geometry changes with the thrust chamber and nozzle cross-sectional area. Each channel runs approximately the same length down the chamber or nozzle. With knowledge of the number of channels and chamber and nozzle geometry, this assumption allows us to determine the total heat transfer surface area.

The DEAN cooling channels are modeled as rectangular channels, as shown in Fig. (17)[5] (government work with permission).

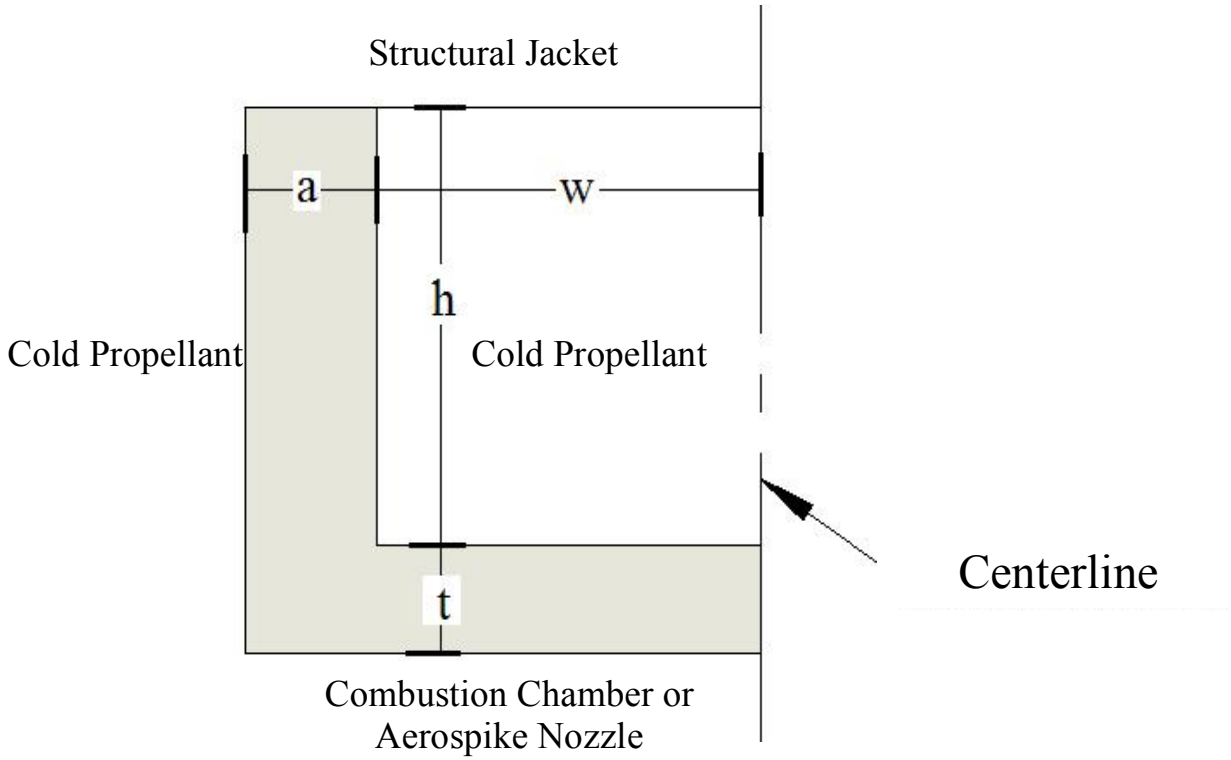

Fig. 17 Cooling Channel Cross-Sectional Geometry[5]

The length parameters are defined as follows: *a* is the half-spacing between channels, *w* is the half-width of a single channel, *t* is the wall thickness between the channel and combustion chamber, and *h* is the channel height. Computationally, *a* and *w* are set by the user inputs (lower bound dictated by manufacturing limits), then the number of channels is determined by the chamber circumference.

The maximum velocity within the cooling volumes was controlled such that it remained at just a fraction of the speed of sound to ensure that the fluid velocity, pressure drop, and channel geometry are constrained within physical limits. Subsequently, results suggested that increasing the fluid velocity is needed to ensure sufficient heat transfer rates can be met. For regenerative cooling systems, the pressure drop in the cooling jacket varies on average between

10-20% of the chamber pressure[1]. The modified DEAN computational model used in this research incorporates a more accurate representation of the physics involved in fluid flow.

In general, it is necessary to model the heat transfer resulting from combustion in order to determine the appropriate materials to use for the chamber and nozzle walls, cooling channel geometry, and working fluid, as well as any requisite support structure materials that must be implemented. Effective cooling techniques result in a broader trade space for materials because more efficient cooling means more materials may be considered for application. This effectively drives down the cost to manufacture these components and allows a broader range of design for the engineer.

Rocket engine material selection must be optimized based on location, function, and mass of any potential material in the trade space. For example, certain propellants are corrosive under their operating conditions and selecting the wrong material to house them could result in a failure mode. Material selection should consider material corrosiveness, strength, thermal conductivity, melting point, reusability, and manufacturability. Hall determined a set of possible material choices and showed their compatibility with both LOX and LH_2[5]. Hall's research concluded that the aerospike structure jacket, aerospike cooling jacket, and aerospike tip should all be made from oxygen-free copper, while the chamber cooling jacket should be made from silicon carbide, and the chamber structure jacket should be made from aluminum 7075-T6[5]. Simmons's research suggested that all the elements should be made from silicon carbide[2]. The earlier studies for the DEAN were significantly limited and did not include the physical limits and relationships included in this model.

The current one-dimensional heat exchange approximation provides adequate information to a point, but does not incorporate the material properties of the chamber and

nozzle. This is particularly an issue when it comes to determining the mass of the propulsion system and is addressed in Chapter V.

II.5 Dual Expander Aerospike Nozzle

The DEAN is an altitude-compensating engine that allows the flow to expand with changes in ambient pressure, thus providing optimal performance at all points up to the design altitude (pressure). The aerospike itself may take the form of a full or truncated spike, and acts as a plug nozzle[31]. The engine incorporates two unique design features that allow it to be throttled: 1) the plug may be controlled axially, and 2) the mixture ratio may be modified by valves – including the bypass and injector – within the separate fuel and oxidizer expansion cycles.

Standard bell and conical rocket nozzle contours are designed and optimized for particular regions within the flight envelope. The term "flight envelope" is used as a reference to a performance parameter at a given altitude, namely exhaust expansion. Flow expansion is considered in three phases: overexpanded flow, underexpanded flow, and fully developed flow. In the case of overexpanded flow, the ambient pressure is greater than the combustion exhaust pressure, therefore causing flow separation within the nozzle (for bell and conical nozzles). The early separation causes some of the nozzle to be unused, and therefore wastes mass – it is for this reason that nozzles are designed to fully expand, or slightly underexpand, at sea level conditions[17]. In addition to decreased performance, the risk of structural failure exists as a result of uneven overexpanding flow. For underexpanded flow, the exhaust pressure is greater than the ambient pressure, so flow separation occurs at the nozzle exit. In this case, the performance is still reduced, but the structural failure modes are lessened. In any case, rocket nozzles are generally operating in either over- or underexpanded conditions, so the optimal nozzle is the one

that maintains near-fully developed flow for the longest duration. The aerospike nozzle is designed to ideally expand from ignition up to the design altitude, so it is considered fully altitude compensating within those ranges. Beyond the design altitude, the aerospike operates similarly to the bell nozzle and suffers some loss from underexpansion[31].

The DEAN's altitude compensation abilities will be more beneficial for ascent and retropropulsion. The ultimate goal of this research is to apply the success of the DEAN to a booster-class launch engine. The distinguishing characteristic between the DEAN and other upper stage nozzles comes from its mass savings. Considering the significant contribution nozzles make to the overall mass, it is necessary to optimize this component. Comparing between standard nozzle designs (bell and conical) and the aerospike nozzle, we see that the major mass savings comes through minimizing the nozzle surface area. Truncating the nozzle enables higher mass savings. Previous research suggests 20% nozzle truncation reduces thrust performance by less than 1%[32]. The truncated aerospike nozzle flow field is shown, with the flow regions identified, in Fig. (18):

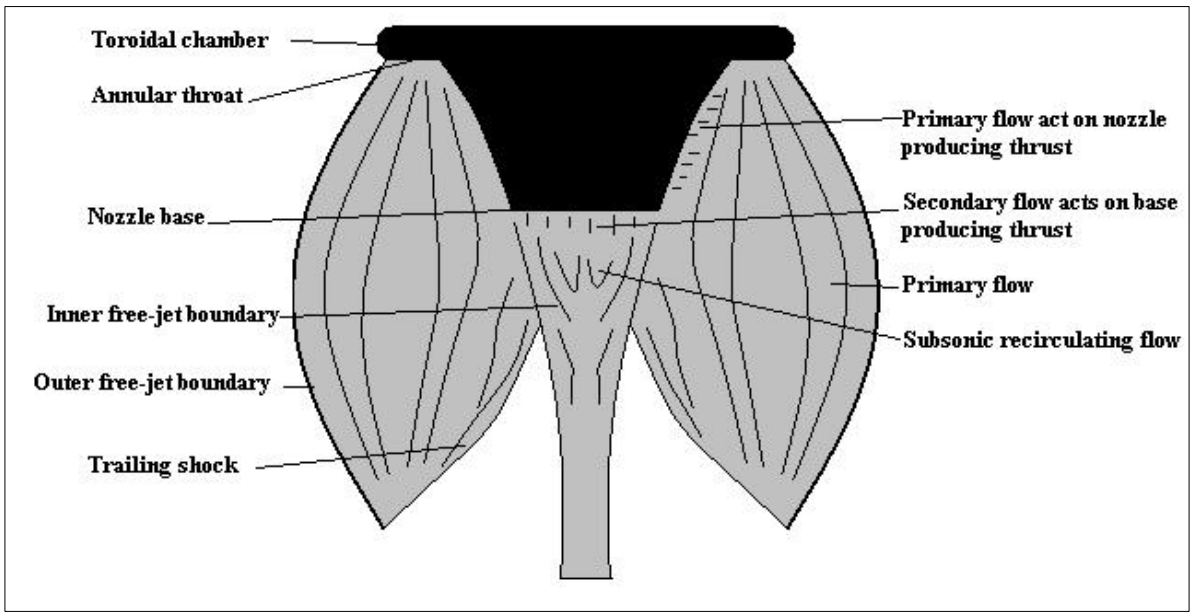

Fig. 18 Truncated Aerospike Nozzle (Inspired by Hill & Peterson)[25]

To reduce recirculating flow into the truncated area, a secondary flow path (approximately 1% of the primary fuel flow) may be needed at the truncated surface, effectively elongating the nozzle and axially directing combustion flow (Fig. (18)). Since the fuel cooling cycle is within the nozzle, there exists no risk for backflow combustion, as the exhausted propellant is already fuel-rich. The performance losses due to this technique would be accounted for in nozzle and propellant efficiency factors.

The nozzle contour for a particular engine must prevent shock waves from occurring within the nozzle while the flow is expanding to ideal or underexpanded flow. As Anderson writes, "The method of characteristics provides a technique for properly designing the contour of a supersonic nozzle for shock free, isentropic flow, taking into account the multidimensional flow inside the duct"[33]. Past research has applied Software and Engineering Associates' Two-Dimensional Kinetics (TDK) software to complete method of characteristics analysis to calculate the nozzle geometry[2,5,10].

II.6 Previous DEAN Research

Researchers at the Air Force Institute of Technology at Wright-Patterson Air Force Base, Ohio have been working on computationally modeling and optimizing the dual-expander aerospike nozzle since 2008 under the Department of Defense Integrated High Payoff Rocket Propulsion Technology program. There have been four primary investigators during this time: David Martin, Joseph Simmons, Joshua Hall, and Michael Moen. The work completed by these gentlemen is discussed below. This research expands their work and incorporates more accurate combustion and heat exchange physics, as well as a more dynamic computational model.

A. David F. Martin, AFIT

Martin's thesis work[10] consisted of three major objectives: 1) to determine the feasibility of the DEAN engine as an orbit transfer vehicle; 2) to implement a design process focused on energy conversion from the combustion chamber and nozzle via a dual-expander cycle; and 3) to perform detailed analysis of the cooling jackets and cooling volume components. To accomplish this work, Martin used two computational modeling programs: TDK, and Numerical Propulsion System Simulation (NPSS) by NASA. TDK was used to design the nozzle and NPSS was used to model the full engine cycle and performance. This effort culminated in the computational design of a LOX/LH_2 DEAN engine with a thrust of 57,231 [lbf] (7,231 above the design point) and I_{sp} of 472 [s] (8 above the design point).

B. Joseph R. Simmons, AFIT

Simmons's dissertation research[2] centered around developing a method to parametrically model the DEAN using NPSS and optimizing that model using Phoenix Integration's ModelCenter. Simmons used SpaceWorks Engineering's REDTOP to analyze ideal performance and real-world performance using estimated efficiencies. Simmons also developed an optimization process to take mission specific requirements and output a Pareto set of possible designs, with the trade space being defined by specific impulse and T/W. Simmons modeled three cases to validate his research: the parametric DEAN, the RL-10 performance-level DEAN, and the X-37 performance DEAN. In the case of the RL-10 performance-level DEAN, Simmons's LOX/LH_2 DEAN engine matched the RL-10's specific impulse of 465 [s] while also achieving T/W of over 135 (compared to the RL-10B-2's 37).

C. Joshua N. Hall, AFIT

Hall's thesis research[5] focused on the following objectives: 1) design a tool to optimize the weight of the DEAN engine and its components; 2) design a tool to evaluate the entire solution space; and 3) improve the design points of the DEAN engine. This research incorporated four modeling and optimization programs: NPSS, TDK, ModelCenter, and Chemical Equilibrium with Applications (CEA) by NASA. Hall identified key areas of improvement to increase the fidelity of the model, including improving the combustion physics within the model and enhanced modeling of the engine's geometry (particularly the combustion chamber). Hall's LOX/LH_2 DEAN engine achieved a thrust of 50,161 [lbf] (161 above the design point), I_{sp} of 430.6 [s] (33.4 below the design point), and T/W of 142.2 (35.7 above the design point).

D. Michael D. Moen, AFIT

Moen's thesis research[27] expanded the previous DEAN design and optimization methods to use methane as the fuel, instead of hydrogen. Moen's work resulted in a thrust of 25,000 [lbf] (at the design point), I_{sp} of 349 [s] (34 below the design point), and T/W of 120 (12 above the design point). Moen's research looked at optimizing T/W over I_{sp}, since both could not be met simultaneously – which accounts for the lower target I_{sp}. Although Moen's research implemented a different working fluid on the fuel side, his program modifications and techniques helped to form a more accurate solving method.

III. METHODOLOGY

Chapter III discusses the methodology applied in the computational design of a DEAN rocket engine and nozzle with the design performance goals of 30,000 [lbf] thrust, 465.5 [s] of specific impulse, and an oxidizer-to-fuel ratio of 5.88. This research was completed using Numerical Propulsion System Simulation (NPSS) and Chemical Equilibrium with Applications (CEA), both developed by NASA.

III.1 Numerical Propulsion System Simulation (NPSS)

The following section provides a top-level description of NPSS and describes how NPSS may be implemented to model rockets and, particularly, the DEAN upper stage rocket engine.

A. NPSS Overview

Numerical Propulsion System Simulation (NPSS) was developed in 1995 by researchers at NASA Glenn Research Center in Cleveland, OH. NPSS is a "full propulsion system simulation tool used by aerospace engineers to predict and analyze the aerothermodynamic behavior of commercial jet aircraft, military applications, and space transportation"[34]. The goal of NPSS is to enable engineers to accurately model, analyze, and optimize aerospace systems without the inherent time and monetary costs that come with the manufacturing and testing of those systems. NPSS may be implemented for both steady-state and transient operating conditions, which makes it ideal in terms of implementation at the system engineer level.

NPSS is a C++-derived, object-oriented simulation environment, and is primarily a flow-network solver[35]. NPSS is therefore able to determine solutions to fundamental power balance

problems, such as with the DEAN's hydrogen and oxygen turbopumps or with the pressure profile over the entire fluid flow path. NPSS defines the simulation environment by the particular thermodynamic gas packages for equations of state (described in Section III.3.B), component elements (described in the next sub-section), linkages between elements, and inputs and outputs for each element. NPSS tracks the flow of data between elements through the use of input and output ports, which are defined based on the information being communicated[35].

The NPSS solver runs the user-defined model to obtain a valid solution for a model operating under the desired end-state conditions, which generally involves particular performance parameters (e.g. thrust, specific impulse, mixture ratios, and volume/weight constraints). The solver "is responsible for iteratively adjusting the values of the model independent variables in order to satisfy the dependent conditions in the system"[35]. The solver essentially exists to balance the mass and energy properties within the system – this includes balancing the fluid flows and mechanical properties. The solver also operates in parallel with transient simulations and provides valid solutions at each discrete point in time. Each element has a set of predefined independent variables and dependent conditions, though user-defined independents and dependents may be added as well. Solvers may also be nested within assemblies of elements such that each assembly may go through its own separate solver sequence before control is returned to the parent solver[35]. In the case of the DEAN NPSS model, the solver iterates until the fluid equations of state match the output geometry. Because the two are so closely related, the model runs through once with initial user-input values and iterates to a converged solution, then sets that solution as the initial input for the second run, thereby ensuring that the interrelationships between the fluid and geometrical properties are accurately modeled.

NPSS utilizes a variety of thermodynamics packages to complete calculations relating to

fluid properties. The available packages include NASA's chemical equilibrium code, the National Institute of Standards and Technology (NIST) gas properties, and Pratt & Whitney's package that implements some humidity and chemical equilibrium capacities. NPSS also allows for user input tables and functions that describe the thermodynamic properties of the fluid more in-depth. This capability is discussed further in Section III.3.B.

B. NPSS Elements

NPSS uses built-in elements to model various engine and nozzle components. Users may customize these elements to fit their particular needs. Elements may contain tables and functions, which operate as subroutines within the element. NPSS was initially created to model air-breathing engines. Many of those initial elements, thermodynamic packages, and flow station capabilities are not valid for use with rocket engines[36]. For this reason, the NPSS Rockets Supplement was created. The applicable NPSS reference sheet for each element used in this research may be found in the NPSS User's Guide and Rocket Supplement documents[35,36]. The following elements are implemented in the DEAN simulation:

1) Starter – The starter element is used to model the propellant tanks and to initiate the fluid flow. The inputs for this element are flow composition, total pressure, and total temperature.

2) Wall2 – The Wall2 element is used to model the heat transfer from the combustion chamber to the fluid flow in the cooling channels. The inputs for this element are thermal conductivity and temperature. This element has one independent variable (material temperature) that the solver varies until the dependent condition (heat flow) is balanced.

3) Valve04 – The Valve04 element is used to model valves and flow channels. This element models a simple flow volume and determines the flow through a valve using the

pressure drop, K-factor, and area. The inputs for this element are K-factor, area, and discharge coefficient, making this element ideal for determining pressure drops in the cooling channels.

4) CoolingVolume02 – The CoolingVolume02 element is a customized variant of the CoolingVolume element described in the NPSS Rockets Supplement. Martin modified the original NPSS element to include a reference value 100 [BTU/lbm] in the total enthalpy calculations[10]. CoolingVolume02 may be used to model either general plumbing or cooling channel volumes. This element completes mass and energy storage calculations and is capable of completing heat transfer applications. The inputs for this element are cross-sectional area, number of channels, and total density. This element has two independent variables (total pressure and total specific enthalpy) and two dependent variables (mass and energy storage). The solver uses the mass and energy derivatives produced by this element to balance the conditions at each of these volume locations. For steady-state conditions, the solver varies the independent variables until the derivatives are zero. This element uses UnReactedFluidPorts to model the weight flow between elements (all CoolingVolume02 elements) and ThermalOutputPorts to model heat exchange (only cooling jacket elements).

5) Pump02 – The Pump02 element is a customized variant of the Pump01 element described in the NPSS Rocket Supplement. Pump02 is modified to provide the needed performance of each of the fuel and oxidizer pumps. Martin modified the original NPSS element to allow the pump design to be an output rather than an input[10]. This element has one independent variable (weight flow) that the solver varies until the dependent variable (pressure ratio) matches the desired exit conditions. The inputs for this element are gear

ratio, weight flow, efficiency, and design pressure ratio. This element uses UnReactedFluidPorts to model the weight flow between elements.

6) Turb03 – The Turb03 element is a customized variant of the Turb02 element described in the NPSS Rocket Supplement. Turb03 is used to model the performance of each of the fuel and oxidizer turbines. The inputs for this element include weight flow and efficiency. This element uses UnReactedFluidPorts to model the weight flow between elements.

7) CavVenturi – The CavVenturi element is used to model cavitating fluid flow through a volume. The inputs for this element are flow area and K-factor. This element uses UnReactedFluidPorts to model the weight flow between elements.

8) Shaft – The Shaft element is a standard NPSS element that models the mechanical connections between the turbine (Turb03) and pump (Pump02) elements. The Shaft manages the power balance between all components that are connected to it and ensures that enough power is provided to operate the associated cycle – dual expander cycle, in the case of the DEAN. The input for this element is mechanical speed. The Shaft element has one independent variable (mechanical speed), which it varies to balance the dependent variable (net torque) to zero.

9) RocketNozzle02 – The RocketNozzle02 element is a customized variant of the RocketNozzle element described in the NPSS Rocket Supplement. RocketNozzle02 is used to model the rocket nozzle – aerospike nozzle, in the case of the DEAN – and calculates the nozzle performance parameters, such as specific impulse, thrust, and weight flow. For these calculations, it is assumed that the flow is always choked and that the isentropic parameter, gamma, is constant for the nozzle conditions. The inputs for this element include expansion ratio, throat area, ambient pressure, nozzle loss coefficients, and

heat transfer rates.

10) RocketComb1 – The RocketComb1 element is used to model the thrust chamber by combining and combusting the oxidizer and fuel flows. This element determines the heat transfer coefficient for the chamber and nozzle wall and cooling jacket. The Bartz and Colburn equations, as well as the fluid property table (FPT) thermodynamic package, are used to complete the heat transfer calculations. The user inputs for this element are propellant type, chamber radius (constant section), chamber volume, O/F ratio, weight flow through the chamber, initial chamber temperature, and initial chamber pressure. This element has three independent variables (chamber total pressure, chamber total temperature, and chamber O/F), which the solver varies until the exit conditions are met. For steady-state conditions, the exit conditions are as follows: 1) the weight flow at the nozzle is equal to the weight flow at the injector (balance of mass storage); 2) the time derivative of the temperature equals zero (balance of energy); and 3) the time derivative of O/F is equal to zero (balance of the composition). This element uses UnReactedFluidPorts to model the weight flow between elements.

C. DEAN NPSS Model

NPSS was used to model and evaluate the DEAN architecture both for performance and for engine feasibility. The major research objectives are split into two components: performance objectives and size objectives. The performance objectives include thrust of 30,000 [lbf], specific impulse of at least 465.5 [s], and an oxidizer-to-fuel ratio of 5.88. The size envelope objectives include maximum diameter of less than 60 [in] and maximum length of less than 90 [in]. The performance and size objectives were established as a baseline of comparison for the DEAN and RL-10B-2 engines. The only difference in the performance parameters is that the

DEAN is being designed for a thrust of approximately 5,000 [lbf] more than the RL-10B-2. The size envelope constraints are consistent for the upper-stage engine class. For the upper stage DEAN engine, the major performance advantages over the RL-10 series lies in its thrust-to-weight; the altitude compensation ability does not play a major role because it is operating primarily beyond the design point (highly underexpanded flow), where the exhaust flow behavior is similar to the bell nozzle design. Engine viability was also determined based on maximum wall temperatures in the combustion chamber and nozzle of less than 1800 [°R] – the limit set by material properties for oxide free copper. The DEAN NPSS LOX expander cycle schematic is shown in Fig. (19) – the LH_2 expander cycle has the same components and order.

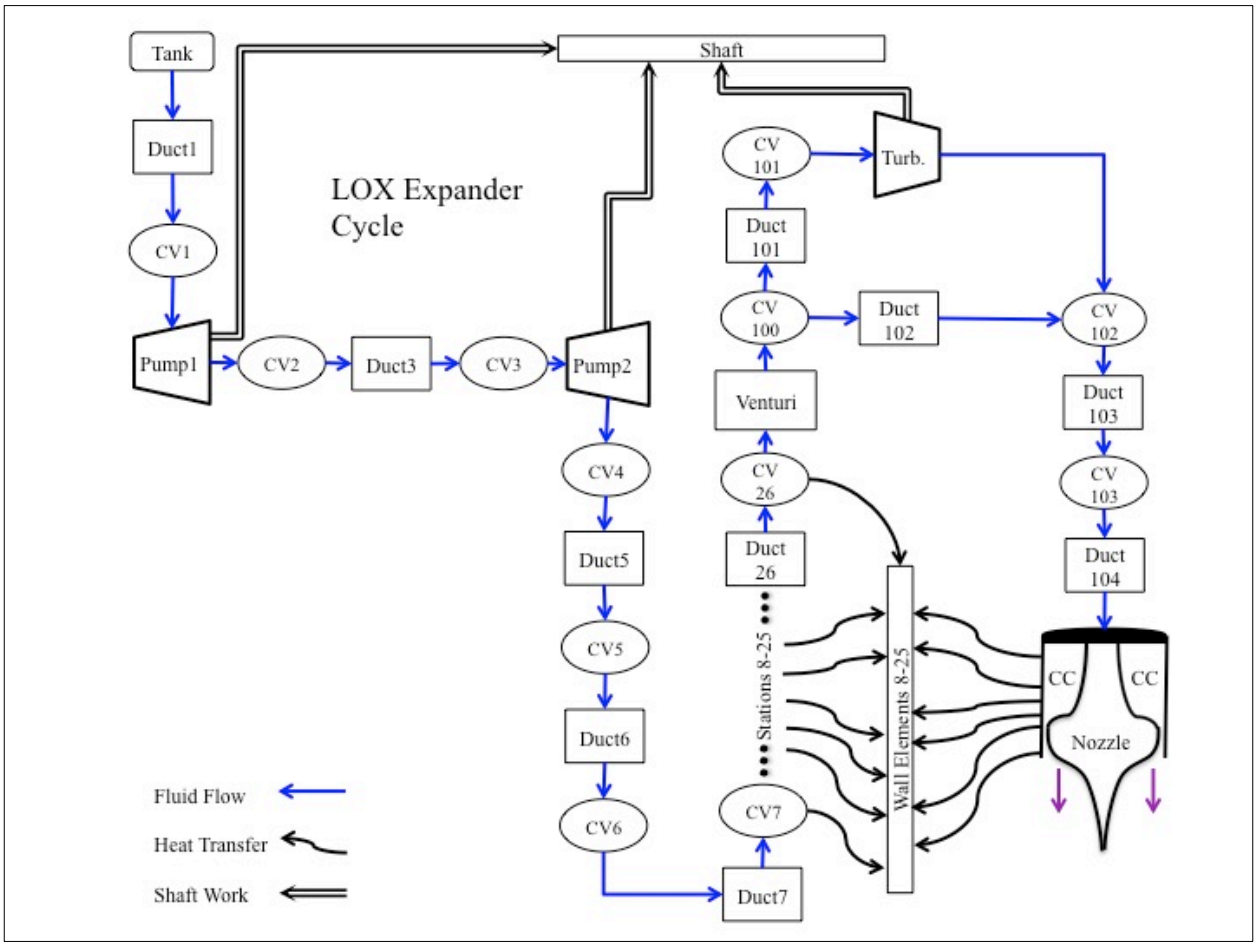

Fig. 19 DEAN NPSS LOX Expander Cycle Schematic

Alternating ducts and cooling volumes (CV) were implemented to capture static conditions and pressure losses throughout the propellant feed system. A cavitating venturi is used as a flow control and to prevent pressure disturbances from propagating from the combustion region up to the turbomachinery. The turbopump pressure ratios are outputs for this model whereas in past models, these have been inputs. Implementing the pressure ratios as independent variables that the solver sequence iterates provides further validation for converged solutions, particularly when they match measured data, as with the RL-10 validation study.

The current DEAN NPSS model maintains the same general structure as Hall and Simmons's models in terms of data files, but differs significantly in terms of geometrical inputs, fluid properties, and RL-10A-3-3A heat exchange methodology validation. The major geometric modifications are in regards to the chamber and nozzle contours – Hall and Simmons implemented linear representations for the contours whereas the current DEAN model uses curved representations. This model also uses a more accurate fluid property table to evaluate the working fluid equations of state as well as the state properties of the combustion products. Finally, the current DEAN model uses K-factor scaling that has been validated by the NPSS RL-10A-3-3A model using the same design methodology.

III.2 DEAN Engine Geometry

The DEAN engine geometry is divided into three segments – thrust chamber, engine throat, and nozzle – and three surface contours – outer chamber surface, inner chamber surface, and nozzle surface. The segment geometry is described using basic rocket engine geometrical equations described by Humble[1]. The surface contours are based on the RL-10, using the DEAN's geometry to scale the contour (i.e. throat radius, chamber radius).

A. Segment Geometry

The DEAN outer throat radius is a function of the expansion ratio and throat area. This radius is determined for the design altitude, at the condition in which the flow is fully expanded.

$$r_{t,o} = \sqrt{\frac{\varepsilon * A_t}{\pi}} \tag{25}$$

The inner throat is a function of the outer throat radius and the throat area.

$$r_{t,i} = \sqrt{{r_{t,o}}^2 - \frac{A_t}{\pi}} \tag{26}$$

The geometry of the DEAN allows for a fairly wide range of expansion ratios and throat areas without changing the throat gap ($r_{t,o} - r_{t,i}$) significantly. The throat gap is constrained by a manufacturing limitation of no less than 0.1 [in].

The outer chamber radius is set to equal the outer throat radius and is modeled as constant for the length of the nozzle. In reality, the chamber outer radius would converge (this portion is called the "lip") immediately after the throat to direct the exhaust flow towards the nozzle surface, which then ideally expands the flow for the design altitude. NPSS only requires surface contours to calculate flow areas, flow rates, and K-factors, which are used in thermal ports and NPSS elements to evaluate pressure drops and engine performance. The chamber lip does not contribute to the determination of the required performance parameters, so it was not necessary.

For the initial approximation, the inner chamber radius is calculated from Eq. (27).

$$r_{c,i} = \sqrt{{r_{c,o}}^2 - \left(\frac{A_c}{A_t}\right) * \frac{A_t}{\pi}} \tag{27}$$

Here, $\frac{A_c}{A_t}$ is the chamber ratio (i.e. ratio of the chamber area to the throat area). The actual inner chamber radius at any point along the length of the chamber is determined by the inner chamber surface contour, discussed in Section III.2.B. Hall's cross-sectional lateral schematic of the

DEAN engine (Fig. (20), government work with permission) shows the general geometry (the real contours are smooth curved, not linear), the heat exchange subsystems, and the nozzle manufacturing features (the length of the fuel cooling channels into the nozzle are user-determined, as is the nozzle truncation location).

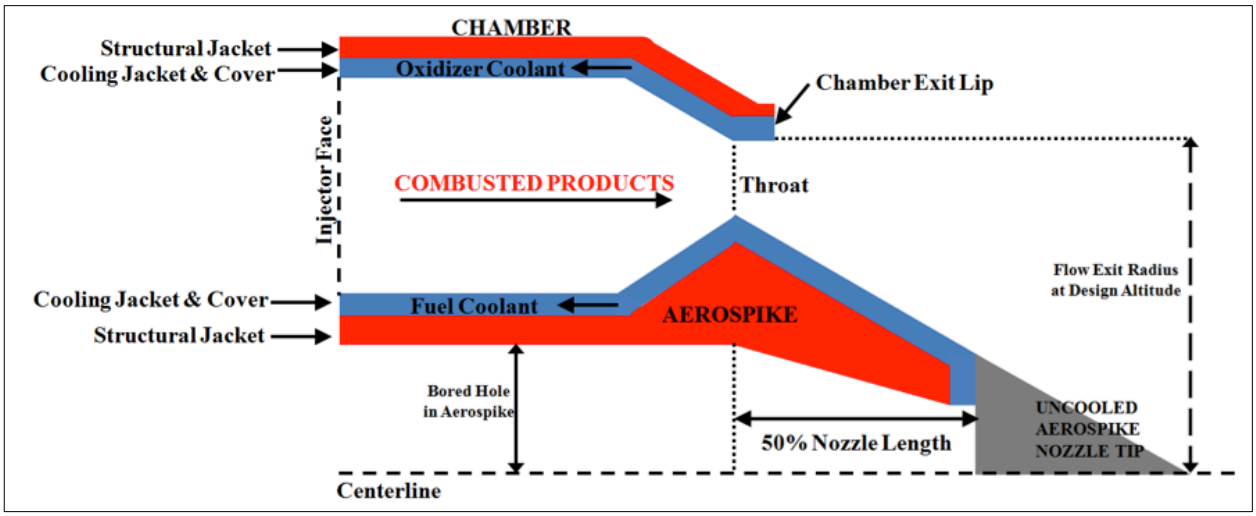

Fig. 20 DEAN Engine Cross-Sectional Schematic[5]

The major considerations regarding the oxidizer and fuel cooling jackets involve the amount of heat transfer and the pressure drop that occurs over those lengths. Noting the square-cube law discussed in Section II.2, there is a fine balance between the amount of heat transfer necessary to run the expander cycles and the amount of pressure drop obtained by the increased surface area for that same heat transfer.

Knowing the values for throat area and characteristic length, both of which are user inputs, the approximate chamber volume may be determined using Eq. (16) – this is the chamber volume necessary for maximized propellant combustion. As discussed in Chapter II, L^* is a combustion performance parameter and is defined empirically for different O/F mixtures to ensure complete combustion (at least to the ideal combustion that the mixture allows). We therefore want to minimize L^* so we can have only the minimum required volume for complete

combustion and the smallest engine possible. In the case of the DEAN engine, where heat exchange is necessary to operate the dual-expander cycle, we must also ensure that L^* is large enough (implies greater surface area) so that adequate heat transfer may occur. These competing constraints suggest an optimal L^* – no excess weight, thereby providing more payload to orbit. For standard cylindrical thrust chambers, the chamber length may be calculated as

$$L_c = \frac{4*V_c}{\pi*{D_c}^2} \tag{28}$$

The DEAN thrust chamber has a varying inner chamber radius and a constant outer chamber radius. The chamber length must be determined to ensure that the volume meets the needs of the desired combustion. This was resolved in NPSS by establishing an iterative scheme that approximates the difference between the theoretical chamber length and the actual chamber length, and then adjusts the volume accordingly.

The nozzle length is determined by approximating the nozzle to be conical. The length is then a function of the cone half-angle, α, given as

$$L_n = \frac{r_{t,i}}{\tan(\alpha)} \tag{29}$$

The aerospike nozzle contour is then modeled after the RL-10 bell nozzle. The curve is scaled with DEAN geometric parameters and provides an accurate method to determine surface area for the heat transfer relationships. For the current DEAN analysis, the conic half-angle was 25 [deg] in order to ensure that sufficient heat transfer occurred over the nozzle surface. Future work will focus on computationally determining an optimized nozzle contour for a set of inputs – the outputs of this work would include an exact nozzle length.

The total engine length is simply the sum of the chamber length and nozzle length, and is given by Eq. (30).

$$L_e = L_c + L_n \tag{30}$$

The chamber, nozzle, and engine lengths are necessary for determining the surface areas of each section because they provide the lower and upper bounds for the integration.

B. Surface Contours and Surface Area Calculations

This research implemented three contours: inner chamber radius, nozzle, and outer chamber radius. As stated earlier, the outer chamber radius is modeled as constant. Both the inner chamber and nozzle radii are modeled after the RL-10 geometry. These relationships take the RL-10 contour and flip them inside out. The chamber contour that normally converges towards the throat for the RL-10 now diverges for the DEAN, and the DEAN nozzle contour now converges from the throat. This geometry gives a proven flight model to base the performance and heat transfer analysis. The long-term aerospike design, however, will include optimization software (e.g. Two-Dimensional Kinetics) to parametrically develop each of these contours as a function of the user geometrical inputs.

The inner chamber contour is a power function that was determined as a function of inner throat radius, chamber length, nozzle length, and axial position (measured from the injector face). The inner chamber contour is defined as Eq. (31).

$$y_{c,i} = \frac{r_{c,i} * r_{t,i}}{\sqrt{(r_{t,i} - r_{c,i}) * \left(\frac{L_c - x}{L_c}\right)} + r_{c,i}} \tag{31}$$

Here, x is the axial position from the injector face.

The nozzle contour is also a power function and was determined as a function of inner chamber radius, inner throat radius, chamber length, and axial position (measured from the throat). The nozzle contour is defined as Eq. (32).

$$y_n = r_{t,i}\left(1 - \left(\frac{x - L_c}{L_n}\right)^{0.715}\right) \tag{32}$$

Here, x is the axial position up to the nozzle tip – note that the tip may be full or truncated.

The surface contours are necessary for the surface area calculations, which are used to determine flow rates, K-factors for the pressure drops, and heat exchange from the combustion chamber to the cooling channels. The surface area for a given contour is determined as follows:

$$SA = \int_a^b 2\pi y \sqrt{1 + \left(\frac{dy}{dx}\right)^2}\, dx \tag{33}$$

The lower and upper bounds, a and b, for the inner chamber surface area are 0 (the injector face) and L_c, respectively. The lower and upper bounds for the nozzle surface area are L_c and $c_n * L_e$, respectively, where c_n – the nozzle truncation coefficient – varies between 0 and 1. The nozzle and inner chamber surface area for a DEAN at the optimal design point (including 50% truncation factor) is shown in Fig. (21). The throat area is 23 [in^2], expansion ratio is 30, L* is 90 [in], and truncation factor is 50%.

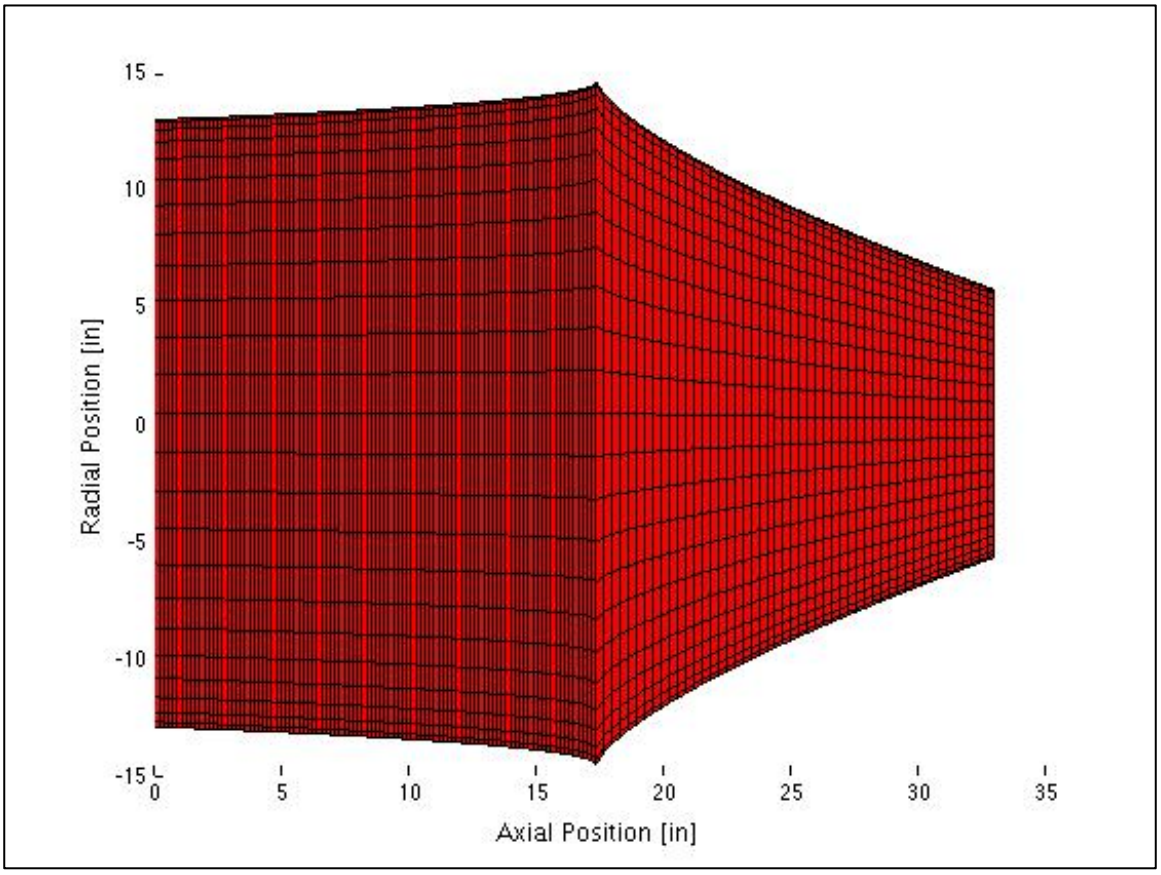

Fig. 21 Truncated DEAN Nozzle Contour Plot

Figures (22) and (23) depict an isometric view and a side view of the truncated DEAN with the inner chamber, outer chamber, and full nozzle surface areas shown.

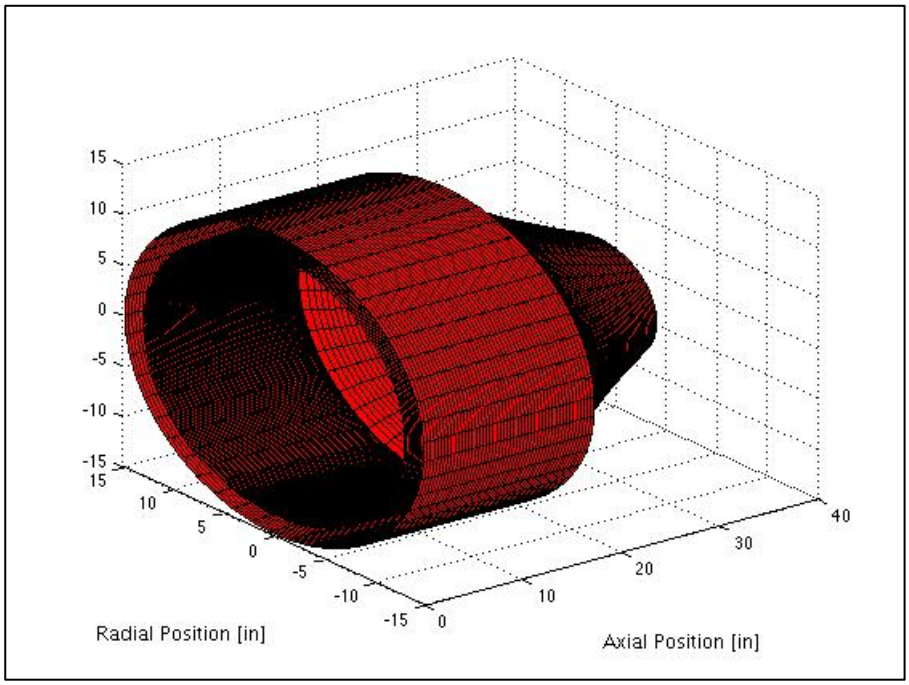

Fig. 22 Truncated DEAN Isometric View

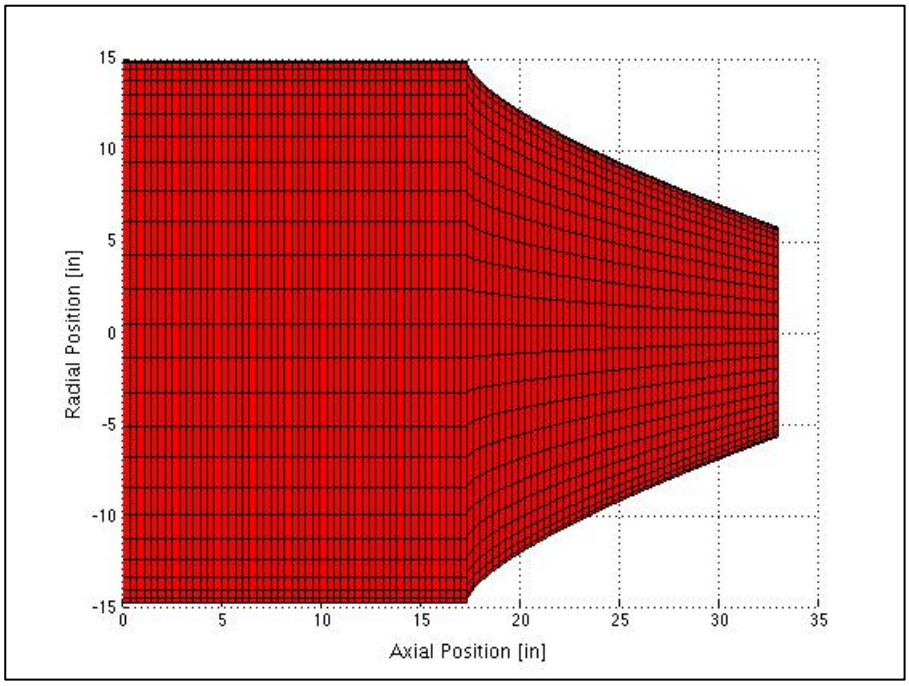

Fig. 23 Truncated DEAN Side View

The volume enclosed by the inner chamber surface would include cooling channels directly on the surface's interior, and the rest would be filled with the cooling jacket structural support material.

The four particular geometrical parameters in this trade space analysis are throat area (A_t), expansion ratio (ε), chamber ratio coefficient (c_{CR}), and characteristic length (L*). As has been shown, each of these elements is a major driver in terms of defining the overall engine and nozzle geometries. To determine the test matrix needed for the NPSS DEAN model, an initial study was completed to analyze and predict any major geometric constraints and variations that the model would exhibit while processing the entire solution space. The survey helped to model the interdependencies, resolve computational impediments, and establish operating ranges for the four parameters. As an example, Figs. (24) and (25) depict the plots for total surface area as a function of L* and c_{CR} – these were determined to be the most effective variables of the four in terms of their impact on the total geometry and surface area. For each plot, the other three variables are held constant.

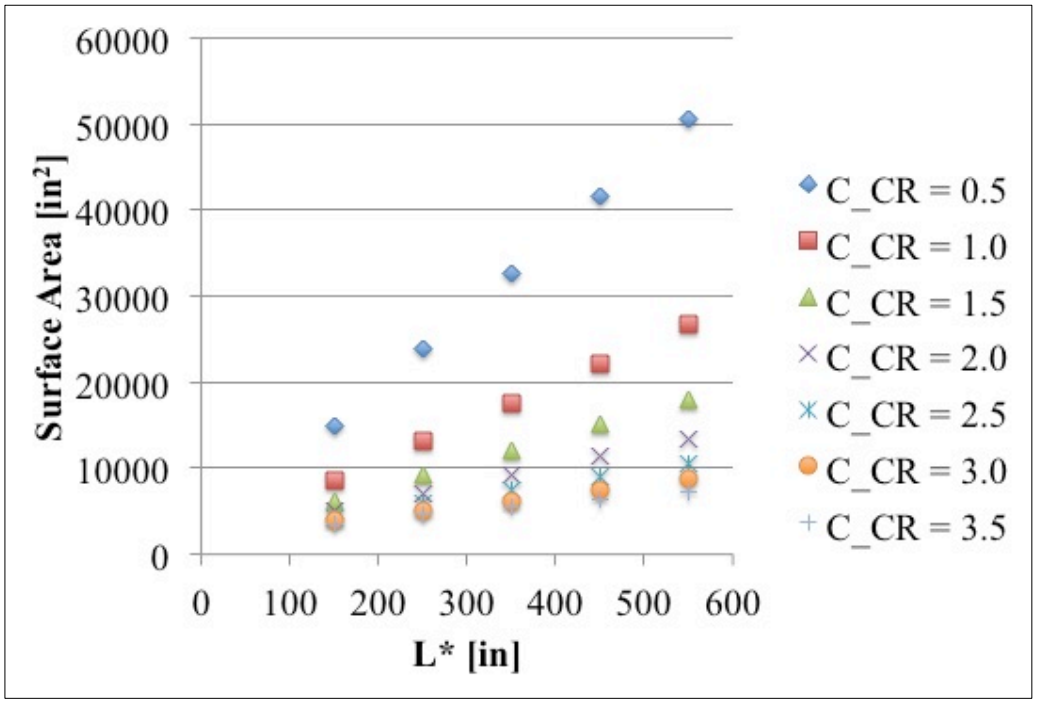

Fig. 24 Total Surface Area as a Function of Characteristic Length

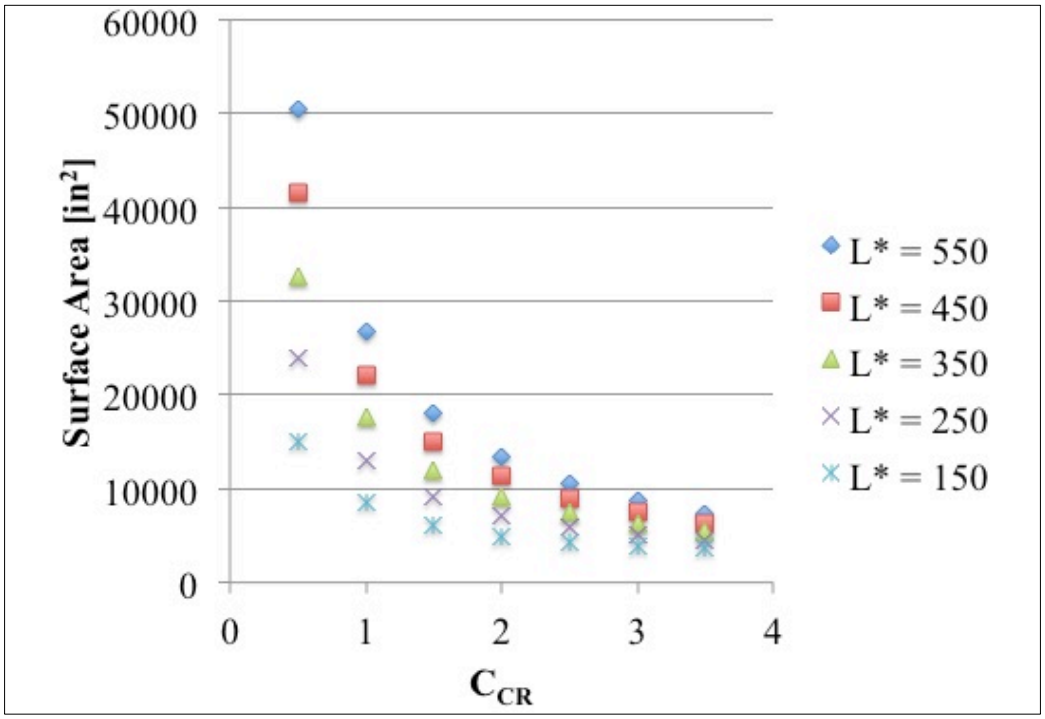

Fig. 25 Total Surface Area as a Function of Chamber Ratio Coefficient

Changes in chamber ratio coefficient had the largest effect on overall surface area, and therefore size, of the modeled DEAN engine. The chamber ratio is first determined from a database of historical engines that use the same propellants. The chamber ratio is then varied using the chamber ratio coefficient, allowing the researcher to explore operational space around known viable operating conditions. The total surface area exhibited relatively high sensitivity at c_{CR} values less than 2.5. The effects from characteristic length were relatively stable – the relationships appear to be nearly linear and the difference between data set plots is roughly a constant multiplier. Chapter IV reviews these parameters further in terms of how they affect the DEAN performance parameters.

III.3 DEAN Thermochemistry

The NPSS DEAN model applies general heat transfer methods and equations to solve for complex fluid flows and power balances that occur throughout the dual-expander cycle. This research implemented an updated user-input thermodynamic package to provide more accurate inputs to the fluid equations of state. The following sections discuss the implementation of these methods and how they were applied to obtain necessary geometries and flow parameters.

A. DEAN Heat Exchange Model

The DEAN combustion process and heat transfer to the working fluids in the dual-expander cycle are modeled by representative physics. Standard heat exchange relationships are used to determine heat transfer from convection (due to combustion/exhaust and coolant flow over the respective surfaces) and heat transfer from conduction (due to heat transfer through the wall). The convective heat exchange equation is

$$\dot{q} = h(T_h - T_c) \tag{34}$$

This equation is valid for the convection from the hot exhaust gas to the chamber wall as well as for the chamber wall to the working fluid, though different heat transfer coefficients are required for each.

The respective heat transfer coefficients are determined by implementing the Bartz and Colburn equations for the hot- and cold-side heat transfer, respectively. These coefficients are determined from the properties of combustion and the geometric properties of the flow. The hot-side heat transfer coefficient given by the Bartz equation is

$$h_{gr} = 0.026 \frac{k_{gr}}{D_{hyd}} \left(\frac{C_p}{k_{gr} \mu_{gr}} \right)^{0.4} \left(\frac{\dot{m}_g D_{hyd}}{A_{cham}} \right)^{0.8} \left(\frac{T_g}{T_{gr}} \right)^{0.8} \phi_B \tag{35}$$

The cold-side heat transfer coefficient given by the Colburn equation is

$$h_l = 0.023 \frac{k_{c_f}}{D_c} \left(\frac{c_{p_{c_f}}}{k_{c_f} \mu_{c_f}} \right)^{0.4} \left(\frac{\dot{m}_c D_c}{A_c} \right)^{0.8} \phi_{curv} \tag{36}$$

For both equations, k is the thermal conductivity of the fluid, c_p is the heat capacity at constant pressure, μ is the absolute viscosity, $\dot{m}$ is the mass flow rate, D is the hydraulic diameter, and A is the cross-sectional flow area. In the Bartz equation, ϕ_B is an applied correction factor used to match actual engine performance outputs, T is temperature, the subscript g denotes the free-stream gas properties in the combustion chamber, and the subscript r denotes the reference enthalpy conditions. In the Colburn equation, ϕ_{curv} is an applied correction factor for the tube radius of curvature, which is designed to account for the additional heat transfer experienced at, and immediately after, the throat. Also, the subscript c denotes bulk coolant conditions.

The conduction heat exchange equation is given as

$$\dot{q} = -k\left(\frac{T_c - T_h}{\Delta L}\right) \tag{37}$$

Here, k is the thermal conductivity of the material, ΔT is the temperature gradient, and L is the distance between the two surfaces. The one-dimensional heat transfer analysis performed in this

research assumes adiabatic wall temperatures (i.e. the wall material is highly conductive, so any temperature gradient is assumed to be negligible). The conduction heat exchange equation is therefore not included in this model.

For steady-state conditions, the convective heat transfer in the chamber must equal the conductive heat transfer through the chamber wall, which then must equal the convective heat transfer in the cooling channel. This equilibrium is shown as

$$\dot{Q} = \dot{q}_i A_i \tag{38}$$

Here, $\dot{Q}$ is the total heat transfer, $\dot{q}$ is the specific heat transfer (defined above for convective and conductive heat transfer), and A is the total surface area over which the heat transfer occurs. Drawing from the cooling channel geometry in Fig. (17) from Chapter II, a relationship for hot-side and cold-side surface areas may be written as

$$SA_c = \left(\frac{w}{w+a}\right) SA_h \tag{39}$$

This relationship is only valid for steady-state, constant wall temperature, and one-dimensional heat transfer.

B. NPSS Thermodynamic Properties

NPSS uses the NIST thermodynamic database to determine state values for the propellants in all phases prior to combustion; more specifically, the solver draws from the NIST database to acquire fluid properties as it iterates towards a solution. The NIST Chemistry WebBook was created to provide standard reference data for chemical and physical properties. NIST provides thermochemical properties such as enthalpy of combustion, enthalpy of reaction, heat capacity, entropy, and vapor pressure[28]. NIST also provides thermophysical fluid properties, including density, heat capacity, enthalpy, entropy, viscosity, and thermal conductivity[28].

A major component of this research focused on the development of a thermodynamics package that was both more complete and more representative of the DEAN operating conditions. Pre-built NPSS thermodynamics packages are somewhat limited in terms of their combustion properties and interpolations. For instance, previous DEAN research used a combustion product thermodynamics package with coarse linear interpolation between only four data points (oxidizer-to-fuel ratios of 5.3, 6.0, 7.0, and 8.0).

Bonnie McBride and Sanford Gordon – researchers at NASA Glenn Research Center – developed the Chemical Equilibrium with Applications (CEA) algorithm and associated transport and thermodynamic property databases to be used in determining combustion properties, rocket performance, and shock-tube parameters, among other things[37]. CEA itself is "a program which calculates chemical equilibrium product concentrations from any set of reactants and determines thermodynamic and transport properties for the product mixture"[37]. NPSS contains a CEA thermodynamics package that, if selected, calls the CEA algorithm for each iteration. Implementing CEA models the states of the products of combustion directly, but it is also very computationally expensive. The CEA model implemented in this research assumes that the flow is frozen, which means that the combustion product composition is the same in both the combustion chamber and at the nozzle exit (end of the aerospike), and that no chemical reactions occur between those elements.

This research applied a middle ground between the highly coarse but computationally inexpensive approximation and CEA's highly smooth but computationally expensive approximation. The new approximation utilizes NPSS's user input capability for fluid property tables (FPT) to store CEA-derived product of combustion state data at discrete points. This technique allows for greater accuracy in the state calculations for combustion products over a

significantly broader range of oxidizer-to-fuel ratios. The new method resulted in the same accuracy as the CEA derived models[27].

Comparisons of the state properties of the oxygen and hydrogen combustion products are presented in Figs. (26-29). These figures show how the previous research was being limited by accuracy of their state relationships; ratio of specific heats (γ), temperature, molecular weight, and specific impulse, all as a function of O/F. The properties were evaluated for a throat area of 25 [in^2], expansion ratio of 25, and L* of 350 [in], and constitute a representative engine to provide fluid property verification. The "good state properties" are the ones using the updated mid-range approximations and the "bad state properties" are the ones using the older coarse approximations.

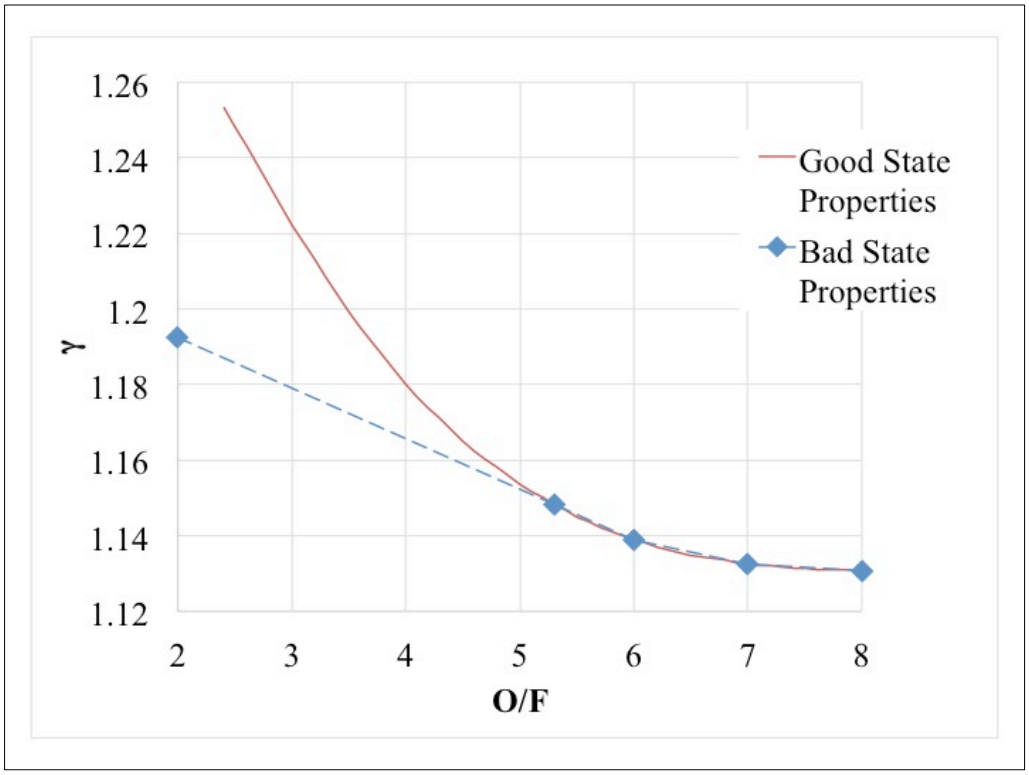

Fig. 26 Ratio of Specific Heats as a Function of O/F

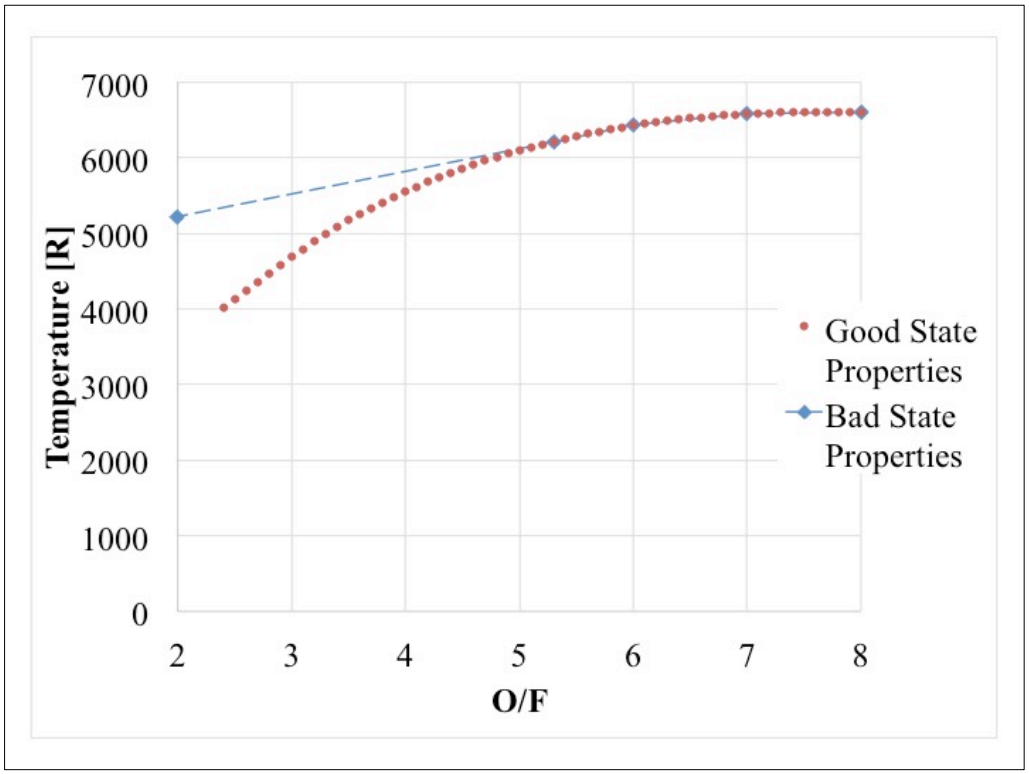

Fig. 27 Temperature as a Function of O/F

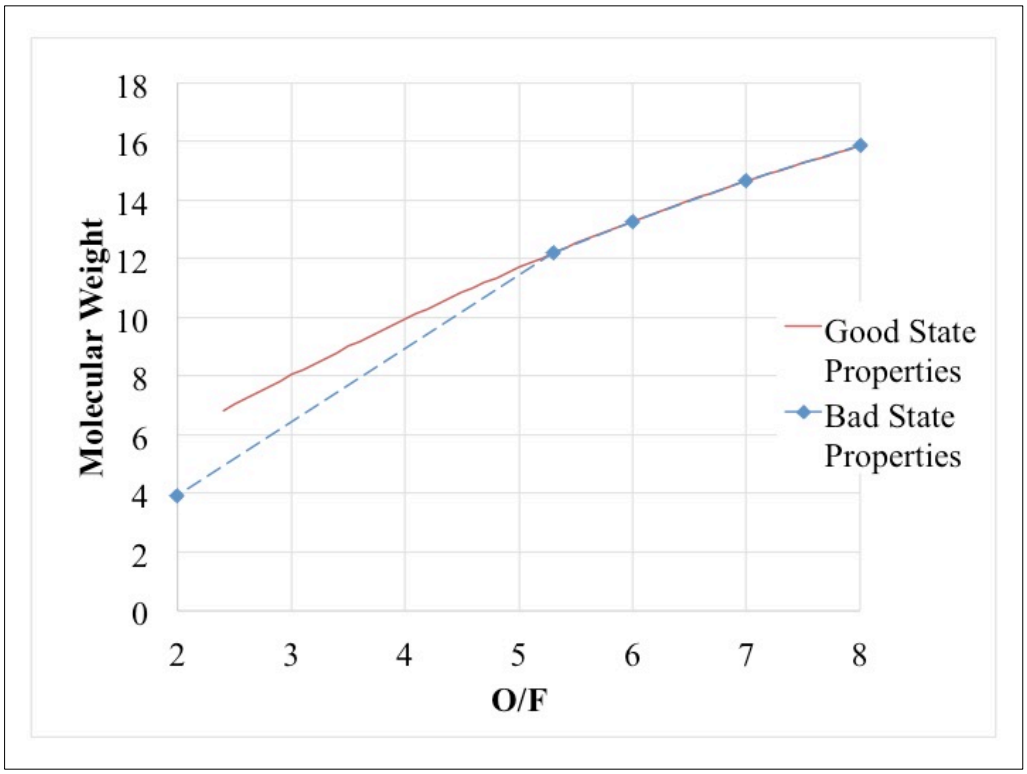

Fig. 28 Molecular Weight as a Function of O/F

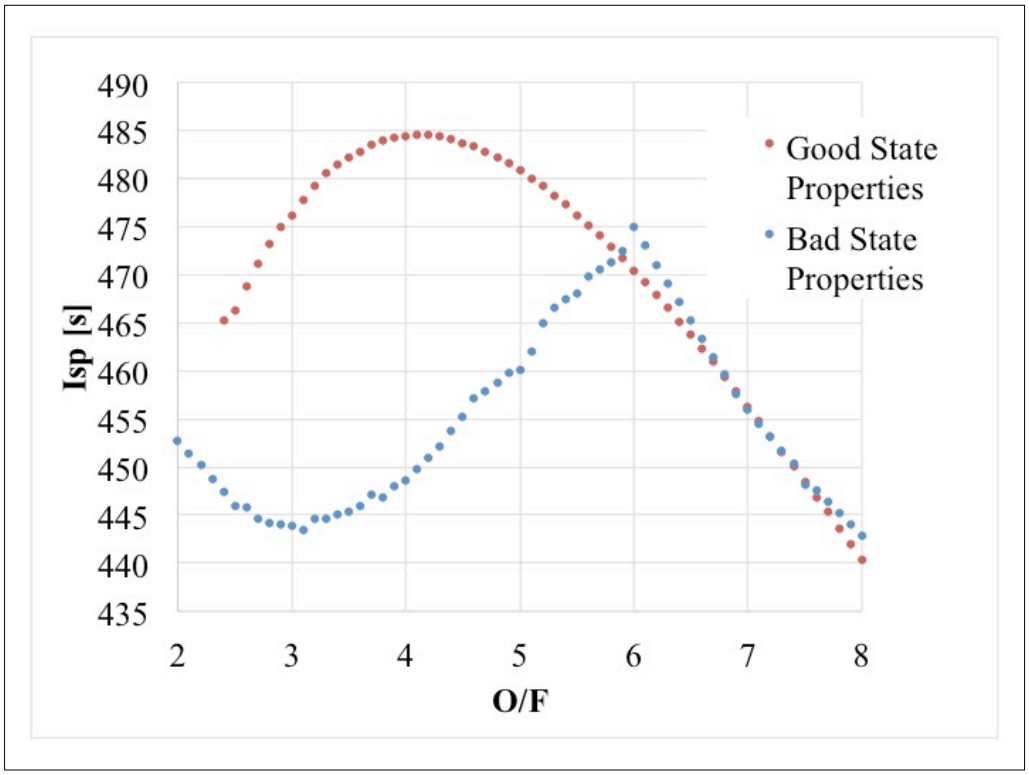

Fig. 29 Specific Impulse as a Function of O/F

The γ, temperature, and molecular weight plots show relatively accurate interpolation within the 5.3-8.0 O/F range. For specific impulse, the curve is not as well behaved outside of the 6.5-8.0 O/F range. In all cases, the original linear interpolation is inaccurate for O/F values less than 5.3. The "good state properties" curve matches that obtained from standard rocket theory (Eq. (1)).

Initial state values must be provided for the fluid conditions in order to determine the initial engine geometry and start the NPSS solver sequence, which then adjusts them as necessary. The data plotted above was determined for oxygen and hydrogen mixtures based on a chamber pressure of 1000 [psia]. Relations for characteristic velocity, γ, and combustion temperature were also determined for the same chamber pressure and O/F ranges of 2.0-8.0. The relations are shown below in Eqs. (40-42).

$$c^* = 8.1151 * \frac{O^3}{F} - 154.05 * \frac{O^2}{F} + 689.73 * \frac{O}{F} + 7325.3 \quad (40)$$

$$\gamma_c = -0.000158 * \frac{O^4}{F} + 0.0029 * \frac{O^3}{F} - 0.013 * \frac{O^2}{F} - 0.0313 * \frac{O}{F} + 1.3765 \quad (41)$$

$$T_{c,i} = -114.46 * \frac{O^2}{F} + 1621.8 * \frac{O}{F} + 821.97 \quad (42)$$

These approximations contribute most to initial error due to the assumption of a constant pressure. These relationships were then used to determine exit Mach number and to size the engine.

C. Working Fluid Discussion

The state, and properties at that state, of working fluids is of fundamental importance in rocket engine design. The working fluid is the mechanism by which the energy is transferred through the engine; in the case of the DEAN, the working fluids are oxygen and hydrogen. Both oxygen and hydrogen exist in only liquid or supercritical states throughout the propellant feed system (tank to injector). Vaporized propellant could result in flow instabilities and potential turbomachinery cavitation[27]. The liquid state properties of oxygen and hydrogen are well known for various applications, but the supercritical state properties are less known and therefore present a source of error, particularly in terms of high energy systems. In order for any fluid to obtain a supercritical state, the temperature and pressure must both be higher than the critical point. Table 3 lists the critical point temperature and pressure for both hydrogen and oxygen.

NPSS includes fluid temperature and pressure outputs at different points (stations). The heat exchange that occurs from the combustion and exhaust to the oxygen and hydrogen cooling volumes is of particular interest to this research because the energy that is transferred must be sufficient to run the respective expander cycles. The heat exchange to the cooling volumes is modeled using 40 total flow stations in the chamber and nozzle sections (20 for each propellant). In general, applying more nodes (flow stations) leads to higher resolution of the static flow

conditions (pressure and temperature). This is particularly important in terms of material selection because higher resolution provides more accurate wall temperature profiles. However, higher nodal resolution may be computationally expensive without improvement in resolution. An analysis was completed to determine the reasonable number of nodes that provide accurate data without severely affecting computational efficiency. The DEAN was modeled with 10, 20 and 25 cooling volumes for each propellant. The solutions at 20 nodes showed sufficient resolution in wall temperature profile to warrant the increased computational penalty. Results at 25 cooling volumes showed very little improvement.

The current DEAN model accounts for both hydrogen and oxygen compressibility in their respective equations of state. Hydrogen is considered incompressible in liquid form and compressible in supercritical form, while oxygen is considered incompressible for both states. The hydrogen K-factors were determined by the equations of state and then validated using the RL-10 outputs; because the RL-10 uses a hydrogen expander cycle, this is considered to be an equivalent comparison. Our current research is constrained by fluid properties of oxygen at a supercritical state, particularly in terms of how well it behaves as a working fluid. Spencer and Rousar determined a heat transfer correlation for liquid oxygen cooling of rocket thrust chambers, but this analysis was only completed for limited temperature and pressure ranges and the resulting correlation was only shown to accurately predict the heat transfer to within ±30%[38]. Outside of this limited study, there has not been significant research in terms of using oxygen as a working fluid in an expander cycle. Further research needs to be completed to understand whether supercritical oxygen can function adequately for an expander cycle.

Additional material research should be completed to understand the effect of subsonic high-temperature supercritical oxygen on the turbomachinery. In designing an expander cycle

oxygen pump, Buckman et al. found that low pressure ratio and low temperature required to meet the power balance are desirable conditions for low metal ignition risk[39]. That same study selected Monel alloys (nickel copper alloy) as the choice material because of their low ignition potential and high strength[39]. An essential component of the DEAN engine research and development will focus on designing and manufacturing turbopumps that can operate effectively in the extreme conditions presented by the utilization of liquid and supercritical oxygen as the working fluid.

III.4 RL-10A-3-3A Validation

Past DEAN research using NPSS only included partial-validation and did not incorporate a validated engine model to test the design and programming methodology. The major validation points centered on comparing the performance, size, and property outputs to those of similar upper stage class engines (i.e. RL-10 series engines). This research applies methods, physics, and properties that are validated using an NPSS model of the RL-10A-3-3A upper stage engine. This section outlines the RL-10 engine series, NPSS methods applied to the RL-10 and DEAN NPSS models, and a steady-state result comparison of the RL-10 NPSS model with NASA's ROCket Engine Transient Simulator (ROCETS) analysis.

A. RL-10 Series Overview

The RL-10 engine series has been in production since the 1960s, with several improvements and new versions being developed since. While each new model has included technological advancements that have enhanced the engine's performance, the core elements have remained intact – those being the use of LOX/LH_2 as the oxidizer/fuel mixture and the implementation of a single-expander cycle. Table 4 outlines the performance parameters for each RL-10 upgrade, from inception of the program, in order by completion date.

Table 4 Summary of RL-10 Engine Series Performance[7,8]

	Thrust [lbf]	I_{sp} [s]	Expansion Ratio [ ]	T/W [ ]
RL-10A-1	15,000	422	40:1	50:1
RL-10A-3	15,000	427	40:1	50:1
RL-10A-3-1	15,000	431	40:1	50:1
RL-10A-3-3	15,000	442	57:1	50:1
RL-10A-3-3A	16,500	444	61:1	55:1
RL-10A-3-3B	15,000	436	61:1	50:1
RL-10A-4	20,800	449	84:1	56:1
RL-10A-5	14,560	368	4.3:1	46:1
RL-10A-4-1	22,300	451	84:1	61:1
RL-10B-2	24,750	465.5	285:1*	37:1

*Includes Nozzle Extension

By comparison, the RL-10 and DEAN engines have many similarities. The core difference is the dual-expander cycle implementation for the DEAN, versus the single-expander cycle implementation for the RL-10. This difference is manifest primarily in terms of the turbomachinery. The RL-10 engines implement a single turbine to operate the fuel and oxidizer pumps. The turbine is driven entirely by warm hydrogen from the expander cycle. The DEAN implements entirely separate turbopump systems for the fuel and oxidizer expander cycles. Similar to the DEAN engine, the RL-10 uses a two-stage fuel pump – allowing more pressure buildup for the lower density hydrogen. Contrastingly, the RL-10 oxidizer side uses a single-stage pump, while the DEAN uses a two-stage pump. Future work will determine the necessity of a second stage pump for the oxygen side. The entire RL-10A-3-3A expander cycle schematic is shown in Fig. (30).

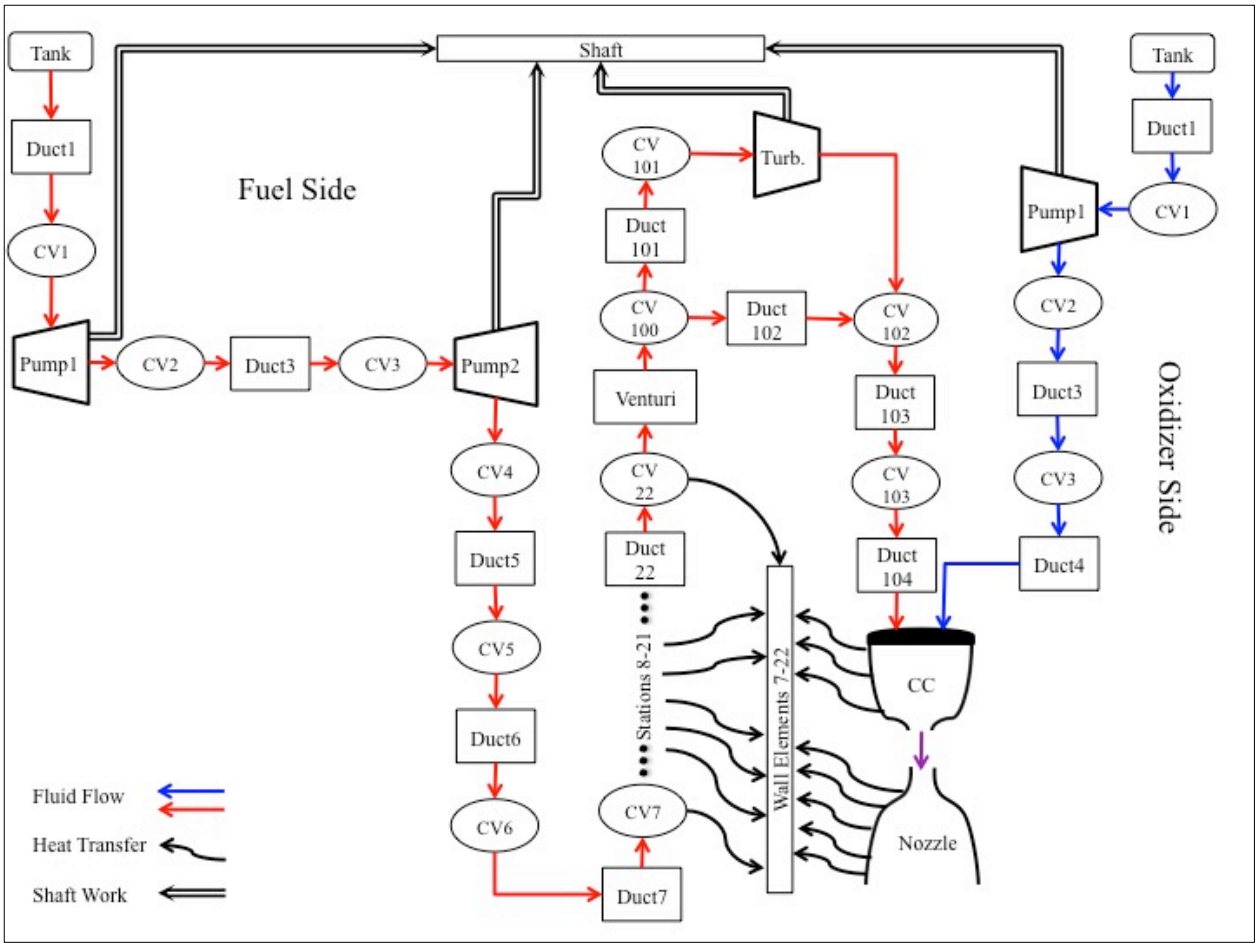

Fig. 30 RL-10 Expander Cycle Schematic

Comparison of Fig. (30) with Fig. (19) provides insight into how similar the DEAN and RL-10 engines are. Apart from the separated turbomachinery and general geometry, the expander cycles are identical. For single-expansion cycles, such as the RL-10, the turbine exhaust gas (hydrogen) and liquid oxygen are injected (vapor-liquid injection) and combusted in the thrust chamber. For dual-expander cycles, the turbine exhaust gases include both hydrogen and oxygen, which are injected (vapor-vapor injection) and combusted.

B. RL-10A-3-3A Methodology

The RL-10A-3-3A was modeled in NPSS in order to adequately validate the methodology and the convective heat transfer coefficient inputs used to model the DEAN engine. The primary difference between the RL-10 and DEAN NPSS models is the geometry definition. The RL-10 model serves to recreate an already established engine – since the geometries are known for the actual engine, they are set as constants in the program. The DEAN applies a much more dynamic process, by way of geometrical relations and standard rocket theory, which allows for trade space analysis (the DEAN trade space is analyzed in Chapter IV). The critical aspects of modeling the RL-10 and DEAN engines were the fluid properties and the associated friction losses in the cooling jackets. The fluid property tables developed for this research and discussed in Section III.3.B were implemented for both the RL-10 and DEAN models. This research also developed a method by to accurately represent the pressure losses in the cooling jackets.

The cooling jacket is responsible for receiving the thermal energy of combustion and transferring that energy to the working fluid and then to the turbines, which drive the expansion cycles. The NPSS solver operates to balance the mass and power of the entire system and therefore must determine the pressure drop across each component in the propellant feed system. In order to calculate those pressure drops, however, the state properties of the working fluid must be accurately known. The following analysis provides a method by which to approximate the friction factors, and therefore pressure drops, across the cooling channel.

The annular flow area, A_{phys}, is defined as the total cross-sectional area of the cooling channels (i.e. cross-sectional area if all the channels were combined into one), at a given axial location. Rearranging Eq. (9) gives A_{phys} as a function of the fluid flow and as a function of the channel geometry.

$$A_{phys} = \frac{\dot{m}}{\rho v} = \frac{\pi {d_{hyd}}^2}{4} n_{channels} \quad (43)$$

The annular flow area may be approximated as a circular cross-section by using the hydraulic diameter, d_{hyd}, as the ratio of the cross sectional area to the perimeter times 4. The hydraulic diameter for a rectangular duct is:

$$d_{hyd} = \frac{4bd}{2(b+d)} \quad (44)$$

Where b is the width and d is the depth of the cross-sectional area. NPSS tracks the mass flow throughout the system, ρ is determined from the equations of state at those particular conditions. The initial velocity is defined to size the A_{phys}.

$$v = 0.2 * a_{H_2} \quad (45)$$

$$v = 0.1 * a_{O_2} \quad (46)$$

Here, a is the speed of sound of the working fluid. The Mach number is set for each fluid based on constraints occurring from high-speed fluid flow. Holding all else constant, higher fluid velocities will drive down the channel areas beyond manufacturing capabilities. Once A_{phys} is determined – and width is given from the user inputs – the height of the individual cooling channels may be calculated:

$$h = \frac{A_{phys}}{(2wn_{channels})} \quad (47)$$

Here, w is the half-width of the cooling channel and $n_{channels}$ is the number of channels in the cooling jacket. Knowing the height of a channel and having already set the channel width as a user input, the individual channel geometry may be determined. Since it is rectangular, the channel cross-sectional area is simply

$$A = 2wh \quad (48)$$

The pressure drop across the cooling channel is defined as in Eq. (49).

$$\Delta P_{cool} = f(\frac{L}{D})\frac{\rho V^2}{2} \tag{49}$$

The K-factor is also called a "loss factor" or "resistance coefficient" and is defined by the friction factor and the flow geometry (length and diameter).

$$K = f(\frac{L}{D}) \tag{50}$$

The friction factor is based on the surface roughness of the tube and the state properties of the fluid flowing through it. The friction factor for this research is based on a curve-fit for Crane's Reynolds number for compressible flow friction factor data[40]. The flow is fully turbulent. The K factor is defined for one individual channel.

$$f = 0.3515 * Re^{-0.203} \tag{51}$$

The Reynolds number (Re) is the ratio of inertial forces to viscous forces and is primarily used to characterize the laminar (low Re) and turbulent (high Re) flow regimes.

$$Re = \frac{\rho V L}{\mu} \tag{52}$$

The new K-factor dependent pressure drop equation for the cooling channels is

$$\Delta P_{cool} = K\frac{\dot{m}^2}{2\rho {A_{phys}}^2 g_0} \cdot (\frac{SA_{Total}}{SA_{Virtual}}) \tag{53}$$

NPSS calculates the flow properties and pressure drops based on A_{phys} (i.e. combined area), so a scaling factor must be used to account for the sum of the individual surface areas across all the channels. SA_{Total} is the total surface area of the cooling channels over some length, L. $SA_{Virtual}$ is the surface area of a single tube, if all the cooling channels were combined together. The ratio of the two is given as

$$\frac{SA_{Total}}{SA_{Virtual}} = \frac{L\pi d_{hyd} n_{channels}}{L\pi d_{vir}} \tag{54}$$

The virtual diameter, d_{vir}, is given by Eq. (55):

$$d_{vir} = \frac{4ab}{2(a+b)} = \sqrt{\frac{4A_{phys}}{\pi}} \tag{55}$$

Substituting Eq. (55) into Eq. (54) and cancelling like-terms, the final equation for the pressure drop over the cooling channels is given as

$$\Delta P_{cool} = K \frac{\dot{m}^2}{2\rho {A_{phys}}^2 g_0} \cdot \sqrt{n} \tag{56}$$

This equation is now a function of K-factor and accounts for actual surface area of the cooling channels.

The results of this study show accurate representation of the pressure drop across the cooling jacket, which is significant in terms of balancing the pressure profile of the engine. The total pressure drop, however, is due to a combination of different factors, including friction. Little information is available for the friction factors, and therefore K-factors, for supercritical hydrogen and oxygen. The RL-10A-3-3A model, which uses the same propellants as the DEAN engine, provides some insight into the magnitudes of the hydrogen K-factor values – this is due to hydrogen being the working fluid in the RL-10 expander cycle. Further research and experimentation will be necessary in order to better understand the friction losses associated with supercritical oxygen.

C. RL-10A-3-3A Steady-State Comparison of Results

NASA Lewis Research Center developed a computational model of the RL-10A-3-3A engine in 1990 in response to investigations of two instances of in-flight failures. The ROCETS code was created to provide a method to model and simulate the RL-10A-3-3A engine (with expansion capabilities for future models)[41]. The code was developed entirely from test, component, and analysis data and information from Pratt & Whitney.

The ROCETS code was designed to model both steady-state and transient operating conditions. The component-level inputs used in the NPSS analysis are the exact same inputs used in the ROCETS analysis, which allows for direct comparison of results. The cooling jacket heat transfer was modeled using NASA's Rocket Thermal Evaluation (RTE) program. RTE is a one-dimension heat transfer program that determines hot-gas-side heat transfer based on the enthalpy gradient and also calculates heat transfer effects due to tube curvature. Combustion analysis was completed using a set of NASA and industry-standard prediction algorithms, including Chemical Equilibrium with Transport Properties (CET93), ROCket Combustor Interactive Design (ROCCID), and TDK. CET93 is an earlier version of CEA, which is used in the NPSS models – comparisons between the two models due to fluid property calculations are nearly identical. Also, NPSS uses similar combustion solver equations and models to the ROCCID code – these were discussed in-depth in Section III.3.A. The ROCETS model includes heat transfer at the injector face, which was beyond the scope of this research, and is therefore not included in the NPSS analyses.

The predicted values from the ROCETS model were found to match the measured test values "within 10% for all parameters on all tests" and that most were "within 4% of the test results"[41]. The ROCETS analysis also determined that deviation of heat transfer from the predicted value might result from inconsistencies in the manufacturing process, causing variations in cooling channel surface areas. A table of detailed NASA ROCETS performance predictions can be found in Appendix A[41]. Table 5 outlines the performance values that were considered for comparison in this research. The RL-10 measured values are not known, so the percent difference is shown as a method of comparison between the NPSS and ROCETS models.

All values besides pressure drop in the cooling jacket are within 10% for each model. The predicted pressure drop in the cooling jacket is within 20% for each model.

Table 5 RL-10A-3A Model Performance Comparison

	[Unit]	NPSS	NASA ROCETS	% Difference
Chamber Pressure	[psia]	455.97	475.5	4.19%
Engine Thrust	[lbf]	16500	16412	0.53%
Specific Impulse	[s]	449.4	445.6	0.85%
Combustion O/F	[ ]	5.5	5.055	8.43%
Mass Flow	[lb/s]	36.71	36.921	0.57%
Fuel Consumption	[lb/s]	5.648	6.161	8.69%
Oxidizer Consumption	[lb/s]	31.06	30.76	0.98%
Cooling Jacket delta-P	[psia]	234.1	195.7	17.87%
Cooling Jacket delta-T	[°R]	321.7	326.3	1.43%
Cooling Jacket delta-h	[BTU/lb]	1257.8	1268.3	0.83%
Total Heat Pick-Up	[BTU/s]	7365.8	7714.2	4.62%
Max. Metal Temperature	[°R]	1530.7	1500.8	1.97%

The maximum difference in the pressure profile occurred at the turbine exit and was determined to be 10.4%. The maximum differences in the temperature and enthalpy profiles each occurred at the cooling jacket. All other percent differences for each parameter were less than 6%, most were less than 3%. The significant enthalpy difference was largely due to a sign difference, which is likely from differences in the heat transfer predictions for each model. The larger pressure drop in the NPSS analysis is the result of more conservative estimates to ensure that we were accounting for the worst-case possible surface roughness. In addition to general performance comparisons, pressure, temperature, and enthalpy profiles were also plotted for each model, and are shown below in Figs. (31-33). The profiles begin at the inlet of the first fuel pump and progress to the second fuel pump, the cooling jacket, the turbine, and then through the injector to the combustion chamber. Due to limited scaling, the combustion chamber value was only shown for the pressure profile plot. Points along the cooling jacket are not shown for the ROCETS model because they were not provided in the NASA analysis documentation.

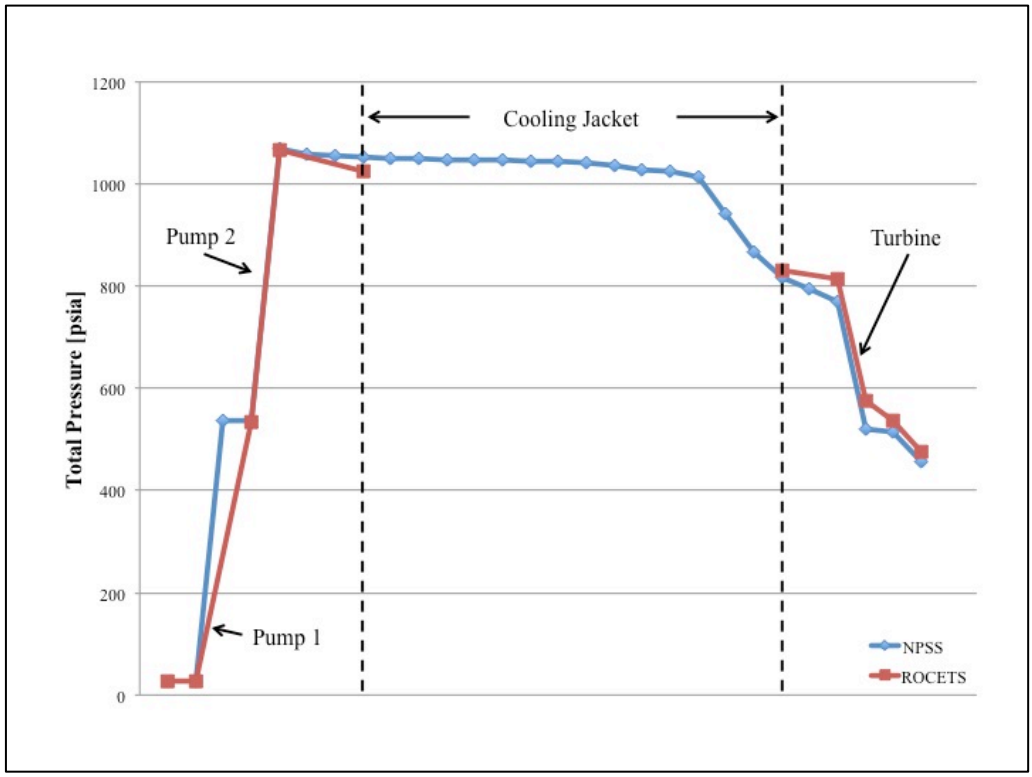

Fig. 31 RL-10A-3-3A Model Pressure Profile Comparison

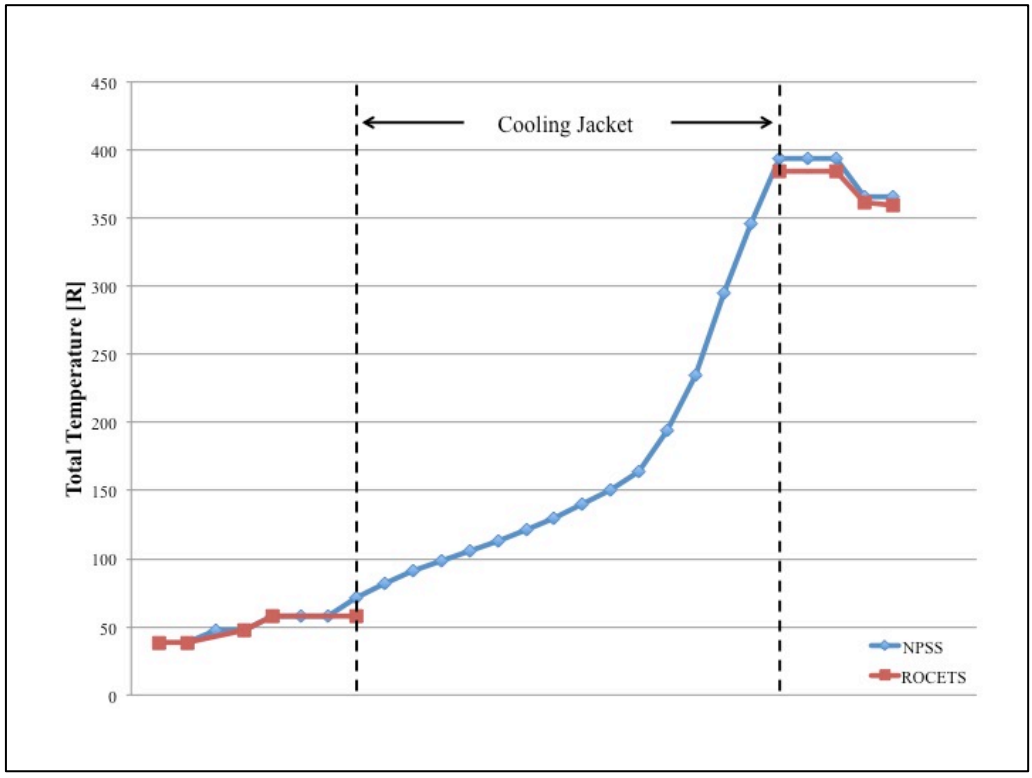

Fig. 32 RL-10A-3-3A Model Fluid Temperature Profile Comparison

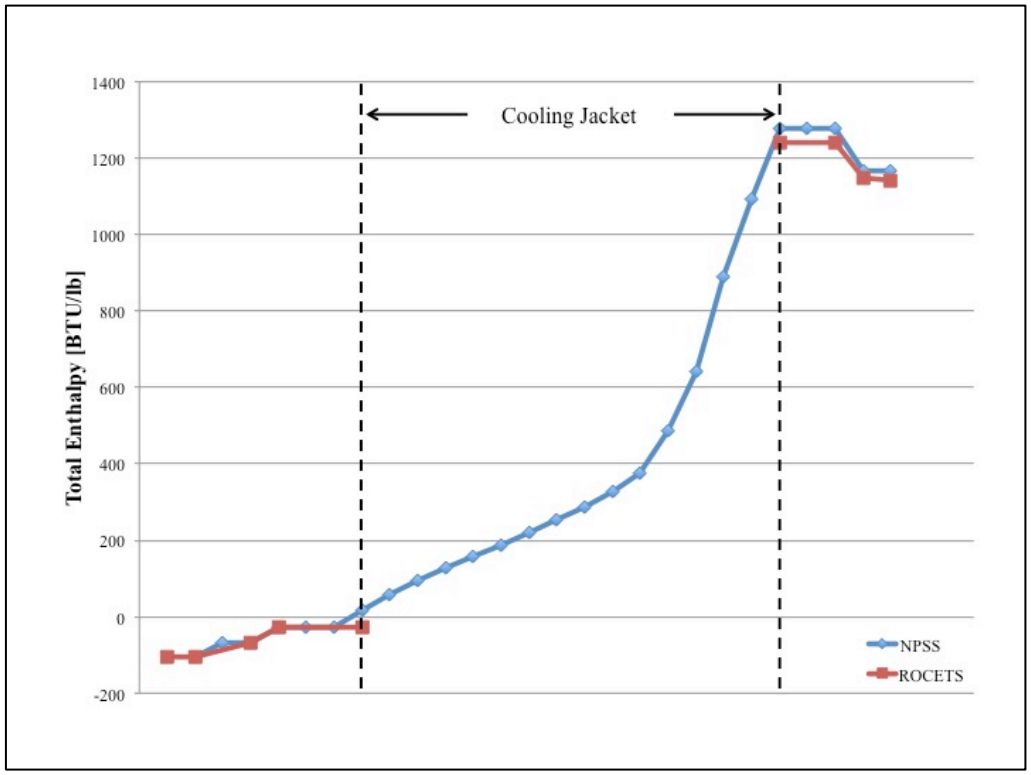

Fig. 33 RL-10A-3-3A Model Enthalpy Profile Comparison

Two major areas determined to be under-examined for past DEAN studies were the fluid property calculations and the friction losses in the cooling jackets. This research implemented new fluid property tables and pressure drop evaluations to better represent the physics of the working fluids in the expander cycles. The results derived from the RL-10A-3-3A NPSS model validated the methodology is accurate. The pressure profile validates the cooling jacket methodology and that the pressure drop calculations are accurate. The total heat pick-up in the cooling jacket being within 5% of the predicted value between models shows that the hydrogen friction factors, and therefore K-factors, are fairly well represented. Experimentation needs to be conducted to determine how oxygen operates in these conditions, because there is not currently a baseline for comparison. The DEAN NPSS model applied the same methodology as was validated using the RL-10 model. Chapter IV reviews and discusses the results of that research.

IV. RESULTS AND ANALYSIS

Chapter IV summarizes and discusses the results obtained from the trade studies performed using the methodology outlined in Chapter III and validated using an NPSS modeled RL-10A-3-3A engine. Sensitivities were completed to determine how the geometrical inputs L*, A_t, ε, and c_{CR} affect the performance of the DEAN engine. Two particular design points are reviewed in-depth and compared with the performance and size objectives. Finally, the optimal design point determined by this trade study is compared with its RL-10B-2 upper stage counterpart.

IV.1 Discussion

Trade studies are implemented in engineering analysis to determine broad, macro-level, trends and system drivers that may be more significant and impactful than others. In general, trade studies help to bound the solution space and provide insight into possible areas of optimal performance. Further, trade studies can help to determine the feasible solution space when constraints are implemented that reflect physical, cost, performance, or other limitations within a given design. Once the general trade space is determined, sensitivity analyses may be performed. These allow for more direct understanding of the micro-level interactions within the system.

This research evaluated the performance and size of the DEAN architecture by completing a trade study and subsequent sensitivity analysis of four geometric parameters: L*, A_t, ε, and c_{CR}. The research objectives are linked to both performance and size outputs: thrust of

30,000 [lbf], specific impulse of 465.5 [s], less than 90 [in] engine length, and less than 60 [in] maximum diameter. Additionally, a maximum allowable wall temperature constraint of 1800 [°R] was established to maintain the solution space within the feasible physical realm. Two design options were selected: the optimal design and a robust design. The optimal design was selected based on being the smallest engine that still achieved the performance objectives.

An initial trade study was completed to better understand the effects of changes in each geometric input. Section III.2.B showed significant effects on surface area for lower chamber ratio coefficients (c_{CR}). In an attempt to determine the smallest engine, c_{CR} was held at unity – this also allows for better comparison with the RL-10, which also has a c_{CR} of 1. Table 6 displays the ranges that were selected based on the desire to determine the smallest possible engine.

Table 6 DEAN Trade Study Inputs

	[Unit]	Minimum	Maximum	Step Size
Throat Area	[in^2]	15	30	5
L*	[in]	75	150	25
Expansion Ratio	[ ]	30	75	15

A total of 57 cases converged of the possible 64 cases ran. Not all converged solutions are within the feasible solution space for the DEAN architecture, which is determined based on the desired performance outputs. All of the converged solutions – displayed in Fig. 34 – were within the maximum performance objectives (max length and diameter). A programmatic goal of this research is to establish a replacement for the RL-10B-2; therefore, that size envelope is also displayed, with most of the converged solutions fitting within that bound. Finally, the optimum design point is labeled – some converged solutions were less than this bound. The establishment of these boundaries provides a clear minimum and maximum size envelope for this study, with

the minimum being the optimum size and the maximum being the RL-10B-2 size (as the programmatic goal of this research is to provide a replacement for the RL-10 series).

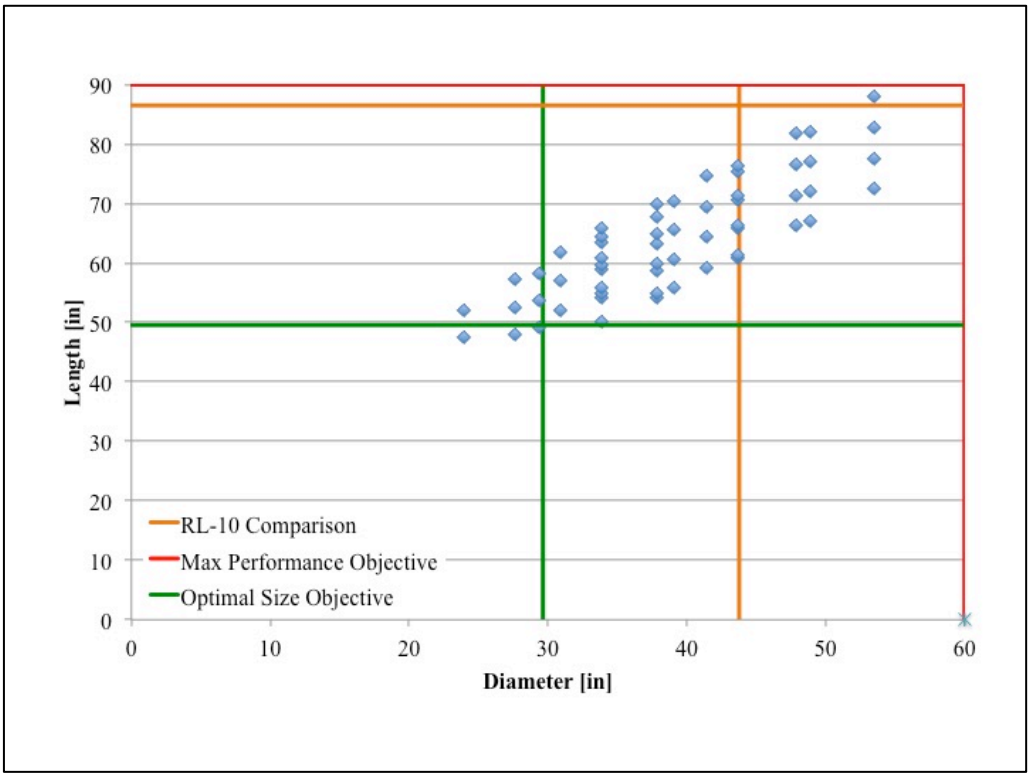

Fig. 34 DEAN Size Envelope Solution Space

The geometry of the DEAN engine implies that the maximum diameter must occur at the throat area location – also, the combustion chamber, propellant feed system, and gimbal are all within that outer throat diameter envelope. The maximum diameter may then be determined as a function of the exit area, which is derived from Eq. (7) as the throat area multiplied by the expansion ratio (i.e. two of the four geometric inputs). The vertical sets shown for different diameters is based on similar exit areas. The total engine length is the summation of the chamber and nozzle lengths, which are each dependent on the four geometric inputs.

The chamber pressure is inversely proportional to the throat area; smaller throat area implies higher chamber pressure and therefore smaller combustion chambers. From the set of solutions, it was determined that convergence was highly dependent on the input L* value.

Lower L* values (multiple cases at L* of 75 and once at 100) did not converge, showing not enough energy was being transferred to the cooling flows to achieve the required pressure drops for the shorter engines. The trade space was fairly robust at L* set at 150, the remaining trade study analyses apply this value (Figs. (35-37)). It is noted that the other input L* values produced similar developments and that the following plots shown are representative of the overall trend. The converged solution chamber pressure outputs are compared in Fig. (35) over a range of throat areas (abscissa) and expansion ratios (defined in the legend).

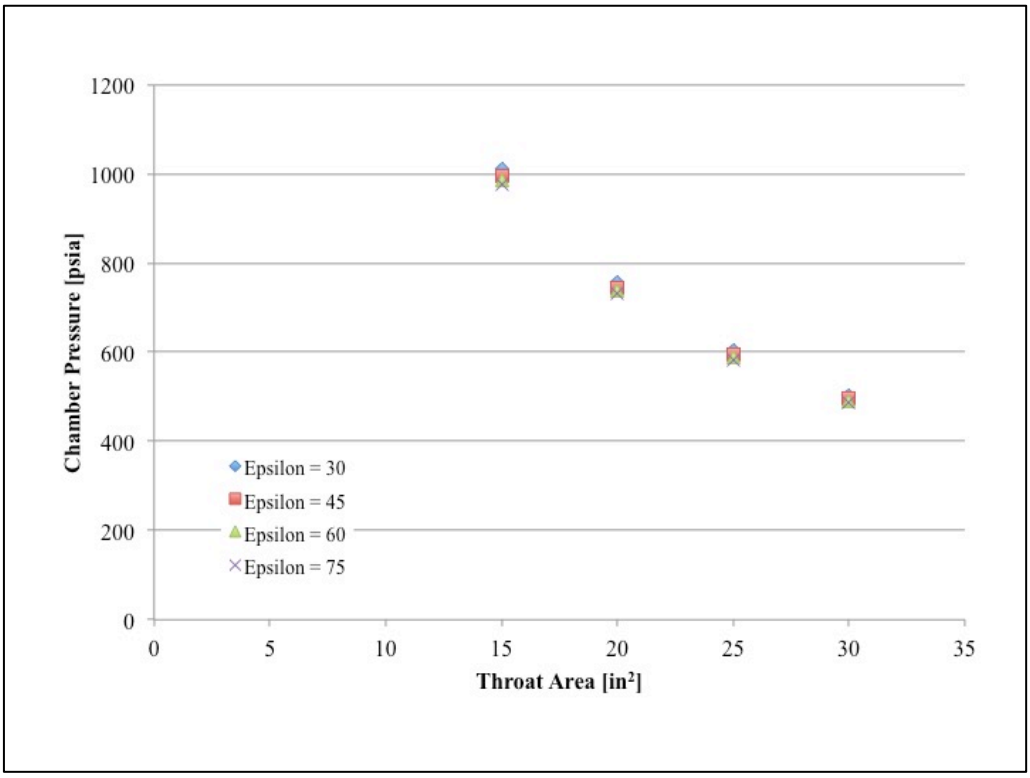

Fig. 35 DEAN Chamber Pressure Correlation with Throat Area

The trend between throat area and chamber pressure is exactly what we would expect from standard rocket theory (Eq. (5)) – increased throat area produces decreased chamber pressure.

Copper was selected as the material of choice for this research because of its high heat conductivity, which is necessary for the regenerative cooling technique used for the dual-expander cycle. The selection of copper as the design material inherently sets the maximum wall

temperature constraint. NASA studies have shown copper alloys with zirconium additives maintain their structural integrity to temperatures just above 1800 [°R][42] (or about 75% of the melting point). This therefore established a constraint on our feasible solution for maximum wall temperature. Future work will include temperature exposure and duration as a means of evaluating reusability.

For any given set of geometrical inputs, the maximum wall temperature occurred in the oxidizer cooling jacket at the throat location. This critical maximum was therefore selected as the primary focus for the general temperature analysis. The temperature ranges are compared in Fig. (36) over a range of expansion ratios (abscissa) and throat areas (defined in the legend), with the maximum temperature objective displayed. A chamber ratio coefficient of 0.8 was implemented to allow for expansion ratios less than 30, without which they would not have enough surface area to meet the power demands.

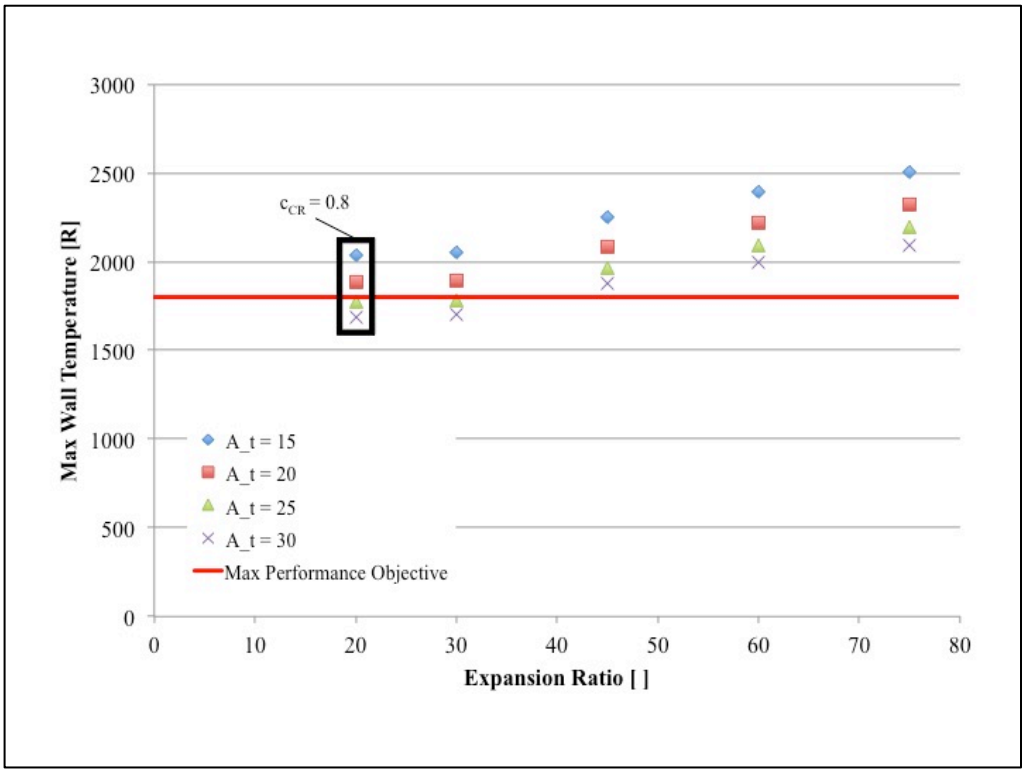

Fig. 36 DEAN Wall Temperature Solution Space

For the standard set of converged solutions, only 6 of the possible 57 converged cases maintained maximum temperatures below the performance objective. Of those 6 data points, all were at expansion ratios of 30 and throat areas of either 25 or 30. Implementing the chamber ratio coefficient of 0.8 allowed for an expansion ratio of 20 to be achieved with similar wall temperatures for the corresponding throat areas.

For conditions where ambient pressure is zero, or near zero, as with an upper stage engine, the thrust always increases with respect to expansion ratio[44]. Holding all else constant and remembering that specific impulse is directly proportional to thrust, specific impulse will also increase with expansion ratio for this flight condition, as can be arrived at from Eq. (1). The RL-10B-2 boasts an expansion ratio of 285:1 (fully extended) and produces a 465.5 [s] specific impulse, nearly 15 [s] greater than its nearest competitor. The RL-10's 465.5 [s] I_{sp} was therefore selected as the minimum performance objective for the DEAN architecture in this research. The specific impulse ranges are compared in Fig. (37) for the DEAN trade study over a range of expansion ratios (abscissa) and throat areas (defined in the legend).

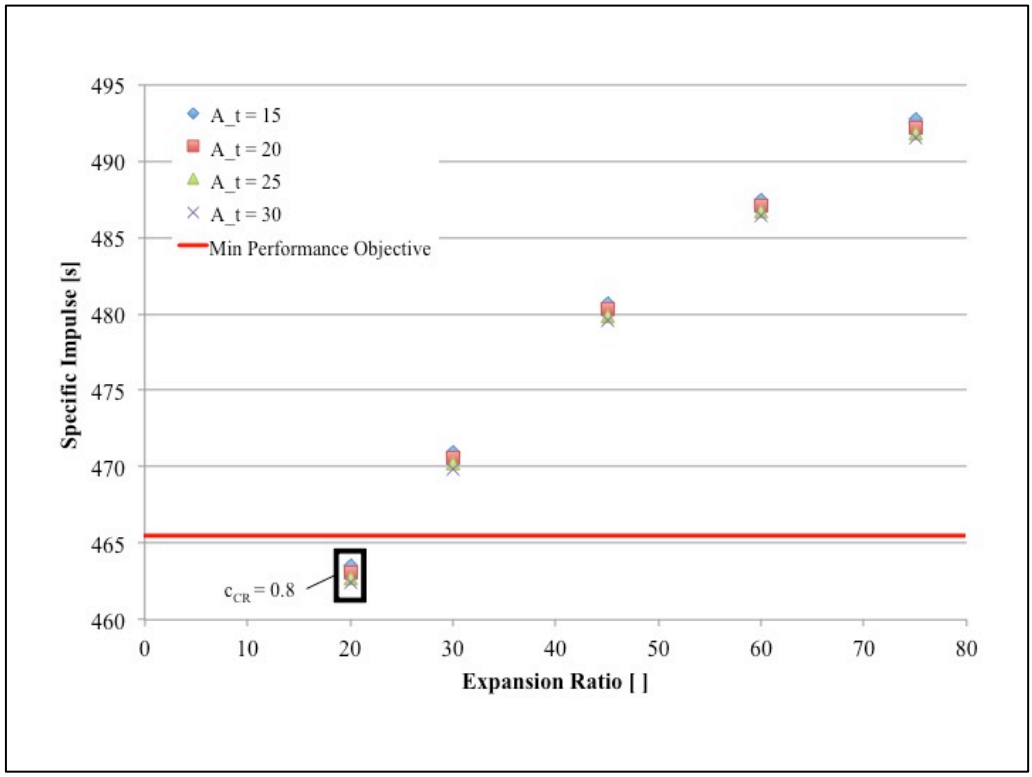

Fig. 37 DEAN Specific Impulse Solution Space

For the standard set of converged solutions, every solution maintained a higher specific impulse than the minimum performance objective of 465.5 [s]. Solutions with chamber ratio coefficient of 0.8 and expansion ratio of 20 do not provide the desirable performance. This result combined with the wall temperature result provides the basis for selecting expansion ratio of 30 as an optimal design parameter. Although increased expansion ratio provides increased specific impulse, it also provides increased mass. The minimum size, and therefore minimum mass, will be for engines just meeting the minimum performance (I_{sp} ~ 464.5 [s]). Setting the chamber ratio coefficient equal to 1.0 also constrains the chamber surface area and allows for a more accurate comparison with the RL-10 engine. No solutions converged for the NPSS model evaluated at expansion ratios less than 30, with chamber ratio coefficient set to 1.0.

The DEAN trade study resulted in boundary definition for the higher fidelity sensitivity analysis. The results of the trade study showed that the optimal expansion ratio was

approximately 30, the optimal throat areas for that expansion ratio were in the range of 25-30, and the optimal chamber ratio coefficient was near 1.0. Table 7 outlines the updated geometrical inputs for the subsequent sensitivity analysis. The sensitivity assumes optimal values for expansion ratio.

Table 7 DEAN Sensitivity Analysis Inputs

	[Unit]	Minimum	Maximum	Step Size
Throat Area	[in^2]	23	30	1
L*	[lbf]	90	160	10
c_{CR}	[ ]	0.6	1.0	0.1

A sensitivity deviating off the optimal point is performed for chamber ratio coefficients in order to validate the analysis performed in Chapter III.

The maximum wall temperature in the oxidizer cooling jacket, with respect to variances in L*, was shown to be negligible (less than 1% change) at the throat location over the range of throat areas. The temperature experienced at the injector face, however, was largely affected by changes in the characteristic length. The oxidizer cooling jacket temperatures at the injector face are compared in Fig. (38) over a range of characteristic lengths (abscissa) and throat areas (defined in the legend); all calculations here utilized chamber ratio coefficient of 1.0. For clarity, the throat areas were limited to the minimum and maximum values from the data set. The same trend occurred for throat areas between these values, with the same relative magnitude (i.e. the curves would have nearly overlapped for added values between the minimum and maximum throat areas).

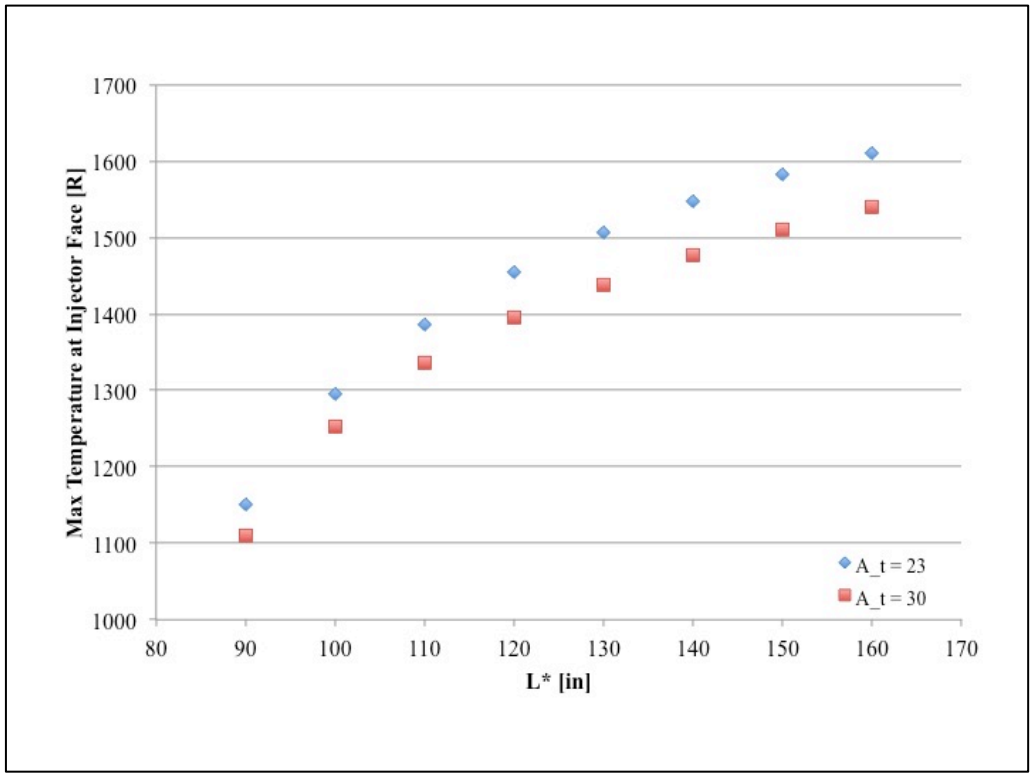

Fig. 38 DEAN Max Injector Face Temperature Correlation with L*

The engine length and total heat pick-up values occurring over the cooling jackets were shown to be nearly linear with respect to changes in characteristic length. These correlations are shown in Figs. (39) and (40) and verify the results obtained in Section III.2.B that predicted linear trends for constant chamber radius coefficients. The engine length is shown for varying L* values and throat areas of 23, 27, and 30 [in^2], as defined in the legend.

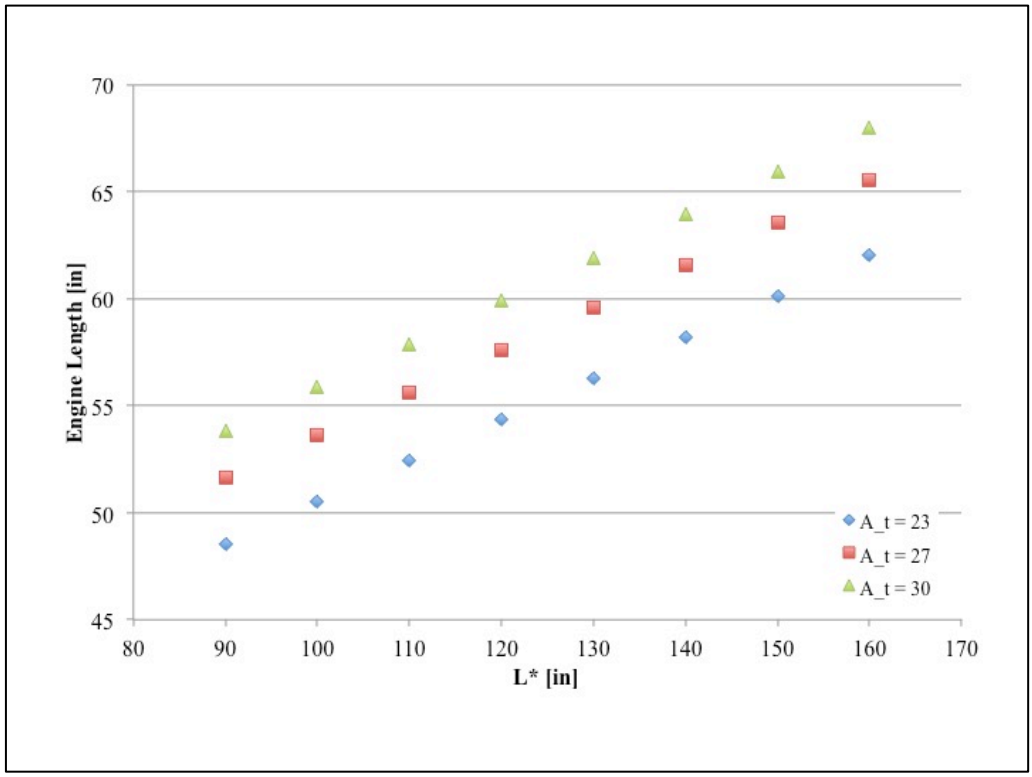

Fig. 39 DEAN Engine Length Correlation with L*

The oxidizer heat pick-up value corresponding to each L* differed at less than 1% over the examined throat area set, with a maximum difference between throat areas of 23 and 30 being 0.96% at 90 [in]. The fuel heat pick-up value corresponding to each characteristic length differed at less than 2.5% over the examined throat area set, with a maximum difference being 2.42% at 90 [in]. For this reason, only the trends for throat area equal to 23 [in^2] are displayed.

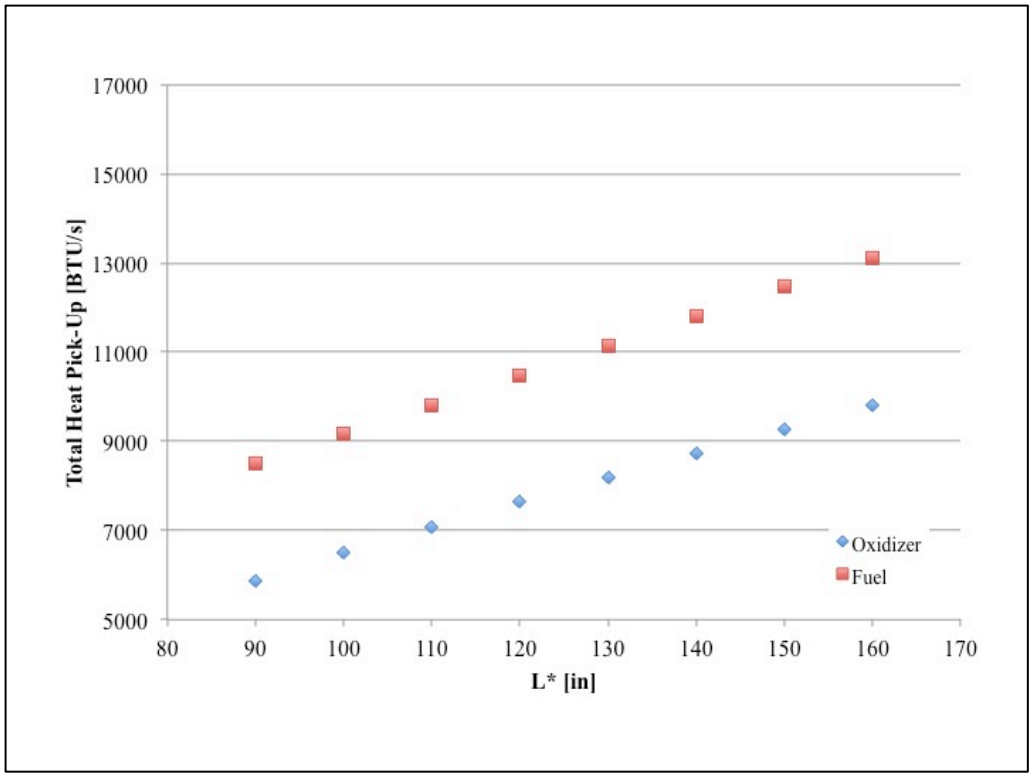

Fig. 40 DEAN Total Heat Pick-Up Correlation with L*

These results are significant both because they show that the model is performing as we would expect from our analysis using standard rocket theory and that the characteristic length may be adjusted to effectively increase or decrease the amount of heat pick-up within the engine. This capability may be applied to future DEAN designs whose surface area does not provide adequate heat transfer to power the turbopumps and run the expander cycles. L* of 90 [in] proved to be the lower bound for an expansion ratio of 30 – an upper bound was not determined because larger L* drives up the chamber volume, and therefore total engine weight. Similar to expansion ratio, the minimum L* required to achieve the performance objectives (i.e. that the chamber is large enough for necessary heat transfer) is the optimal value.

It was determined earlier that the chamber ratio coefficient of 1 was the optimal selection based on minimizing the engine size and being able to compare it directly with the RL-10, whose c_{CR} input is the same. A sensitivity analysis was performed on the chamber ratio coefficient to

fully understand the trends of decreased values on engine length and heat transfer. The engine length and total heat pick-up values across the fuel and oxidizer cooling jackets were shown to be non-linear with respect to chamber ratio coefficient. These correlations are shown in Figs. (41) and (42) and verify the predicted outcomes determined in Section III.2.B.

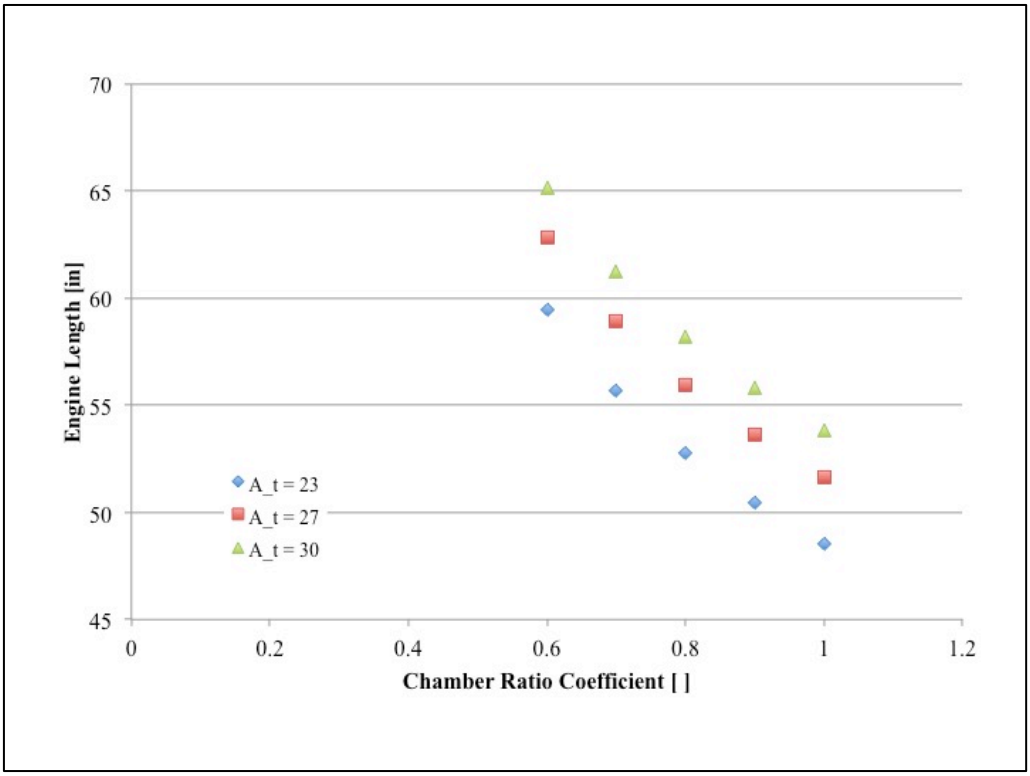

Fig. 41 DEAN Engine Length Correlation with c_{CR}

For expansion ratio of 30, it is shown that the DEAN size envelope is maximized for a c_{CR} value of 1 for any throat area. Additional increase of the chamber ratio was not considered in this research due to the desire to maintain as close to the same scaling inputs as the RL-10B-2.

The oxidizer and fuel heat pick-up values corresponding to each chamber ratio coefficient differed within 1% and 2.5% respectively. The maximum differences were the same as evaluated for L* and occurred at chamber ratio equal to unity. For this reason, only the trends for throat area equal to 23 [in^2] are displayed.

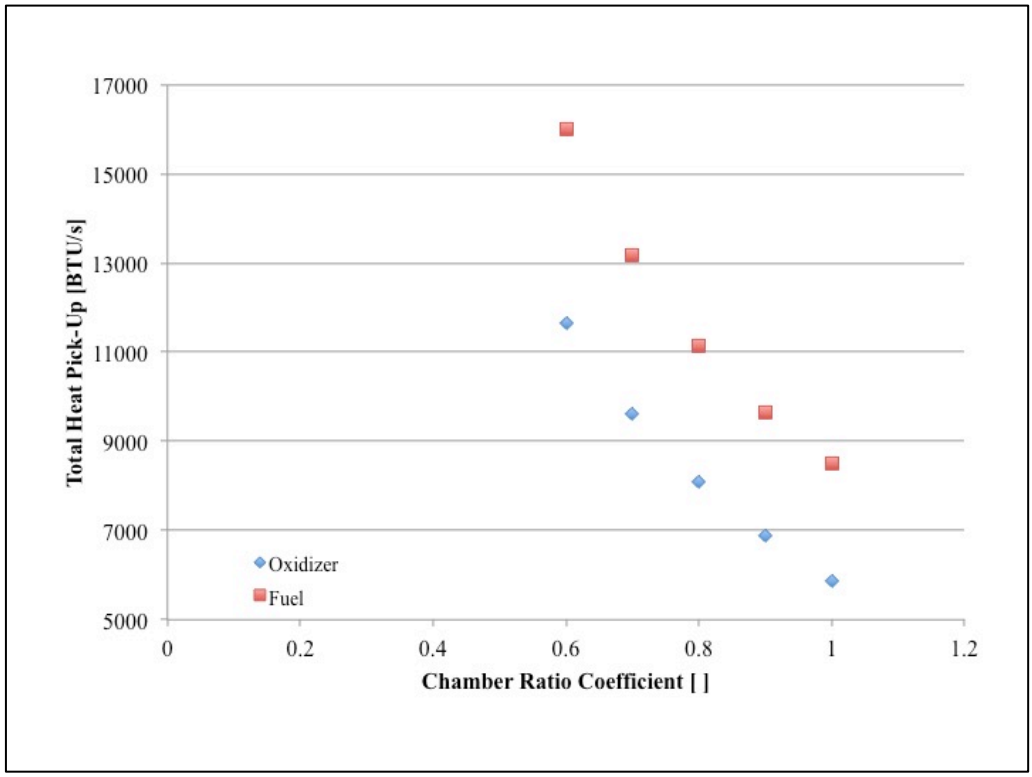

Fig. 42 DEAN Total Heat Pick-Up Correlation with c_{CR}

These results match the predictions in Chapter III that the heat transfer increases non-linearly as the chamber ratio coefficient is decreased.

In summary, the NPSS DEAN model was shown to converge over throat areas between 23-30 [in^2], L* values between 90-160 [in], and expansion ratio and chamber ratio coefficient set at 30 and 1, respectively. In an effort to determine the minimum engine size, it was shown that the optimal value for A_t and L* would correspond to the smallest value for which the performance and size objectives were still achieved.

IV.2 Comparative Design Point Study

From a programmatic perspective, multiple possible design points within the feasible solution space must be identified in order to make adequate decisions on the long-term architecture. Two design points were identified for this research and are discussed and compared

in this section: the optimal design point and the robust design point. The optimal design point is the point at which all geometric inputs provide the minimum size envelope while still achieving the defined performance objectives; the term "optimal" is considered within the scope of the solution space examined in this research and does necessarily apply to the absolute optimal design point. For this research, the optimal design point was determined only for values within the set of converged solutions and within the established performance constraints. In general, an optimal design point may be defined based on current or future state-of-the-art technologies, which provides insight into what would need to be developed or improved in order to obtain the far-reaching performance objectives. The robust design point is selected based on the desire for the system to be able to withstand various geometrical modifications and still produce the desired end-state conditions.

It was shown that the maximum engine diameter was largely affected by the selection of A_t and that the chamber length was largely affected by the selection of L*. Intuitively, a 1 [in^2] change in throat area is significantly more impactful than a 1 [in] change in L*, since A_t sets the diameter of the combustion chamber and nozzle, while L* only really changes the chamber length. In order to account for a variety of possible changes in the chamber and nozzle, it is determined that the desired robust design point (while still remaining somewhat near the optimal design point) should be a modification of the throat area. The optimal and robust throat areas were selected as 23 and 27 [in^2], respectively. The expansion ratio of 30, L* of 90 [in], and chamber ratio coefficient of 1 were established as constant for both design points. Figures (43-48) provide fuel and oxidizer wall temperature, fluid temperature, and total pressure profiles. The abscissa axis for each plot constitutes the corresponding axial flow station, and all stations are plotted equidistantly apart. In actuality, only the stations in the cooling jacket are equally

spaced, the others are entirely dependent on the location of the component they represent. The flow stations are numbered with the left-most stations being furthest from the injector face and the right-most stations being closest to the injector face. The density of the flow stations per section is dependent on which cooling jacket is displayed (fuel or oxidizer) and is a function of the geometry of each jacket (i.e. fuel starts at 50% of the nozzle length while oxidizer starts at the throat location).

The maximum wall temperature profiles are shown for the corresponding hot-side wall temperatures of the fuel and oxidizer cooling jackets. The temperature requirements established by this research set the maximum allowable temperature at 1800 [°R]. It is seen in Fig. (43) that the fuel wall temperature is entirely unaffected by this constraint and that it is significantly below that maximum value.

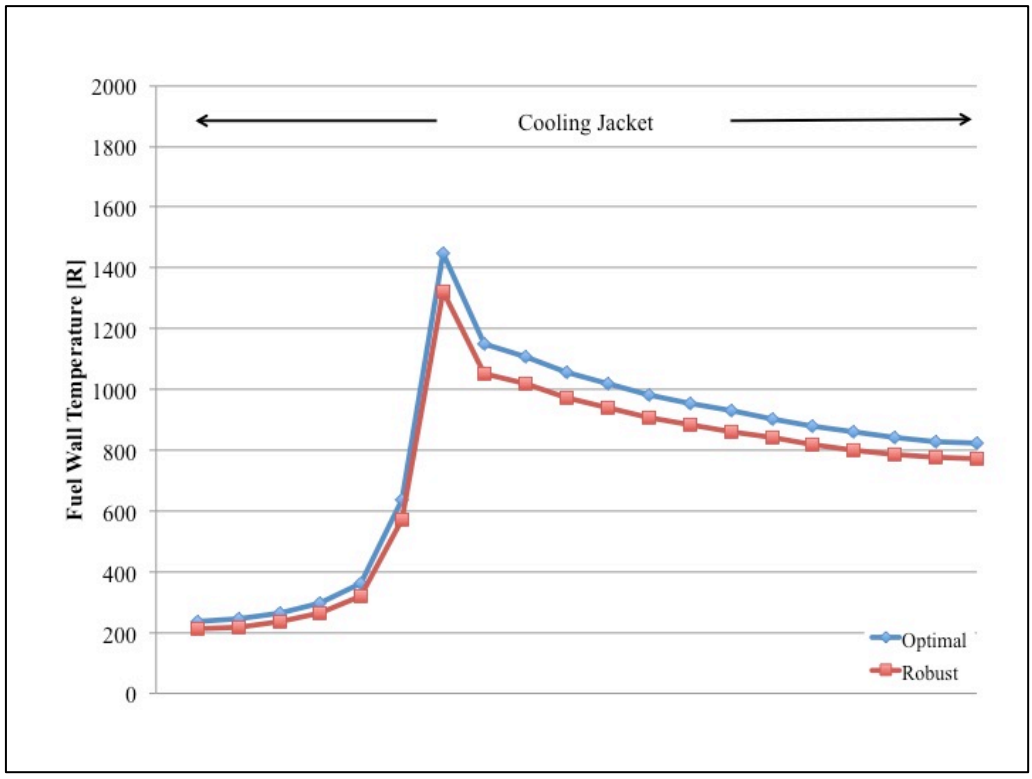

Fig. 43 DEAN Fuel Wall Temperature Profile

The fuel temperature profile shows the maximum value occurring at the throat location. The fuel cooling channels are set to begin at 50% of the nozzle length and move up completely through the interior of the chamber. The wall temperature varies inversely with changes in cross-sectional area, which is why the maximum temperature occurs at the throat location (minimum cross-sectional area).

As stated in Section IV.1, the maximum wall temperature of the DEAN engine was found to occur on the oxidizer cooling jacket at the throat location (as is shown, this location maintained near-maximum temperatures while still operating in the feasible solution space). The oxidizer cooling jacket is set at a constant radius and the resulting wall temperature profile is therefore much different from the fuel-side, as shown in Fig. (44). Two local maxima appear at the throat and injector face locations, though the global maximum still occurs at the throat, as is the case with the fuel side.

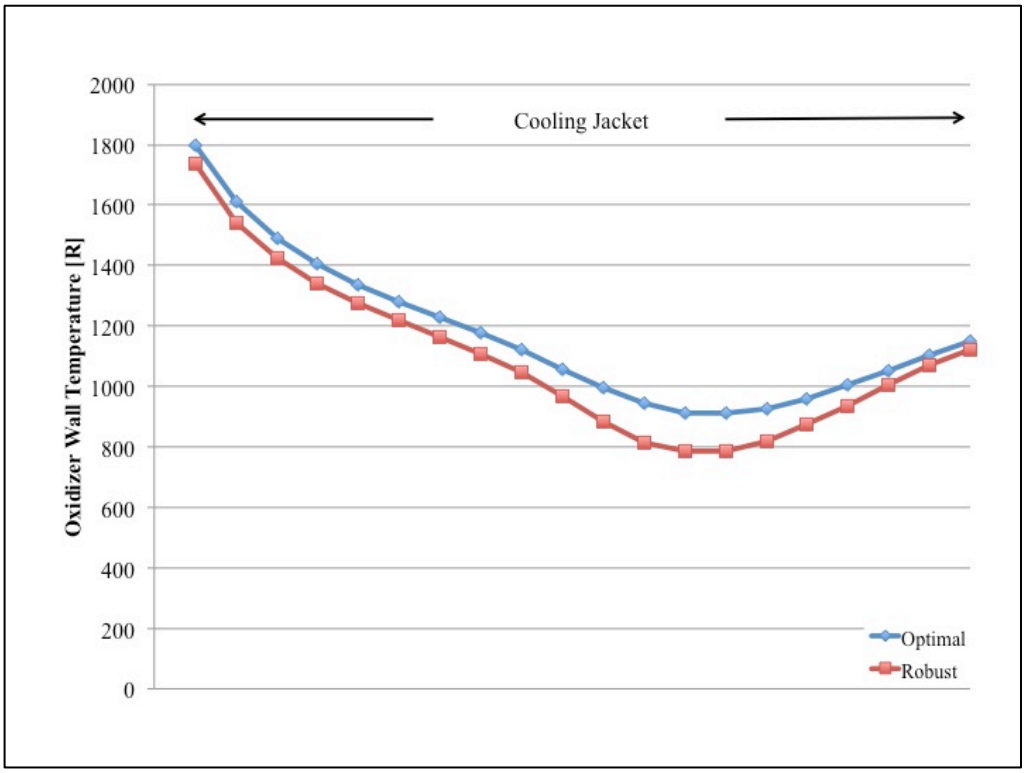

Fig. 44 DEAN Oxidizer Wall Temperature Profile

The oxidizer cooling channels are set to begin at the throat location and move up through the exterior of the chamber to the injector face. The increased wall temperature at the injector face is the result of heat transfer to the oxidizer earlier in the chamber walls. The wall equilibrates at a higher temperature as the fluid temperature in the cooling volume rises as a result of earlier heat transfer.

The fuel and oxidizer fluid temperature profiles over the entire DEAN engine are displayed in Figs. (45) and (46). For both fluids, the maximum temperature gradient occurred across the cooling jackets, as expected. The fuel fluid temperatures did not vary appreciably between the optimal and robust cases. The oxidizer fluid temperatures did vary slightly, particularly near the turbine inlet. For both cases, the temperatures are not significantly high where they would present a concern for ignition, corrosion, etc.

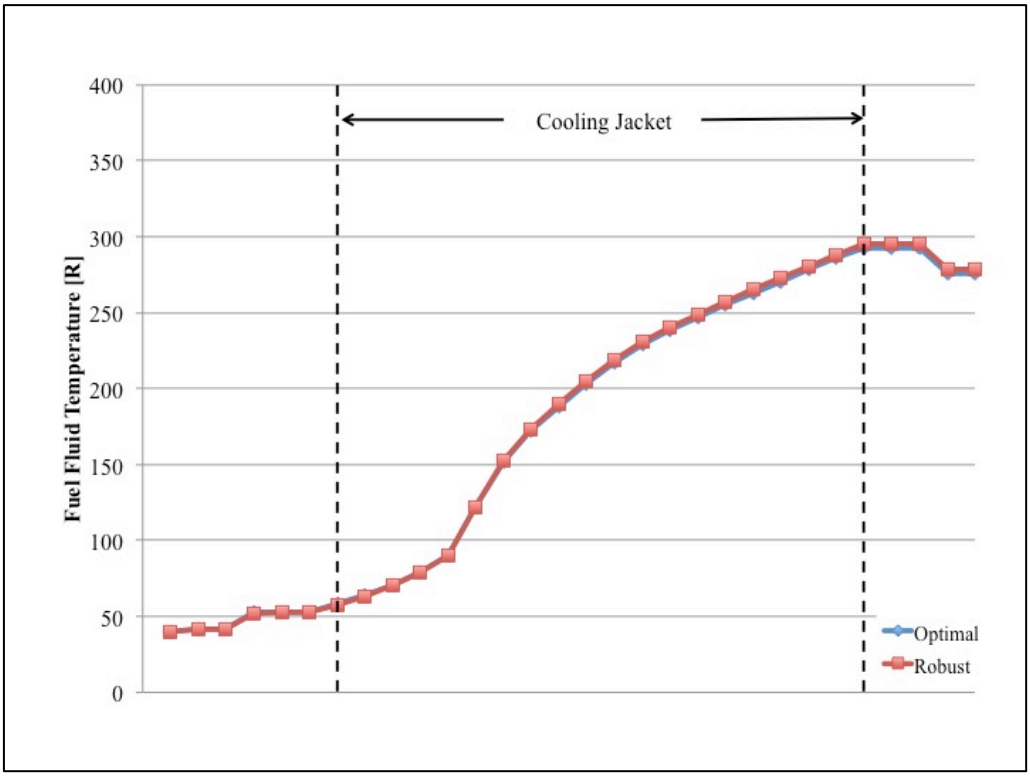

Fig. 45 DEAN Fuel Fluid Temperature Profile

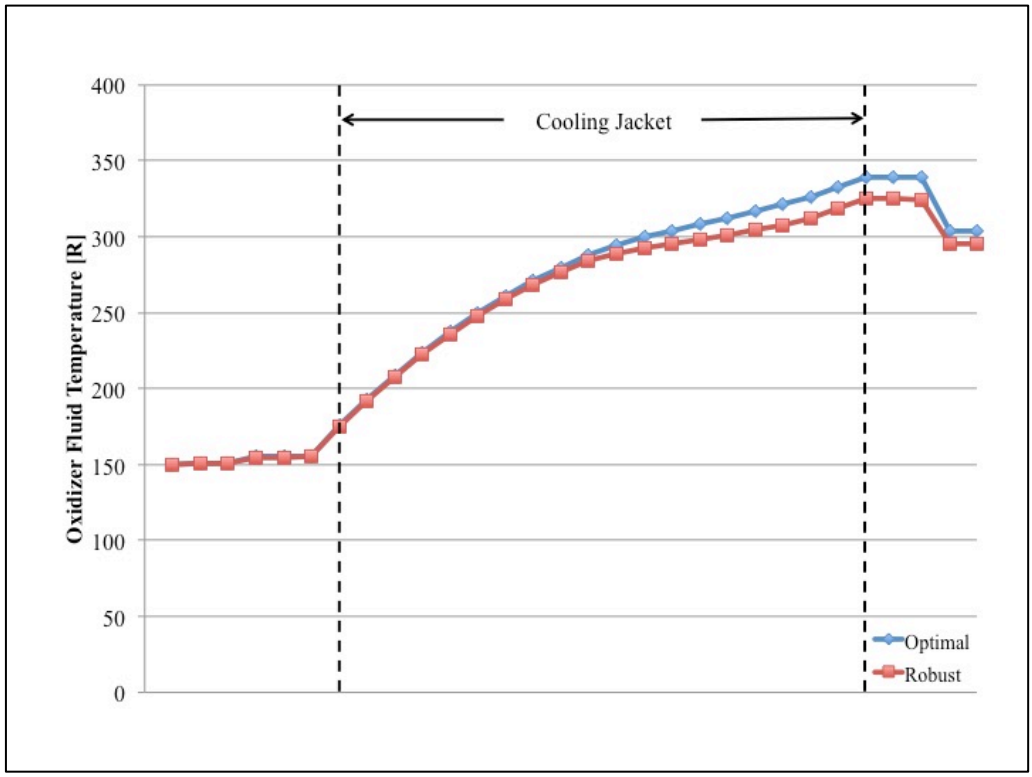

Fig. 46 DEAN Oxidizer Fluid Temperature Profile

The fluid temperatures and pressures are necessary for modeling the state properties of the fluid at any given station. This then assists in defining heat transfer and flow properties, as described in earlier chapters.

The pressure profiles for each fuel and oxidizer feed system are shown in Figs. (47) and (48). The profiles begin at the inlet of the first pump and progress to the second pump, the cooling jacket, the turbine, and then through the injector to the combustion chamber.

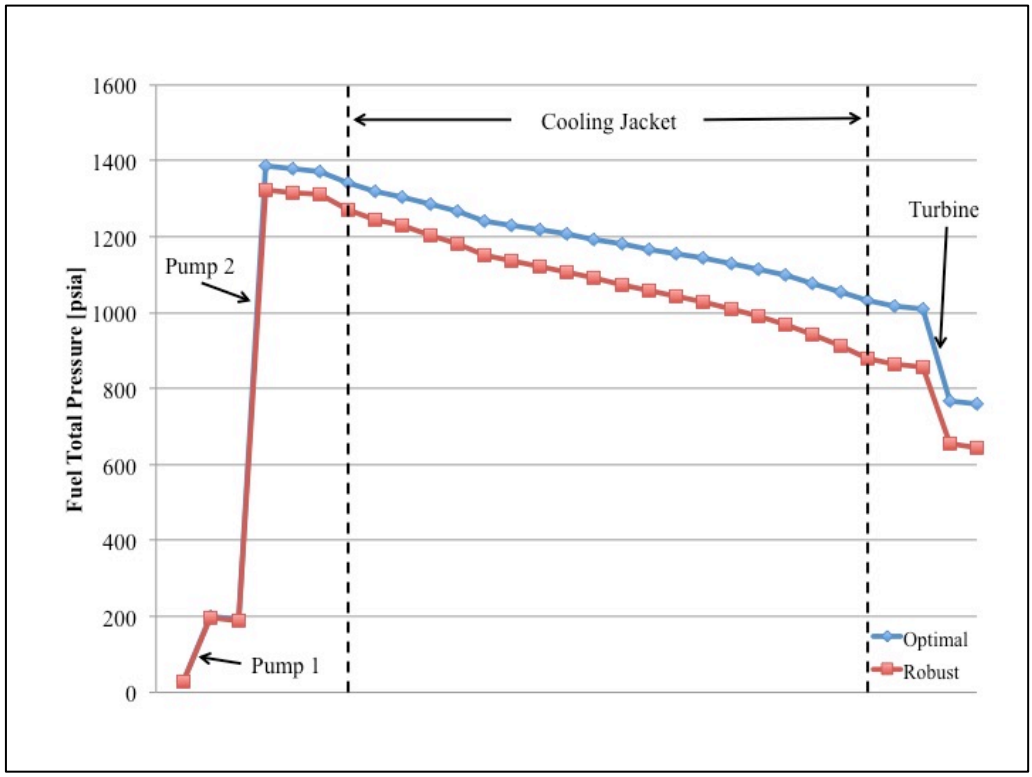

Fig. 47 DEAN Fuel Total Pressure Profile

The difference in maximum fuel total pressures between the optimal and robust cases was 61.2 [psia], or 4.52%. The difference in pressures experienced at the turbine inlet was 156.2 [psia], or 16.7%.

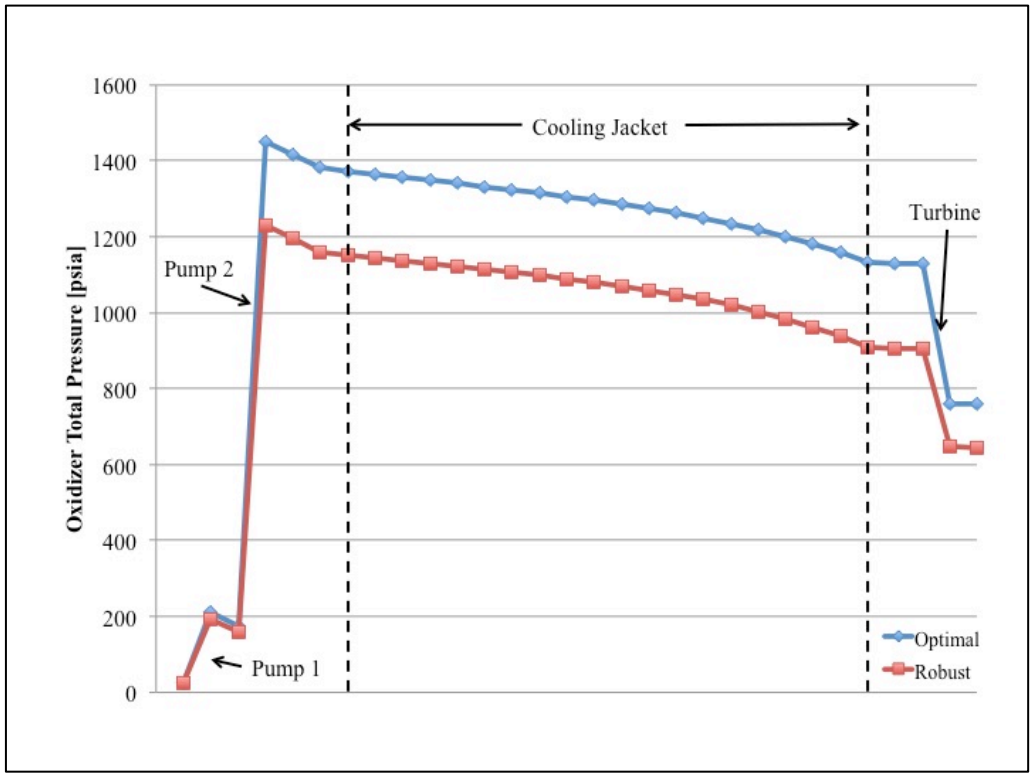

Fig. 48 DEAN Oxidizer Total Pressure Profile

The difference in maximum oxidizer total pressures between the optimal and robust cases was 220.2 [psia], or 16.4%. The difference in pressures experienced at the turbine inlet was 224.5 [psia], or 22.1%.

It is the goal of the engineer to minimize pressure in the propellant feed system as much as possible while still delivering the necessary chamber pressure to achieve the performance goals. In general, lower pressures experienced in the propellant feed system mean less material is required to contain those pressures, which drives down the total engine weight. On the other hand, the pressures must also be high enough to maintain supercritical fluid conditions and to overcome the pressure drop across the cooling jackets.

Table 8 provides a comparison of performance, size, and operating parameters between the optimal and robust design points. The pump discharge pressures are determined at the exit of the second stage ("Pump 2" in the total pressure figures) for each pump.

Table 8 DEAN Design Point Comparison

	[Unit]	Optimal	Robust	% Difference
Throat Area	[in^2]	23	27	16.00%
L*	[in]	90	90	--
Expansion Ratio	[ ]	30	30	--
Engine Length	[in]	49.56	52.67	6.08%
Maximum Diameter	[in]	29.64	32.12	8.03%
Chamber Pressure	[psia]	658.9	560.9	16.07%
Engine Thrust	[lbf]	30,000	30,000	--
Specific Impulse	[s]	467.3	467.1	0.04%
Combustion O/F	[ ]	5.88	5.88	--
Mass Flow	[lb/s]	64.20	64.23	0.05%
Fuel Consumption	[lb/s]	9.33	9.34	0.05%
Oxidizer Consumption	[lb/s]	54.87	54.90	0.05%
Maximum Fuel Wall Temperature	[°R]	1447.8	1321.4	9.13%
Maximum Fuel Fluid Temperature	[°R]	292.9	295.3	0.84%
Maximum Oxidizer Wall Temperature	[°R]	1799.1	1737.5	3.49%
Maximum Oxidizer Fluid Temperature	[°R]	339.4	324.9	4.35%
Fuel Pump Discharge Pressure	[psia]	1385.6	1324.4	4.52%
Oxidizer Pump Discharge Pressure	[psia]	1450.6	1230.4	16.43%

The differences between the optimal and the robust design points are primarily in their geometries. The difference in throat area directly accounts for large differences seen between the maximum diameters and the chamber pressures, and therefore the pump discharge pressures. Similarly, it can be ascertained that the associated wall temperatures should be lower for larger throat areas because wall temperature and cross-sectional areas are inversely proportional. Implementing weight and reusability models into this research may show that the robust design point is more effective due to the fact that the pressures are lower, which implies less material to constrain that pressure. Also, the combination of lower temperatures and pressures is a potential trend that should be examined more closely because the reusability of engines, at least pertaining to their materials, relies heavily on these two operating parameters.

In summary, the optimal and robust design points are both within the feasible solution space and either would be an appropriate programmatic decision based on their performance and size envelopes being better than the RL-10B-2 and the desired project objectives for both cases.

IV.3 Upper Stage Performance Comparison

NASA's Advanced Upper Stage Engine Program requires a new generation upper stage rocket engine to replace the outdated RL-10B-2 technology that is currently in production. This research shows that the DEAN is a prime candidate to meet that need both in terms of performance and size. Table 9 contains a comparison of performance, size, and operating parameters between the DEAN and RL-10B-2 engines. The DEAN contains a two-stage oxidizer pump while the RL-10 contains only one – this is due to the DEAN operating a dual-expander cycle instead of a single-expander, like the RL-10.

Table 9 Upper Stage Performance Comparison[8]

	[Unit]	DEAN	RL-10B-2	% Difference
Engine Length	[in]	49.56	86.5	54.30%
Maximum Diameter	[in]	29.64	43.8	38.56%
Chamber Pressure	[psia]	658.9	644	2.29%
Engine Thrust	[lbf]	30,000	24,750	19.18%
Specific Impulse	[s]	467.3	465.5	0.39%
Combustion O/F	[ ]	5.88	6.0	2.02%
Mass Flow	[lb/s]	64.20	53.10	18.93%
Fuel Consumption	[lb/s]	9.33	7.6	20.45%
Oxidizer Consumption	[lb/s]	54.87	45.5	18.67%
Fuel Pump Discharge Pressure	[psia]	1385.6	1,509	8.53%
Oxidizer Pump Discharge Pressure	[psia]	1450.6	858	51.34%

The DEAN performance is significantly better than the RL-10B-2 at a fraction of the size. Furthermore, higher specific impulse may be obtained by increasing the expansion ratio, as shown in Fig. (37). This increase would add volume and mass, but should still be within the size

envelope of the RL-10 engine. Finally, it is noted that the engine length is for a full nozzle; truncating the nozzle would provide additional mass and length savings, as well as increased performance in terms of thrust-to-weight ratio.

V. CONCLUSIONS AND RECOMMENDATIONS

Chapter V provides final conclusions and a summary of the research, as well as recommendations for future research regarding the DEAN and general dual-expander cycles, particularly in terms of liquid oxygen as a working fluid for an expander cycle.

V.1 Research Conclusions

This research establishes a foundation for dual-expander cycle architecture implementation with a variety of different nozzle configurations, including the aerospike, bell, and conical. The core of this research was to modify past DEAN models with updated physics, geometry, and then to validate and baseline the methods used. This research developed a computational tool to model geometry and performance of a dual-expander aerospike nozzle engine in a near-vacuum environment.

The DEAN upper stage rocket engine was shown to have major advantages over the RL-10B-2 both in performance and size. Three major research objectives were achieved: 1) demonstrate the performance of a LOX/LH_2 dual-expander cycle, 2) validate those results using the same methodology for an RL-10A-3-3A, and 3) determine the optimal design parameters and limitations of the dual-expander model in order to provide a next generation upper stage engine.

V.2 Research Significance

The optimal DEAN design point was shown to achieve a thrust of more than 5,000 [lbf] greater than the RL-10B-2, a vacuum I_{sp} of 1.8 [s] greater, and a significantly reduced size envelope. These results are within the performance and size constraints of NASA's Advanced

Upper Stage Engine Program. The DEAN is shown to be a complete next generation candidate to replace the RL-10 series engines that have been in production since the 1960s.

Finally, the high-performance, small size, and altitude compensation abilities of the DEAN rocket engine would be optimal for both propulsion and retro-propulsion capabilities to support Mars entry, descent, landing, and launch vehicle architectures. Increased thrust and specific impulse at decreased size directly increases the payload to orbit, which implies more mission essential equipment and personnel could be delivered to the Martian surface at a fraction of the cost.

V.3 Recommendations for Future Research

The DEAN is a significant step forward in next generation upper stage engines. While this research achieved substantial advances in terms of accurately modeling the DEAN upper stage rocket engine, a better understanding of the physics of high-energy heat transfer correlations between the combustion chamber and the working fluids is needed. Additional model enhancements should be completed to provide more dynamic modeling of the aerospike nozzle geometry and the performance parameters, such as thrust-to-weight (T/W) ratio.

The heat transfer physics implemented in this research involved more fluid properties of fuel and hydrogen and modeling them such that the fluid properties read by NPSS were developed using the best current information (also ensuring that the range of those values was established for all conditions that the DEAN could operate in). Fluid property information for supercritical oxygen is relatively sparse. More experimental work must be completed to determine oxygen's properties at the operating conditions (pressures and temperatures) of the DEAN, specifically with respect to heat transfer. NPSS uses a flow and power balance solver, so the inaccuracies in oxygen friction factors, and therefore K-factors, will introduce error within

the converged solution. An experimental set-up to model the heat transfer and fluid properties of supercritical oxygen at a range of temperatures and pressures – including the operating conditions – will resolve this concern. Such a platform would also enable an experimental analysis of the range of speeds that the working fluids are effective. The foundation of this model should follow Spencer and Rousar's experimental set-up[38], but extend the convective correlations to higher temperatures and pressures, within and beyond the operating conditions of the DEAN upper stage rocket engine. The NPSS model should also be expanded to enable the handling of multiphase heat transfer systems, such as the DEAN's thrust chamber and nozzle cooling jackets[43].

The NPSS heat exchange model provides an efficient method to perform a trade study on the heat transfer coefficients, cooling channel geometries, and materials. This work should begin by using NPSS to computationally complete a parametric analysis of the speed of sound coefficients for the fluid flow through the cooling chambers. The current maximum Mach numbers are based on the desire to minimize flow instabilities and constrain the cooling channel geometries within manufacturing and safety limitations. Different cooling channel geometries (e.g. circular, oblong, etc.) should also be considered in the trade space as they may provide better heat exchange and overall performance improvements. A nodal analysis for nozzle and chamber sections should be conducted to increase the resolution of static flow conditions and wall temperatures. The number of nodes for the RL-10A-3-3A model was determined based on the ROCETS analysis with a one-for-one implementation, but the optimal resolution should be verified.

The model is currently built for one-dimensional heat exchange. Future work should include representing full heat exchange (and effects) in the chamber and nozzle and to

incorporate material thermal properties. A full materials-based trade study is needed to determine the mass of the engine. The materials sector continues to grow and discover new "state-of-the-art" materials; a sensitivity analysis should be completed to examine what future "state-of-the-art" materials (properties) would need to be advanced for major mass and/or performance savings. The materials trade study allows for implementation of T/W calculations and comparisons. In a general sense, the T/W value signifies how much an engine can accelerate and is, therefore, a major performance parameter for a rocket engine. In order for a full weight calculation to be completed, there must also be a full engine layout with tubing distances between components and accurate component sizing.

The current DEAN model uses RL-10 contours for the chamber and nozzle walls. The geometry (length and width) of each section is dynamically determined based on the geometric and performance inputs. While the RL-10 contour is a proven and well-tested design, it is not optimized for the DEAN. Overall performance of the DEAN engine could benefit greatly with the application of a dynamic contour algorithm. Contours may be established using more general mathematical models such as method of characteristics, or by using more in-depth software such as Two-Dimensional Kinetics (TDK). Past research used the latter software, but the models and input values were not refined enough for it to be effective for this research. Additionally, future models should incorporate combustion flow (computational fluid dynamics) analysis to model the exhaust more accurately and to provide better performance data.

This research focused on steady-state modeling of the DEAN architecture. If the engine is to be considered for manufacture and testing, future computational work must also include transient modeling. The transient case models the entire engine sequence including startup, steady-state, throttling, and shutdown, which allows for more accurate understanding of the

behavior of the engine and the individual components (particularly at the turbomachinery level). Modeling the transient case enables further examination how thrust vectoring and gimbaling affect the engine performance. NPSS is capable of modeling transient conditions, but that work was outside the scope of this research.

Liquid rocket propulsion systems are designed to last multiple uses up to some burn duration and, to this extent, are considered reusable. From a computational modeling perspective, the reusability of a rocket engine can be evaluated based on the material properties, the temperatures experienced, the pressures experienced, and the duration of each. Future research should incorporate a quantitative analysis of the reusability of the DEAN engine and complete a trade study to determine manufacturing and operational costs associated with increasing this capability. One application of a reusable rocket engine is for a Mars access vehicle. Reusable engines will be necessary to deliver payload to and from the Mars sphere of influence without exorbitant launch costs from the Earth's surface. One of the major features of the aerospike nozzle is its altitude compensation ability, which makes it a candidate for a surface access system. A Mars mission would likely require a propellant other than LOX/LH_2 – current Mars architectures are designed for LOX/LCH_4. Future research should examine the performance and operational outputs of different propellants in the DEAN architecture.

REFERENCES

1 Humble, Ronald W., Gary N. Henry, and Wiley J. Larson. “Liquid Rocket Propulsion Systems.” Space Propulsion Analysis and Design. New York: McGraw-Hill, 1995. N. pag. Print.

2 Simmons, J., and R. D. Branam. "Parametric Study of Dual-Expander Aerospike Nozzle Upper Stage Rocket Engine." Wright Patterson AFB, Ohio. Lecture.

3 Greason, Jeff. "Launch Economics & Technology." 23 Mar. 2011. Lecture.

4 “Altitude Compensation,” *Aerospace Web* [online database], URL: http://www.aerospaceweb.org/design/aerospike/compensation.shtml [cited 18 April 2015].

5 Hall, J., and R. D. Branam. "Optimized Dual-Expander Aerospike Rocket." Wright Patterson AFB, Ohio. Thesis.

6 Drake, Bret G., and Kevin D. Watts. *Human Exploration of Mars: Design Reference Architecture 5.0 - Addendum #2*. Publication no. Mars DRA 5.0 Executive Summary. NASA Lyndon B. Johnson Space Center, Mar. 2014. Web. 25 May 2015.

7 Sackheim, Robert L. "Overview of United States Rocket Propulsion Technology and Associated Space Transportation Systems." *Journal of Propulsion and Power* 22.6 (2006): 1310-333. Web.

8 Santiago, Jorge R. "Evolution of the RL10 Liquid Rocket Engine for a New Upperstage Application." *32nd Joint Propulsion Conference & Exhibit*(1996): n. pag. Print.

9 Brinton, Turner. "U.S. Air Force Ponders New Upper-stage Rocket Engine - SpaceNews.com." *SpaceNews.com*. N.p., 15 Oct. 2010. Web. 03 Sep. 2015.

10 Martin, D. "Computational Design of Upper Stage Chamber, Aerospike, & Cooling Jacket for Dual-Expander Rocket Engine." Wright Patterson AFB, Ohio. Thesis.

11 Buzzell, James C. "Testing for the J-2X Upper Stage Engine." *AIAA SpaceOps 2010 Conference* (2010): n. pag. Web.

12 Bullock, J.R., M. Popp, and J.R. Santiago. *Program Status of the Pratt & Whitney RL60 Engine*. Tech. West Palm Beach, FL: Pratt & Whitney Space Propulsion, 2012. Print.

13 "Staged Combustion Cycle." *Project Gutenberg*. N.p., n.d. Web. <http://gutenberg.us/articles/staged_combustion_cycle_(rocket)>.

14 Greene, W. D. "Liquid Rocket Engines (J-2X, RS-25, General)." Liquid Rocket Engines J2X RS25 General. National Aeronautics and Space Administration, n.d. Web. 2 Feb. 2016.

15 "Pressure-Fed Cycle." *Project Gutenberg*. N.p., n.d. Web. <http://gutenberg.us/articles/Pressure-fed_cycle_(rocket)>.

16 Greene, W. "Liquid Rocket Engines." *Liquid Rocket Engines*. National Aeronautics and Space Administration, n.d. Web. 16 Jan. 2016. <https://blogs.nasa.gov/J2X/author/wgreene/>.

17 Sutton, George P., and Oscar Biblarz. *Rocket Propulsion Elements: An Introduction to the Engineering of Rockets*. 7th ed. New York: Wiley-Interscience, 2001. Print.

18 Akin, Dave. "Akin's Laws of Spacecraft Design*." *Akin's Laws of Spacecraft Design*. University of Maryland, n.d. Web. 18 Dec. 2015. <http://spacecraft.ssl.umd.edu/akins_laws.html>.

19 Jensen, J.E.; Brechna, H, Tuttle, W. Stewart, R., "Brookhaven National Laboratory Selected Cryogenic Data Notebook." BNL 10200-R, Revised August 1980.

20 *Turbopump Systems for Liquid Rocket Engines*. Tech. Lewis Research Center, OH: National Aeronautics and Space Administration, 1974. Print.

21 Arguello, M. *The Concept Design of a Split Flow Liquid Hydrogen Turbopump.* MS thesis, AFIT/GAE/ENY/08 M01. Graduate School of Engineering and Management, Air Force Institute of Technology (AU), Wright-Patterson AFB, OH. March 2008.

22 Strain, M. *Design of an Oxygen Turbopump for a Dual Expander Cycle Rocket Engine.* AFIT/GAE/ENY/08-M26. Graduate School of Engineering and Management, Air Force Institute of Technology (AU), Wright-Patterson AFB OH. March 2008.

23 Huzel, D. and Huang, D. Modern Engineering for Design of Liquid-Propellant Rocket Engines. Progress in Astronautics and Aeronautics, Volume 147, AIAA, 1992.

24 Dressler, Gordon A., and J. Martin Bauer. "TRW Pintle Engine Heritage and Performance Characteristics." *36th AIAA/ASME/SAE/ASEE Joint Propulsion Conference & Exhibit* (2000): n. pag. Web.

25 Hill, Philip G., and Carl R. Peterson. *Mechanics and Thermodynamics of Propulsion*. Reading, MA: Addison-Wesley Pub., 1965. Print.

26 Hersch, Martin. *Hydrogen-oxygen Chemical Reaction Kinetics in Rocket Engine Combustion*. Washington, D.C.: National Aeronautics and Space Administration, 1967. Web.

27 Moen, Michael D. "Methane Dual Expander Aerospike Nozzle Rocket Engine." Thesis. Air Force Institute of Technology, 2012. Print.

28 "Welcome to the NIST Chemistry WebBook." *Welcome to the NIST WebBook*. National Institute of Standards and Technology, n.d. Web. 24 Nov. 2015. <http://webbook.nist.gov/>.

29 Pisacane, Vincent L. “Thermal Control.” The Space Environment and Its Effects on Space Systems. Reston, VA: American Institute of Aeronautics and Astronautics, 2008. N. pag. Print.

30 Carlile, Julie, and Richard Quentmeyer. "An Experimental Investigation of High-aspect-ratio Cooling Passages." *28th Joint Propulsion Conference and Exhibit* (1992): n. pag. Web.

31 Hagemann, G., H. Immich, and M. Terhardt. "Flow Phenomena in Advanced Rocket Nozzles - The Plug Nozzle - 34th AIAA/ASME/SAE/ASEE Joint Propulsion Conference and Exhibit (AIAA)." *Flow Phenomena in Advanced Rocket Nozzles - The Plug Nozzle - 34th AIAA/ASME/SAE/ASEE Joint Propulsion Conference and Exhibit (AIAA)*. Aerospace Research Central, 1998. Web.

32 Ladeinde, Tayo, and Hsun Chen. "Performance Comparison of a Full-Length and a Truncated Aerospike Nozzle." *46th AIAA/ASME/SAE/ASEE Joint Propulsion Conference & Exhibit* (2010): n. pag. Web.

33 Anderson, John D. "Numerical Techniques for Steady Supersonic Flow." *Modern Compressible Flow: With Historical Perspective*. Third ed. Boston: McGraw-Hill, 2003. N. pag. Print.

34 *Numerical Propulsion System Simulation (NPSS): An Award Winning Propulsion System Simulation Tool*. NASA Glenn Research Center, June 2002. Web. <http://ntrs.nasa.gov/archive/nasa/casi.ntrs.nasa.gov/20050214739.pdf>.

35 *NPSS User Guide*. Rep. Cleveland, OH: Ohio Aerospace Institute, 2012. Print. 2.4.1.

36 *NPSS Rockets Supplement*. Rep. Glenn Research Center, OH: National Aeronautics and Space Administration, 2006. Print. 1.6.4.

37 McBride, Bonnie J., and Sanford Gordon. "NASA Chemical Equilibrium with Applications (CEA)." *NASA Chemical Equilibrium with Applications (CEA)*. NASA Glenn Research Center, n.d. Web. 10 Feb. 2016. <http://www.grc.nasa.gov/WWW/CEAWeb/>.

38 Spencer, R.G., and D.C. Rousar. *Supercritical Oxygen Heat Transfer*. Tech. N.p.: n.p., n.d. *Supercritical Oxygen Heat Transfer*. Aerojet Liquid Rocket Company. Web.

39 Buckmann, P. S., N. R. Shrimp, F. Viteri, and M. Proctor. "Design and Test of an Oxygen Turbopump for a Dual Expander Cycle Rocket Engine." *Journal of Propulsion and Power* 8.1 (1992): 80-86. Web.

40 *Flow of Fluids through Valves, Fittings, and Pipe*. New York, NY: Crane, 1988. Print.

41 Binder, Michael, Thomas Tomsik, and Joseph P. Veres. *RL-10A-3-3A Rocket Engine Modeling Project*. Tech. Lewis Research Center, OH: National Aeronautics and Space Administration, 1997. Print.

42 Ellis, David L. *GRCop-84: A High-Temperature Copper Alloy for High-Heat-Flux Applications*. Tech. Glenn Research Center, OH: National Aeronautics and Space Administration, 2005. Print.

43 Ransom, David. "Numerical Propulsion System Simulation (NPSS®) Consortium." *Numerical Propulsion System Simulation (NPSS)*. Southwest Research Institute, 05 May 2015. Web. 21 Dec. 2015. <http://www.swri.org/npss/>.

44 Braeunig, Robert A. "Basics of Space Flight: Rocket Propulsion." *Basics of Space Flight: Rocket Propulsion*. N.p., n.d. Web. 05 Feb. 2016. <http://www.braeunig.us/space/propuls.htm>.

APPENDIX A: NASA ROCETS Steady-State Performance Predictions[41]

Steady-state Cycle Performance Prediction for the RL10A-3-3A

NASA Lewis Research Center RL10A-3-3A Engine Model Output

OVERALL ENGINE PERFORMANCE

Chamber Pressure (at injector face)	475.5	psia
Engine Thrust	16412	lbf
Engine Inlet O/F	4.993	
Combustion O/F	5.055	
Specific Impulse	445.6	sec
Fuel Consumption	6.161	lb/sec
Oxidizer Consumption	30.76	lb/sec

COMBUSTION CHAMBER / NOZZLE

Nozzle Stagnation Pressure	473.5	psia
Combustion Temperature	5816	R
c* Efficiency	0.9892	
c* (ideal)	93885	in/sec
Engine Exit Pressure (ambient)	0.01	psia
Fuel-LOX heat transfer at injector	40.36	BTU/sec

TURBOMACHINERY PERFORMANCE

	delta-Head (feet)	Volume Flow (gpm)	Speed (rpm)	Torque (lbf-in)	Efficiency
Fuel Pump					
1st stage	16858	637.8	31494	645.5	0.5854
2nd stage	17901	641.0	31494	700.7	0.5686
LOX Pump	1212	199.9	12598	529.1	0.6408

Turbine Pressure Ratio (T-S)	1.402	
Turbine Exit Pressure (static)	580.6	psia
Turbine Exit Temperature	360.9	R
Turbine delta-H	92.02	BTU/lb
Turbine Efficiency	0.7353	
Turbine Torque	1577.8	lbf-in
Veocity Ratio (U/Co)	0.4581	

COOLING JACKET PERFORMANCE

Cooling Jacket delta-P (total)	195.7	psid
Cooling Jacket delta-T	326.3	R
Total Heat Pick-up	7714.2	BTU/sec
Maximum Metal Temp	1500.8	R

VALVE PERFORMANCE

Thrust Control Open Area	.004836	sq.in.
Turbine Bypass Flow	.02634	lb/sec
Oxidizer Control Open Area	.5783	sq.in.
OCV primary flow	28.10	lb/sec
OCV bypass flow	2.659	lb/sec

FUEL-SIDE ENGINE CONDITIONS

Location	static pressure (psia)	total pressure (psia)	total temp (deg R)	mass flow (lb/sec)	density (lb/cu.ft)	total enthalpy (BTU/lb)
Fuel Tank	27.68	27.68	38.60	.....	4.337	-105.1
Fuel Pump Inlet	26.08	27.19	38.6	6.161	4.337	-105.1
Fuel Pump Interstage	532.2	534.8	47.65	6.118	4.285	-68.21
Fuel Pump Discharge	1058.9	1067.3	57.63	6.082	4.220	-27.84
Cooling Jacket Inlet	1018.3	1026.6	57.94	6.082	4.185	-27.84
Cooling Jacket Exit	816.8	830.9	384.2	6.082	0.3855	1240.5
Turbine Inlet	796.7	813.8	384.2	6.056	0.3767	1240.5
Turbine Hlusing Exit	562.2	576.2	361.1	6.082	0.2868	1149.2
Fuel Injector Plennum	537.9	537.9	359.4	6.082	0.2742	1142.4
Chamber	475.5					

OXIDIZER-SIDE ENGINE CONDITIONS

Location	static pressure (psia)	total pressure (psia)	total temp (deg R)	mass flow (lb/sec)	density (lb/cu.in)	total enthalpy (BTU/lb)
Oxygen Tank	42.35	42.35	174.7	.....	69.07	66.42
Ox Pump Inlet	36.33	39.96	174.7	30.76	69.07	66.42
Ox Pump Discharge	601.5	621.1	178.6	30.75	69.02	68.84
Oxid. Injector Plennum	529.4	539.3	182.1	30.75	68.31	70.15
Chamber	475.5					